

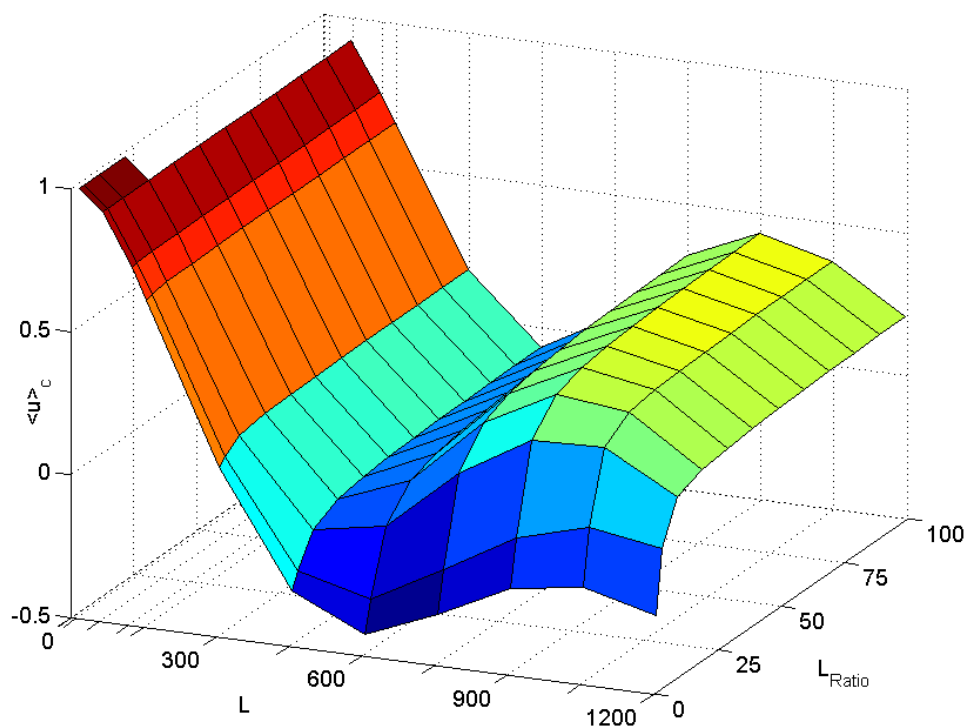
Technical Report



DEPARTMENT OF MATHEMATICS

Temporal correlation of average population densities of adjacent spatial domains

Research Project



Students Name:	Daniel Neumann
Supervisor:	Dr. Sergei Petrovskii
Date of first Submission: (<i>rough-and-ready</i>)	14. Juli 2011
Date of final Submission:	09. August 2011

ABSTRACT

Animal populations are not constant in space and time but reveal temporal oscillations. Since the beginning of the 20th century this is a widely accepted fact [Elton, 1924, Lotka, 1925, Volterra, 1926]. Volterra [1931] and Lotka [1934] suggested the first mathematical predator-prey model for describing these oscillations. Within the following decades many different new models have been proposed and several population cycles of various species have been observed. Murray [1989] [or Murray, 2008, 2003] gives a good overview over many models. Especially the population cycles of the snowshoe hare and the Canadian lynx have been studied extensively and are said to be the best documented ones [MacLulich, 1937, Elton and Nicholson, 1942, Chitty, 1948, 1950, Finerty, 1979, Smith, 1983, Krebs et al., 1986, Smith et al., 1988, Sinclair et al., 1988, 1993, Ranta et al., 1997b, Krebs et al., 2001].

The monitoring of wildlife animal populations provides mean populations sizes for large spatial domains. In the case of many time series of the snowshoe hare population these domains have the area of several thousand square kilometres. Motivated by this, we analyse the effect of the size and position of spatial domains on the mean animal populations within these domains. No real observations but a mathematical predator-prey-model are used for this purpose. The model was used by Petrovskii and Malchow [1999] [see also Murray, 1989, Sherratt and Smith, 2008] and describes the propagation and interaction of a predator and a prey species. It is formed by two coupled partial differential equations: Both species diffuse with the same diffusion coefficient, the prey grows logistically, both equations are coupled by a Michaelis-Menten-Kinetics term [Michaelis and Menten, 1913] as hunt-term and the mortality term of the predator is a first order kinetic. For the appropriate choice of parameters, the population densities oscillate either chaotically or regularly depending on the initial conditions. After discussing the model and the used numeric tools in chapter 2, we introduce two adjacent spatial domains, change their size - relative to each other and relative to the whole space - and position and compute average population densities which we compare in chapter 3.

The pde system offers different possibilities to vary parameters, initial conditions and the model itself. Uncoupled from the practical motivation, parameter and model variations and their results are discussed and presented in the chapters 4, 5 and 6. In chapter 4 we vary especially the prey's growth rate and the predator's mortality. The results are traveling waves [Sherratt and Smith, 2008], unexpected less regular regular oscillations and chaotic oscillations which evolve slightly different than those observed before. Further in chapter 5 we introduce noise with the intention to produce more realistic regular oscillations which we can use for further works on the topic of chapter 3. However, we hit some snags and discuss the results without working with the both spatial domains and computing average population densities. Finally in chapter 6 spatio-temporal chaos lies in the focus. We observe areas of regular oscillations in a chaos-dominated system and try to reproduce results of Petrovskii et al. [2010].

ZUSAMMENFASSUNG

Tierpopulationen sind nicht zeitlich und räumlich konstant, sondern zeigen Schwingungen in der Zeit. Seit Anfang des 20. Jahrhunderts ist dies eine weitgehend akzeptierte Tatsache [Elton, 1924, Lotka, 1925, Volterra, 1926]. Als erste schlugen Volterra [1931] und Lotka [1934] ein mathematisches Modell zur Beschreibung dieser Oszillationen vor. Innerhalb der folgenden Jahrzehnte wurden viele verschiedene neue Modelle aufgestellt und etliche Populationszyklen unterschiedlicher Tierarten aufgezeichnet. Murray [1989] [or Murray, 2008, 2003] bietet einen guten Überblick über einige dieser Modelle. Besonders die Populationszyklen des Schneeschuhhasen und des Kanadischen Luchses wurden ausführlich studiert und sollen zu den am umfangreichsten dokumentierten gehören [MacLulich, 1937, Elton and Nicholson, 1942, Chitty, 1948, 1950, Finerty, 1979, Smith, 1983, Krebs et al., 1986, Smith et al., 1988, Sinclair et al., 1988, 1993, Ranta et al., 1997b, Krebs et al., 2001].

Im Allgemeinen liefert die Beobachtung wild lebender Tierpopulationen lediglich über ein großes räumliches Gebiet gemittelte Populationsgrößen. Im Fall von Zeitreihen des Schneeschuhhasen umfassen diese Gebiete mehrere tausend Quadratkilometer. Hierdurch motiviert analysieren wir den Effekt der Größe und Position solcher Gebiete auf die dort drin ermittelten mittleren Tierpopulationen. Hierfür werden keine realen Tierbeobachtungen sondern ein mathematisches Räuber-Beute-Modell verwandt. Das Modell wurde bereits in Petrovskii and Malchow [1999] genutzt [siehe auch Murray, 1989, Sherratt and Smith, 2008] and beschreibt die Ausbreitung und Interaktion einer Räuber- und einer Beutespezies. Es besteht aus zwei gekoppelten partiellen Differentialgleichungen: Beide Spezies diffundieren räumlich mit dem gleichen Diffusionskoeffizienten, die Beute wächst logistisch, beide Gleichungen sind über eine als Jagd-Term genutzte Michaelis-Menten-Kinetik miteinander verbunden und der Räuber stirbt mit einem Reaktionsterm erster Ordnung. In Kapitel 2 werden das Modell und die genutzten numerischen Hilfsmittel vorgestellt. Bei passend gewählten Parametern schwingen die Populationsdichten abhängig von den Anfangsbedingungen entweder chaotisch oder geordnet. Anschließend führen wir in Kapitel 3 zwei räumlich benachbarte Domänen ein, verändern ihre Größe - relativ zueinander und relativ zum gesamten Raum - und ihre Position und berechnen mittlere Populationsdichten, die wir miteinander vergleichen.

Das gegebene System an partiellen Differentialgleichungen bieten verschiedene Möglichkeiten Parameter, Anfangsbedingungen und das Modell selbst zu verändern. Losgelöst von der praktischen Motivation diskutieren und präsentieren wir Variationen der Parameter und des Modells und deren Auswirkungen in den Kapiteln 4, 5 und 6. In Kapitel 4 konzentrieren wir uns speziell auf die Variation der Wachstumsrate der Beute und der Sterberate des Räubers. Die Ergebnisse sind Travelling Waves (dt.: *reisende Wellen*) [Sherratt and Smith, 2008], unerwartet weniger regelmäßige geordnete Schwingungen und chaotische Schwingungen, die sich etwas anders entwickeln als die bisher beobachteten. Weiter in Kapitel 5 führen wir Noise (dt.: *Rauschen*) mit der Intention ein, realistischere reguläre Schwingungen zu erzeugen, die wir für weitere Arbeiten zum Thema von Kapitel 3 verwenden können. Allerdings treffen wir auf einige Hinderniss und diskutieren lediglich die

Ergebnisse ohne mit den beiden räumlichen Domänen zu arbeiten und gemittelte Populationsdichten auszurechnen. Schließlich liegt in Kapitel 6 raum-zeitliches Chaos im Fokus. Wir beobachten Gebiete geordneter Schwingungen in einem von Chaos dominierten System und versuchen Ergebnisse von Petrovskii et al. [2010] zu reproduzieren.

Acknowledgement

My master research project I performed at the Mathematics Department of the University of Leicester. Without the following people and organisations, which supported my stay, the preparation of my project and the realisation of it in different ways, it would have been more difficult to organise or not have been possible.

First of all, I want to thank Dr. Sergei Petrovskii of the Mathematics Department of the University of Leicester. Since the beginning of 2008 we had contact via email concerning an exchange semester in Leicester for a research project or a bachelor's or master's thesis. We kept contact and finally agreed on a research project within the winter semester 2010/11. Sergei gave me an interesting and fascinating topic on which I worked during my projects core phase from January to April 2011. While a two weeks stay for preparation in November 2010 and my proper stay in Leicester, he took the time for an introduction into the topic and discussions about my work and population dynamics in general. He pushed me to write my report parallel to the computer simulations I performed and gave me advices. Moreover Sergei supported me in organising my accommodation and other things around my stay.

Another thanks goes to Prof. Dr. Horst Malchow of the Institute of Environmental Systems Research of the University of Osnabrück. He established my contact to Sergei Petrovskii and answered all questions concerning the integration of my research project in Leicester.

The PhD-Students of the University of Leicester and Kristina Burns who worked in the same graduate computer room as I did, have also to be mentioned. They answered my question to technical topics, the university and travelling at the weekends.

Two organisations supported my project. The University of Leicester did it indirect by providing a workplace, a good working environment and the possibility to take part in courses of the Sports & Recreation Service of the University. The Foundation of German Business (Stiftung der Deutschen Wirtschaft, sdw) paid an *Auslandspauschale* (\approx sponsorship abroad) and a refund of my travelling expenses with which my accommodation and flights were funded. Concerning the sdw, special thanks goes to Girina Holland who is desk officer at the sdw and my contact person there.

Finally, thanks to my parents Hannelore and Dietrich Neumann who supported my stay in Leicester in various ways.

Contents

1	Introduction	7
1.1	Motivation I	7
1.2	The model	9
1.3	Course of Action	10
2	Definition of Model and Domains	12
2.1	Parameters initial conditions, stationary states and system behaviour	12
2.2	Numerical Solution of the PDE	13
2.3	Choice of Parameters and Initial Conditions	15
2.4	Definition of the Domains	16
2.5	Comparison of the Average Densities	18
3	Correlation of average Densities	21
3.1	Size of the Domains	21
3.2	Different Locations of the Domains	23
3.3	Comparison of average Predator- and Prey Densities	26
3.4	Parameter Set C	26
3.5	Different Diffusion Coefficients	27
3.6	Summary first Analysis and Outlook	28
4	Variation of Parameters	30
4.1	Chaos through parameter variation	31
4.2	Varying the growth rate	33
4.2.1	Simulation results for changed growth rate	34
4.2.2	Attempts to explain the simulation results	37
4.3	Spatially Varying parameters	38
4.3.1	Effects of variation in the initial conditions	40
4.3.2	Velocity of travelling waves	42
4.4	Summary Parameter Variation	45
5	Introduction of Noise	47
5.1	Motivation II: Why noise?	47
5.2	Application and Implementation of the Noise I	47
5.3	First Observations I: Strong dependence on size of time steps	49
5.4	First Observations II: Different system behaviour for different sets of parameters	52
5.5	Summary, Outlook and Noise II	54
6	Chaotic System	56
6.1	Islands of Order	56
6.2	Chaos Suppression through noise	57
7	Summary and Outlook	60

1 Introduction

1.1 Motivation I

It is a well known fact, that animal populations show oscillations in time. But it is still hotly discussed which factors and mechanisms lead to these oscillations and influence them. In discussion are external factors as weather [Elton, 1924] or solar activity [Sinclair et al., 1993], just random influences [Cole, 1951, 1954] or species interactions over two or more trophic levels. A classical and simple model for the latter one is the predator-prey model by Lotka and Volterra [Lotka, 1934, Volterra, 1931]. Additionally, in some datasets a spatial variation of animal populations can be identified [Smith, 1983, Ranta et al., 1997b]. Smith [1983] proposed the idea that the spatial inhomogeneous distribution of populations can be described by diffusion. Whereas other authors assume a homogeneous animal distribution, disturbed by stochastic or local influences.

Two species for which much data is available are the snowshoe hare (*Lepus americanus*) and the Canadian lynx (*Lynx canadensis*): Fur records of the Hudson Bay Company of the 19th and 20th century [hare and lynx respectively: MacLulich, 1957, Elton and Nicholson, 1942], hare observations of the Canadian Snowshoe Rabbit Enquiry 1931-1948 (e.g. [Chitty, 1948],[Chitty, 1950] or the journal *The Canadian Field-Naturalist* from 1934 to 1950 in general), hare countings with modern equipment [Krebs et al., 1986]. Also secondary data as marks at tree barks is used to reconstruct time series of hare population [Sinclair et al., 1993]. For the interested reader: Finerty [1979] discusses possible corruption of the data by human hunting habits.

The published data of the Canadian Snowshoe Rabbit Enquiry 1931-1948 was re-evaluated and analysed by Smith [1983]. Canadian Snowshoe Rabbit and Canadian Snowshoe Hare are identical. At this enquiry not the number of hares was counted but it was noted whether the hare population increased, decreased or stayed equal compared to the year before. For each year about 300 valid data points distributed over whole Canada are given. This dataset is one of the most detailed ones which is available. Unfortunately the original data is not available. In the published data [Chitty, 1948, 1950] the observations are assigned to squares in a grid map of Canada or to the Canadian provinces. Squares and man-made boundaries are probably not fitting to the catchment areas of the hare and hence are no good choice for subsuming the data. Smith [1983] reworked the published data set and looked at the hare oscillation in different areas of Canada. It became obvious that the temporal oscillations at different spatial positions are not always in phase. Figure 1.1 shows the phase shifts in years compared to the national mean oscillation. Figure 1.1 is equal to figure 2 of Smith [1983] but coloured and a legend is added. The color indicates the size of the phase shift. A whole hare population cycle has a length of about 9 to 11 years.

A patchy pattern is clear to see in the given figure. It indicates that some spatial motion exists and a spatial homogeneous model is not enough to explain the population dynamic of hares. Therefore we will use a continuous spatio-temporal population model introduced by Murray [1989] and Shigesada and Kawasaki [1997] and discussed amongst others by Petrovskii and Malchow [1999] and DeRoos et al. [1991]. The model is a system of two partial differential equations (pde) and describes the interaction, distribution and evolution of a prey and a predator population. These can be for example the Canadian snowshoe hare and the Canadian lynx. Simulations with this model in two spatial dimensions show similar patchy shapes. We will only

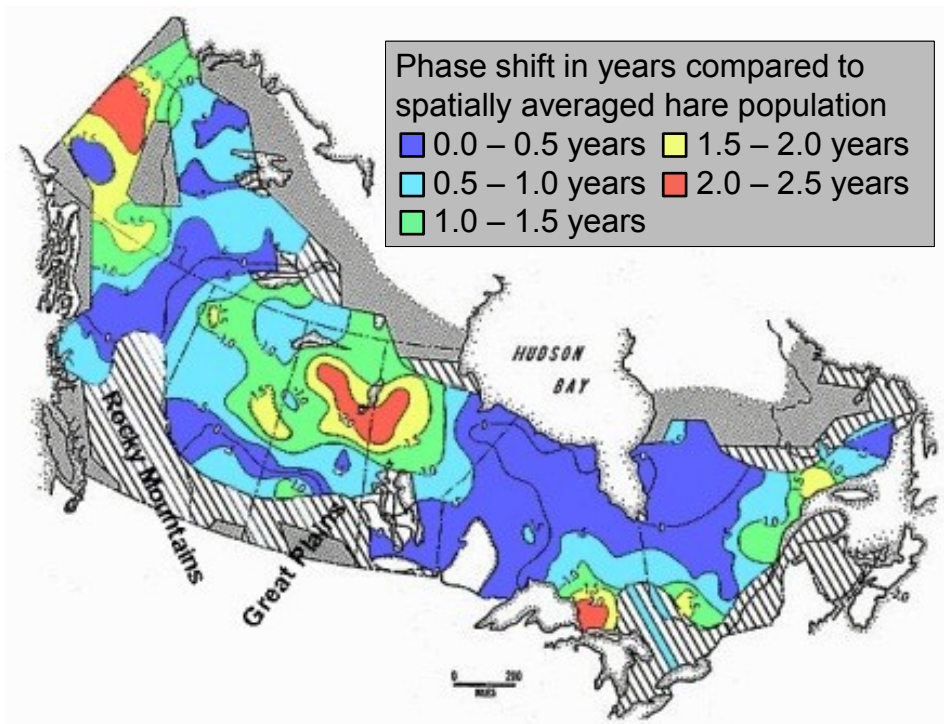


Figure 1.1: Map of Canada from Smith [1983] in coloured form. The lines with the numbers ± 0.5 till ± 2.0 indicate the phase shift in years of the local temporal oscillation compared to the mean Canadian oscillation of the snowshoe hare population. The colors indicate also the time shift in years as follows: blue = less than 0.5 years, light blue = between 0.5 and 1.0 year, green = between 1.0 and 1.5 years, yellow = between 1.5 and 2.0 years and red = above 2.0 years.

work in one spatial dimension. In the next subsections the model will be further discussed.

The real world data often consists of average values for large areas [e.g.: Chitty, 1948, 1950]. Moreover the areas have different size. The Canadian provinces shown in figure 1.2 are a nice example for this problem. Because the model is continuous in time and space, *exact* animal populations at each position and time point are computed but no average data. Thus real world data and model results are not directly comparable.

The problem of comparability of model and real world data should be fixed. Therefore we introduce two domains of different sizes into the model and compute average population densities for these domains. In other words: We discretise the model. It is better to start on a low level of complexity. Thus two domains and not three or more are introduced. One next logical step is, to compare the average model data with real world observation. We do not go this step but another one. Smith [1983] mentioned a phase shift between temporal oscillations of hare populations between different areas in Canada. Ranta et al. [1997b] compared hare population cycles of different provinces in Finland. He observed similar period times for the cycles but phase shifts depending roughly on the distance between the provinces as well. The continuous model explains these phase shifts but how does the relation between the discrete average densities look like? Further, both authors did not regard the size of the domains. Here we start. Or first questions are: What is the influence of the domain size on the observed average population and especially on the correlation between the population oscillations of two adjacent domains? Can we estimate a critical size for an observation area above which the resulting data is averaged too much and therefore useless? In particular, what are the answers of these questions if noise of different intensities is added to the model? Another question which is moved to another work:



Figure 1.2: Map of Canada with its provinces [WikiCommons et al., 2007]

How strong does the phase shift of the oscillations depend on the distance of two domains?

1.2 The model

Equations 1.1 and 1.2 describe predator and prey populations in time and space. The variable for time is t and for space x . At first we consider only one spatial dimension. u is the prey and v the predator population density. The first term on the right-hand side of each equation is spatial diffusion of both species. The second term in equation 1.1 is logistic growth of the prey. The third term in equation 1.1 and the second one in equation 1.2 is the food intake of the predator of Holling-type II by the Michaelis-Menten formula. The constant κ reflects the effectiveness of the food conversion. The mortality of the predators is given by the third term. The first term in each equation we call the diffusion term and the second and third one the reaction term.

$$\frac{dU}{dt} = D_u \frac{d^2U}{dx^2} + \frac{a}{u_1} \cdot U \cdot (u_1 - U) - \gamma \cdot \frac{U}{U + h} \cdot V \quad (1.1)$$

$$\frac{dV}{dt} = D_v \frac{d^2V}{dx^2} + \kappa \cdot \gamma \cdot \frac{U}{U + h} \cdot V - \mu \cdot V \quad (1.2)$$

For more detailed information concerning the different terms and alternative ones see Murray [1989], Petrovskii and Malchow [1999] or Sherratt and Smith [2008]. The equations are used for the simulation of different species population (cf. Murray [1989], Malchow et al. [2002], Medvinsky et al. [2002], Sherratt and Smith [2008]).

To improve the readability of the equations the following short forms are used: $\frac{df}{dt} = f_t$, $\frac{d^2f}{dx^2} = f_{xx}$

Introducing dimensionless variables and assuming $D_u = D_v = D$ leads to equations 1.3 and 1.4. Where $H = h/u_1$ (Michaelis-Menten constant), $m = \mu/a$ (mortality) and $k = \kappa\gamma/a$ (effectiveness of food conversion) are the dimensionless parameters. The proof of these parameters is left for the reader.

$$u_t = u_{xx} + u(1-u) - \frac{u}{u+H}v \quad (1.3)$$

$$v_t = v_{xx} + k\frac{u}{u+h}v - m \cdot v \quad (1.4)$$

If the diffusion coefficients D_u and D_v are unequal, the ration d_{ratio} between D_v and D_u appears in one of the equations (See equations 1.5 and 1.6 with $d_{ratio} = \frac{D_v}{D_u}$). Here $D_u \neq D_v$ is only shortly discussed in section 3.5.

$$u_t = u_{xx} + u(1-u) - \frac{u}{u+H}v \quad (1.5)$$

$$v_t = d_{ratio}v_{xx} + k\frac{u}{u+h}v - m \cdot v \quad (1.6)$$

The system is interesting to analyse. It is a known fact about complex systems that they exhibit chaotic or non-chaotic behaviour depending on the parameters of the system [e.g.: Lorenz, 1963, Rössler, 1976]. In the given system (equations 1.3 and 1.4) for a fix set of parameters k , m and H some initial conditions lead to spatio-temporal chaos and some others not. Without the diffusion term we would have a system of ordinary differential equations. In this system no chaos would evolve. The systems of Lorenz [1963] and Rössler [1976] consist of ordinary differential equations and exhibit temporal chaos. It is important to distinguish between spatio-temporal chaos and temporal chaos. Different topics concerning the chaotic behaviour of predator-prey systems are discussed in Pascual and Levin [1999], Petrovskii and Malchow [1999], Durrett and Levin [2000], Petrovskii and Malchow [2001] and Petrovskii et al. [2003]. Apart from sections 4.1, 5.3 and 5.4 and chapter 6 we work with initial conditions and pde parameters which lead to non-chaotic system behaviour. We call it regular system behaviour (irregular = chaotic).

1.3 Course of Action

In section 2 the model is presented deeper in detail and technical things as solving the pde system and implementation issues are discussed. Amongst others the following questions are answered: Which sets of parameters are used? Which initial conditions are chosen? How are the two spatial domains defined? In which way the time series of average population densities are compared? Which numerical solutions are applied to equations 1.3 and 1.4?

Chapter 3 deals with the comparison of the time series of average densities for the given system with non-chaotic behaviour and one spatial dimension. For this comparison the size and position of the two domains are varied. Furthermore, the pde parameters are changed exemplary in some cases.

To make the system more realistic, noise is introduced in chapter 5. It is motivated at first (section 5.1), then the implementation is described (section 5.2) and observations of the noisy system are discussed (sections 5.3 and 5.4). The noise leads to unexpected and partly interesting system behaviour. Unfortunately the chosen kind of noise is not appropriate for our purpose. Finally a second kind of noise is defined (section 5.5) but because of the lack of time and further interesting findings no new simulations are performed and analysed.

In Chapter 4 the system behaviour under variation of some pde parameters is discussed. The first two sections deal with simple changes of the parameter values and the resulting change in system behaviour. In the third section the effects of linear in space increasing parameters are presented. Beneath other things, travelling waves evolve.

Chapter 6 deals with spatio-temporal chaos. When spatio-temporal chaos prevails in the given system, small sections of regular oscillations appear at some positions in space for a short period of time. This is topic in section 6.1. In section 6.2 we work on the suppression of chaotic oscillations through noise on one of the pde parameters. This is a reproduction of some results of Petrovskii et al. [2010].

Finally in chapter 7 we give an outlook for further work on this topic.

2 Definition of Model and Domains

2.1 Parameters initial conditions, stationary states and system behaviour

At first we consider the stationary states of the system of partial differential equations given by equations 1.3 and 1.4 without the diffusion term. Further we are interested in the stability of these states. This work helps us later to find a sensible parameter space of H , m and k for the simulations. The system is called stationary or steady if all temporal derivatives are equal zero [Tabor, 1989]. Two steady states are obvious (trivial): $(u = 0, v = 0)$ and $(u = 1, v = 0)$. Additionally, one non-trivial stationary state (u^*, v^*) exists.

$$u^* = \frac{pH}{1-p}, \quad v^* = (1-u^*)(H+u^*), \quad \text{with } p = m/k \quad (2.1)$$

If we perform a linear stability analysis [Tabor, 1989], we get the following results: The state $(u = 0, v = 0)$ is always a saddle point. $(u = 1, v = 0)$ is stable if $H > (1-p)/p$ and a saddle point otherwise ($H = (1-p)/p$ we ignore here). The stability analysis of (u^*, v^*) is more complicated. If $H < (1-p)/(1+p)$ the non-trivial steady state is unstable, if $(1-p)/(1+p) < H < (1-p)/p$ it is stable and if $(1-p)/p < H$ it is a saddle point. At $H = (1-p)/(1+p)$ is a Hopf bifurcation [Hopf, 1942, Marsden and McCracken, 1976, Morawitz et al., 2002] where the stability changes from a stable focus to unstable focus with a stable limit cycle. We do not need k and m explicitly to express the stabilities of the steady states. This is quite convenient. If we want to distinguish between a stable/unstable node and a stable/unstable focus we need m or k . At this point we go not into detail. Petrovskii and Malchow [1999] and Petrovskii et al. [2004] discuss this matter deeper.

The densities u^* and v^* should be located in a biological meaningful region ($u^* \leq 0, v^* \leq 0$). Using formulas 2.1 we arrive at $0 < p < 1$ and $H < (1-p)/p$. Hence in our case $(u = 1, v = 0)$ is always a saddle point and (u^*, v^*) is stable or unstable. The most interesting and realistic system behaviour takes place if (u^*, v^*) is an unstable focus with a stable limit cycle. Therefore we chose our parameters later in a way that $H < (1-p)/(1+p)$ is fulfilled.

The initials and boundary conditions are chosen as in Petrovskii and Malchow [1999].

Initial condition:

$$u(t=0, x) = u^* \quad (2.2)$$

$$v(t=0, x) = v^* + (\epsilon(x - x_0) + \delta) \quad (2.3)$$

The system behaviour - chaotic or regular oscillations - depends on the choice of ϵ , x_0 and δ . For $\epsilon \neq 0$ the function $v(t=0, x)$ is a increasing or decreasing line (see figure 2.1). The parameters x_0 and δ could be replaced by one parameter but working with these two parameters is more descriptive: δ is the distance of $v(t=0, x)$ to v^* at the spatial position x_0 . Further, if $\delta = 0$, x_0 is the spatial position where $v(t=0, x)$ and v^* intersect.

If $v(t=0, x) = v^*$ for at least one $x \in]0, X[$ (fig. 2.1 right), chaos evolves in the system. The chaotic oscillations start at the position of intersection of $v(t=0, x)$ and v^* and spread slowly

over the whole domain. If $v(t=0, x) \neq v^*$ for all $x \in [0, X]$ and if ϵ is not too large (fig. 2.1 left) then the system behaviour stays regular. If ϵ is larger than some critical value ϵ^* , chaos emerges also in the latter case. In subsection 4.2.2 we generate regular oscillations which seem to be near the boundary to chaotic ones. For further discussion of these initial conditions and of ϵ^* and for other initial conditions see Petrovskii and Malchow [1999] and Petrovskii and Malchow [2001].

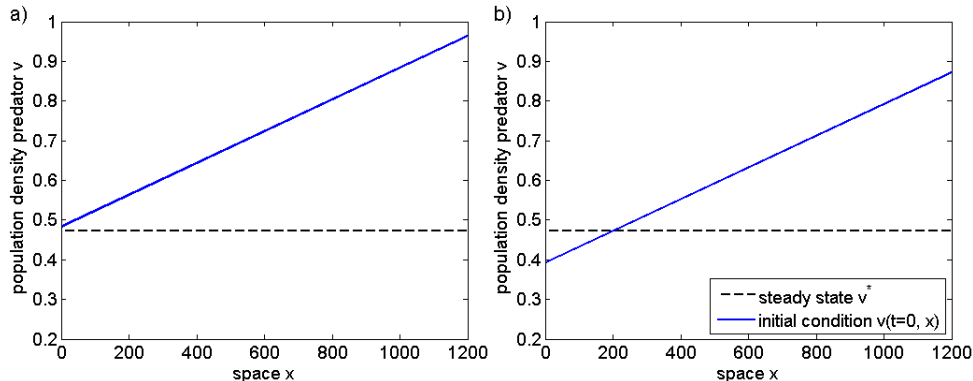


Figure 2.1: Plots of the initial conditions for different values of the parameters ϵ , x_0 and δ . Left: $v(t=0, x) > v^*$, no intersection between $v(t=0, x)$ and v^* . Right: $v(t=0, x)$ and v^* intersect in x_c .

As boundary conditions *von Neumann* boundary conditions are chosen. They are also called zero-flux boundary conditions.

Neumann boundary conditions

$$\left. \frac{du(t, x)}{dx} \right|_{x \in \{0, X\}} = 0 \quad (2.4)$$

2.2 Numerical Solution of the PDE

In the current program version the pde system (equations 1.3 and 1.4) is solved in two steps. In the following the variable for time is t and for space is x .

1. Solve the reaction term explicit forward in time with an error of first order (“euler scheme”) $O(\Delta t)$. [cf. Hairer et al., 2010]
2. Solve the diffusion term implicit forward in time and centered in space with an error of first order in time $O(\Delta t)$ and second order in space $O(\Delta x^2)$ [cf. Richtmyer and Morton, 1994].

For the solution of the reaction term a more accurate scheme could be used. This is not sensible, because the implicit solution of the diffusion term has an error of first order in time. The chosen implicit scheme leads to an tridiagonal matrix which has to be inverted. The inversion of a tridiagonal matrix can be done by the so-called Thomas Algorithm (cf. Conte and De Boor [1980] or Schwarz and Koeckler [2009]) which is not as computing time consuming as other algorithms for the inversion of more general matrices. Therefore it is sensible to use this scheme.

The simplest implementation of the zero-flux initial conditions is to set $u(0) = u(-\Delta s)$. This leads to an error of first order in space for the boundary. It is not nice, because for the remaining space the error is of second order. Therefore it is sensible to find a more accurate discretisation for the boundary conditions. Here a discretisation suggested in Brauer [2005] with an error of second order in space is used. We will derive it briefly in the paragraph after the next. The important point of this discretisation is that the matrix of the implicit scheme stays tridiagonal.

The left boundary in space is at $x = 0$ and the right is at $x = X$. The time starts at 0 and ends at T . X should be at least 1200. If X is smaller than 1200, the system behaviour changes. For more information on this see Petrovskii and Malchow [1999]. In some figures S appears instead of X . S and X are equal. Normally we solved the pde till $T = 4000$ or $T = 10000$. Spatial step Δx and time step Δt are both 0.1 if not otherwise mentioned. In section 5.3 the effects of different Δx and Δt are compared. Because an implicit scheme is used, Δx and Δt are independent of each other [Richtmyer and Morton, 1994]. The steps for the user output (Δx_{Out} and Δt_{Out}) are 1 by default but can be changed.

We discretise space and time and get a grid with P steps in spatial and Q steps in temporal direction. The spatial steps are numbered from 0 to $P - 1$. The index is called p . Whereas $p \cdot \Delta x = x$. The temporal steps are numbered accordingly and their indices are called q with $q \cdot \Delta t = t$. Further, $u(x, t)$ is equal to $u(p \cdot \Delta x, q \cdot \Delta t)$ and u_p^q . We apply a implicit discretisation schema on the diffusion equation $\partial_t u = \partial_{xx} u$ and get equation 2.5.

$$u_p^q = -c \cdot u_{p-1}^{q+1} + (1 + 2 \cdot c) u_p^{q+1} - c \cdot u_{p+1}^{q+1} + o(\Delta x^2) + o(\Delta t) \quad (2.5)$$

with $c = D \frac{\Delta t}{\Delta x^2}$

At the boundaries we get the following discretisations.

$$u_0^q = -c \cdot u_{-1}^{q+1} + (1 + 2 \cdot c) u_0^{q+1} - c \cdot u_{p+1}^1 + o(\Delta x^2) + o(\Delta t) \quad (2.6)$$

$$u_{P-1}^q = -c \cdot u_{P-2}^{q+1} + (1 + 2 \cdot c) u_{P-1}^{q+1} - c \cdot u_P^{q+1} + o(\Delta x^2) + o(\Delta t) \quad (2.7)$$

u_{-1}^{q+1} and u_P^{q+1} are not explicit given and have to be replaced by other expressions. We will do this exemplary for u_{-1}^{q+1} . The replacement of u_P^{q+1} works analogically. For deriving an expression for u_{-1}^{q+1} we need the boundary condition of equation 2.4. To simplify the reading we leave out the index for the time step if it is not necessary.

$$\left. \frac{\partial u(x, t)}{\partial x} \right|_{x=0} = \partial_x u(x=0, t) = 0 \quad (2.8)$$

$$\Rightarrow \partial_x u_0 = 0 \text{ and } \partial_x u_{-1} = 0 \quad (2.9)$$

If we express $\partial_x u_0$ by a first order Taylor expansion and transform the resulting equation, we get an expression for $\partial_x u_0$.

$$\partial_x u_0 = \frac{u_0 - u_{-1}}{\Delta x} + o(\Delta x) \quad (2.10)$$

Using the boundary condition of formula 2.9 on the Taylor expansion 2.10 leads to equation 2.11.

$$u_0 = u_{-1} + o(\Delta x) \quad (2.11)$$

Inserting 2.11 into equation 2.6 we get equation 2.12.

$$u_0^q = (1 + c) u_0^{q+1} - c \cdot u_{p+1}^1 + o(\Delta x) + o(\Delta t) \quad (2.12)$$

Equation 2.12 has an error of first order in space. Whereas the spatial error in equations 2.5 and 2.6 is of second order. Our aim is to improve the order from first order to second order. Therefore we express u_0 and u_1 by Taylor Series. u_0 is expanded towards u_{-1} with as step size of Δx and u_1 is expanded towards u_{-1} with double step size ($2 \cdot \Delta x$).

$$u_0 = u_{-1} + \Delta x \cdot \partial_x u_{-1} + \frac{1}{2} \Delta x^2 \partial_{xx} u_{-1} + o(\Delta x^3) \quad (2.13)$$

$$u_1 = u_{-1} + 2\Delta x \cdot \partial_x u_{-1} + \frac{1}{2} (2\Delta x)^2 \partial_{xx} u_{-1} + o(\Delta x^3) \quad (2.14)$$

If we subtract four times equation 2.13 from equation 2.14, we get equation 2.16.

$$u_1 - 4u_0 = -3u_{-1} - 2\Delta x \cdot \partial_x u_{-1} + o(\Delta x^3) \quad (2.15)$$

$$\Leftrightarrow \partial_x u_{-1} = \frac{-3u_{-1} + 4u_0 - u_1}{2\Delta x} + o(\Delta x^3) \quad (2.16)$$

With formula 2.9 in equation 2.16 and a bit transforming we arrive at equation 2.17. Inserting this into the discretisation at $x = p = 0$ (equation 2.6) leads equation 2.18. The last expression has a second order error in space as we wished. We use this one for our computations.

$$u_{-1} = \frac{4}{3} u_0 - \frac{1}{3} u_1 + o(\Delta x^2) \quad (2.17)$$

$$u_0^q = \left(1 + \frac{2}{3}c\right) u_0^{q+1} - \frac{2}{3}c \cdot u_{p+1}^1 + o(\Delta x^2) + o(\Delta t) \quad (2.18)$$

2.3 Choice of Parameters and Initial Conditions

In Petrovskii and Malchow [1999] two different sets of parameters are applied to the pde system. Set A from them is adopted here. For this set the non-trivial stationary state is unstable but it has a stable limit cycle. Set D is adopted from Petrovskii et al. [2010]. The parameter sets C and E are not adopted. Sets C, D and E lead to the same stability for the non-trivial stationary state as set A but the size and shape of the limit cycle differ. The second set is named C and not B to avoid confusion with Petrovskii and Malchow [1999]. The parameters sets A and C are used generally in the whole work while D is used exclusively in section 6.2 and E only in section 4.3.

$$\text{A: } k = 2.0, \quad m = 0.6, \quad H = 0.4$$

$$\text{C: } k = 1.9, \quad m = 0.8, \quad H = 0.4$$

$$\text{D: } k = 2.0, \quad m = 0.7, \quad H = 0.3$$

$$\text{E: } k = 1.9, \quad m = 0.75, \quad H = 0.4$$

The parameters of the initial conditions of v are also chosen analogical to Petrovskii and Malchow [1999] and Petrovskii et al. [2010]. Here we assign small letters to them. The sets a and b are from the first and d from the second source.

- a (regular system behaviour): $\epsilon = 0.0004$, $x_0 = 0$, $\delta = 0.01$
- b (chaotic system behaviour): $\epsilon = 0.0004$, $x_0 = 200$, $\delta = 0$
- d (chaotic system behaviour): $\epsilon = 0.0004$, $x_0 = 600$, $\delta = 0$

If below the *regular case* is mentioned it denotes a system with regular behaviour. Accordingly, the *chaotic case* means one with chaotic behaviour. Figure 2.2 shows some plots which illustrate the system behaviour. The plots on the left hand side show regular system behaviour. Bottom left a u-v-phase plane with limit cycles of the prey density for two different sets of pde parameters (blue = set A, red = set C) is plotted. The plot top left shows the spatio temporal oscillations of the prey and predator population densities. Contrary, on the right-hand side one can see chaotic oscillations in the u-v-phase plane (bottom right) and the spatial distribution of the populations (top right). For the plots at the top the time $t = 2000$ is chosen and for the plots at the bottom the spatial position $x = 600$.

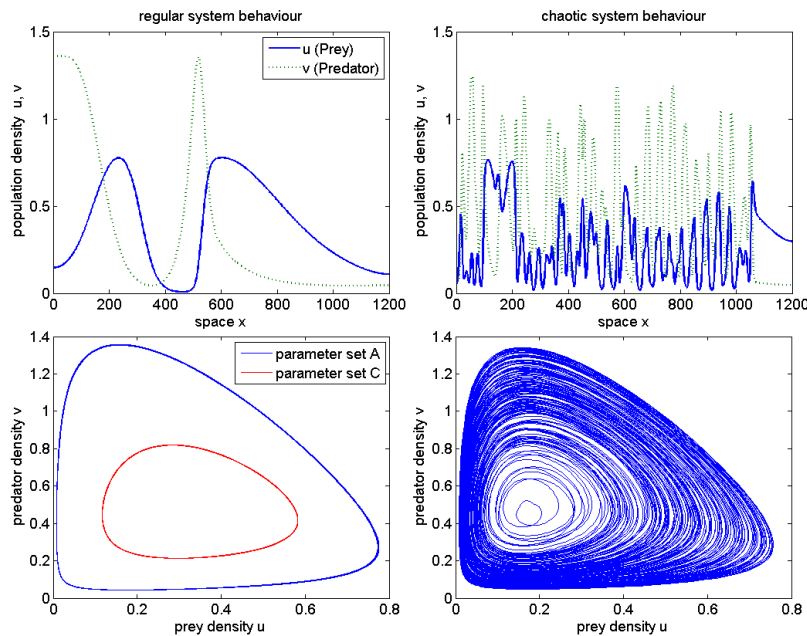


Figure 2.2: Plots of solutions of equations 1.3 and 1.4. The plots on the left hand side show regular (initial conditions a) and on the right-hand side chaotic behaviour (initial conditions b). The plot bottom left shows solutions of the pde system for parameter sets A and C. For all other plotted solutions only the parameter set A is used. The plots at the top show the population densities of prey and predator depending on the space x at the time $t = 2000$. On the left hand side one can see nice regular oscillations with a constant amplitude. On the right hand side the oscillation is chaotic and the amplitudes vary strongly. Nevertheless they stay within a certain interval. The plots at the bottom show the u-v-phase plane for the temporal interval $[3000, 5000]$ and at the spatial position $x = 600$. On the left hand side one can clearly see a limit cycle whereas on the right hand side irregular oscillation is present.

2.4 Definition of the Domains

In this section we introduce the two domains and define parameters which describe these domains completely. Table 2.2 at the end of this chapter contains all parameters with a short description

as overview.

At first we choose two intervals of the length L_1 and L_2 and place them neighbouring to each other somewhere in the space. The space is defined by the interval $[0, X]$. The two intervals are our domains and we call them A_1 and A_2 . Precisely we have up to four intervals: “left of A_1 ”, A_1 , A_2 and “right of A_2 ”. The first and the latter interval exist sometimes and sometimes not. We ignore them. The sum of L_1 and L_2 we call L . Figure 2.3a illustrates this.

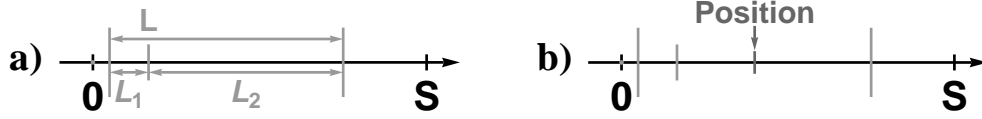


Figure 2.3: Domains A_1 and A_2 in space. **a)** Length of domain A_1 is L_1 and length of domain A_2 is L_2 . L is the sum of L_1 and L_2 . **b)** Position of A_1 and A_2 . The center of $A_1 \cup A_2$ is the point which is positioned.

It seemed sensible to me to choose the cumulated size of both domains L in relation to the size of the whole space X . Thus we define a parameter $L_{fraction}$. In the figures 2.3a, 2.3b and 2.4 the value of $L_{fraction}$ is 0.7.

$$L_{fraction} = \frac{L}{X}$$

$$L_{fraction} \in]0, 1[$$

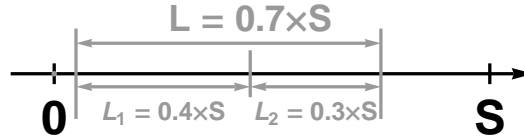


Figure 2.4: $L_{fraction} = \frac{L}{X} = 0.7$ and $L_{ratio} = \frac{L_1}{L_2} = \frac{4}{3} = 1.\bar{3}$

Further we have to define the position of the domains in the space. The center of $A_1 \cup A_2$ is the point we place somewhere (see fig 2.3b). The parameter which contains this information we call $L_{position}$. It seemed sensible to me to use a position relative to size of the space S . Therefore $L_{position}$ is defined as follows.

- $L_{position} = 0$: the center of the domains is in the center of the space ($x_{Position} = 0.5 \cdot X$);
- $L_{position} = 0.5$: the center of the domains is on the left boundary of the space ($x_{Position} = 0$). Half of L is outside the space. Therefore this position is not sensible to use.
- $L_{position} = -0.5$: the center of the domains is on the right boundary of the space ($x_{Position} = X$). Half of L is outside the space. Therefore this position is not sensible to use.
- $L_{position} \in [-(0.5 - L_{fraction}/2), 0.5 - L_{fraction}/2]$

For illustration and examples see figure 2.5.

The size of L_1 and L_2 is defined by their ratio L_{ratio} and their cumulated size L as follows.

$$\frac{L_1}{L_2} = L_{ratio}$$

$$L_1 = \frac{L_{ratio}}{1 + L_{ratio}} L = \frac{L_{ratio} \cdot L_{fraction}}{1 + L_{ratio}} X \quad (2.19)$$

$$L_2 = \frac{1}{1 + L_{ratio}} L = \frac{L_{fraction}}{1 + L_{ratio}} X \quad (2.20)$$

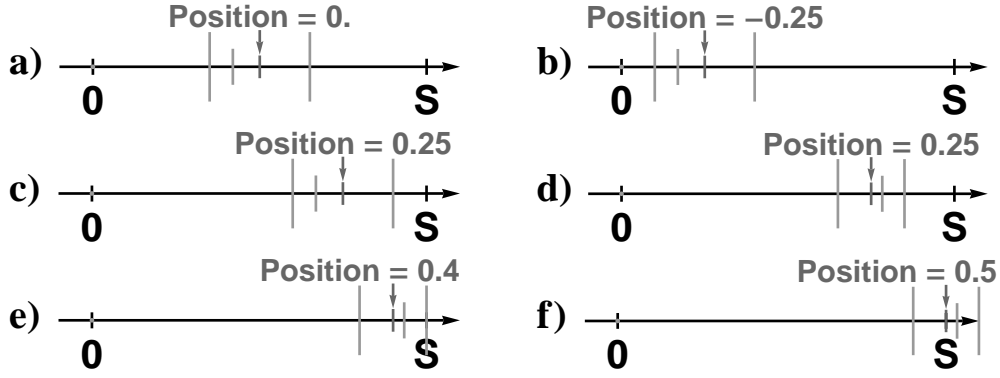


Figure 2.5: Shown are different positions of the domains with given $L_{position}$. Figure f) is for demonstration of $L_{position} = 0.5$ only. The domains can not be defined this way in the simulation because A_2 is not in $[0, X]$.

In figure 2.4 L_{ratio} is $4/3$. We assume, that L_1 and L_2 are interchangeable. Thus L_{ratio} needs only to be *1 and greater 1* or *1 and smaller 1* but not both. Arbitrary we choose the ratio to be greater or equal 1. The assumption is shortly discussed in section 3.1 (see near table 3.2).

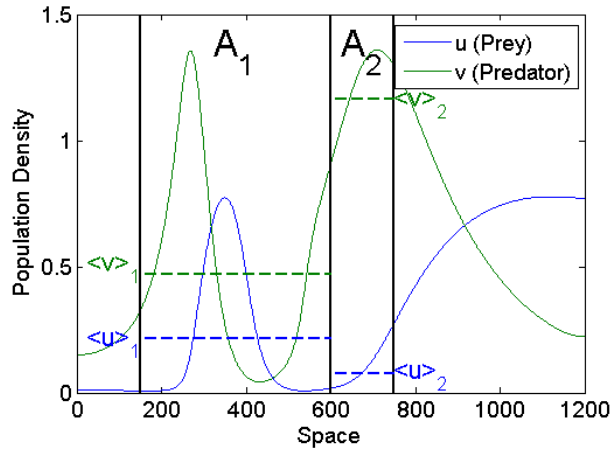


Figure 2.6: The prey (u , blue line) and predator (v , green line) densities are plotted against the space s for a given time t . The chosen set of pde parameters, initial conditions and t are not of interest. The boundaries of the two domains A_1 and A_2 are marked by vertical lines. The average densities $\langle u \rangle_1$, $\langle u \rangle_2$, $\langle v \rangle_1$ and $\langle v \rangle_2$ are represented by horizontal coloured and dashed lines.

For both domains and at each time step the average densities of u (Prey) and v (Predator) are computed - call them $\langle u \rangle_1$, $\langle u \rangle_2$, $\langle v \rangle_1$ and $\langle v \rangle_2$ (see fig 2.6). After each simulation $\langle u \rangle_1$ and $\langle u \rangle_2$ and respectively $\langle v \rangle_1$ and $\langle v \rangle_2$ are compared. For example correlation coefficients are computed or a phase plan of $\langle u \rangle_1$ and $\langle u \rangle_2$ is visualised. More to the comparison in the next section.

2.5 Comparison of the Average Densities

Figure 2.7 shows four plots with $\langle u \rangle_1$ and $\langle u \rangle_2$. The nearer the points are to an arbitrary line (e.g. the black line) the higher is the linear correlation between $\langle u \rangle_1$ and $\langle u \rangle_2$. Therefore the linear correlation in the plot bottom right is considerably higher than in the bottom left and top right one. For comparison the correlation coefficients are shown in table 2.1. The plot bottom

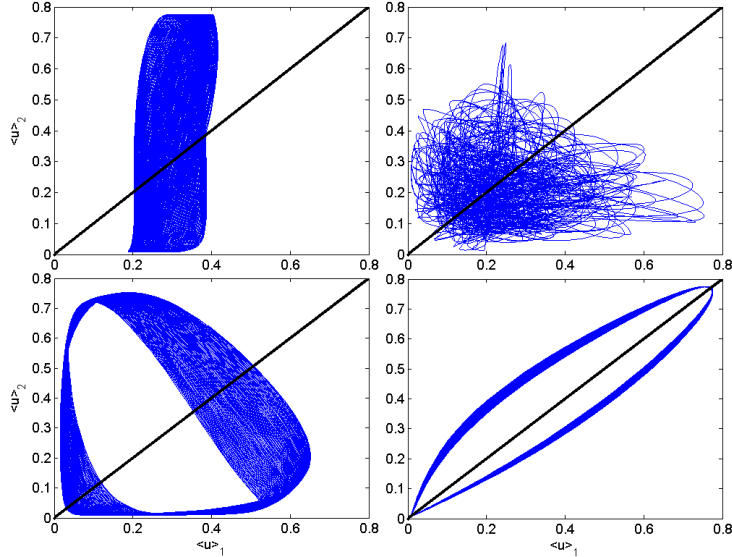


Figure 2.7: Four example plots: The plot top right shows $\langle u \rangle_1$ - $\langle u \rangle_2$ -phase plane for the chaotic regime and the other plots for the regular one. The thick black line in each plot is a line through the origin with a gradient of 1. The plot bottom right has a strong linear correlation and thus the correlation coefficient in table 2.1 is near 1. The correlation coefficient of the plot bottom left is small because of a low linear correlation. Compared to the plot of the chaotic regime top right the plot bottom left has at least some kind of correlation. Top right looks like random data. The plot top left shows a medium linear correlation. One can imagine a nearly vertical line near which the data is gathered. Therefore the correlation coefficient of this plot has a medium size.

$\langle u \rangle_c$	left	right
top	0.4372	-0,0030
bottom	0.1103	0.9255

Table 2.1: Correlation coefficients $\langle u \rangle_c$ corresponding to the plots in figure 2.7

left shows no linear correlation but the points are not distributed randomly as in the plot top right. The plot top left is similar to the one below. Thus, there are three cases: $\langle u \rangle_1$ and $\langle u \rangle_2$ are linear correlated (bottom right and partly top left), they are not linear but in another way correlated (bottom left and partly top left), they are not correlated (top right).

To be able to compare a larger number of different time series of $\langle u \rangle_1$ and $\langle u \rangle_2$ the Pearson's correlation coefficient of $\langle u \rangle_1$ and $\langle u \rangle_2$ is used. It measures the size of the linear correlation between $\langle u \rangle_1$ and $\langle u \rangle_2$. We call it $\langle u \rangle_c$. With the following equation the coefficient is computed:

$$\langle u \rangle_c = \frac{\sum_{i=1}^n \left((\langle u \rangle_{1,i} - \overline{\langle u \rangle_1}) (\langle u \rangle_{2,i} - \overline{\langle u \rangle_2}) \right)}{\sqrt{\sum_{i=1}^n \left((\langle u \rangle_{1,i} - \overline{\langle u \rangle_1})^2 \right)} \sqrt{\sum_{i=1}^n \left((\langle u \rangle_{2,i} - \overline{\langle u \rangle_2})^2 \right)}} \quad (2.21)$$

$\langle u \rangle_{1,i}$ and $\langle u \rangle_{2,i}$ are elements of the two discrete time series of average densities $\langle u \rangle_1$ and $\langle u \rangle_2$ with $i \in \{1, 2, \dots, n\}$ giving the number of the element. $i = 1$ correspondents to time $t = 0$ and $i = n$ to the final time T . $\overline{\langle u \rangle_1}$ is the average value of the time series of $\langle u \rangle_1$ and respectively $\overline{\langle u \rangle_2}$ for the other time series. The correlation coefficients for the density v are computed analogically.

If the correlation coefficient is near 1 or -1 then the data is linear correlated. This means that the plotted data nearly has the shape of a line. If the correlation coefficient is near 0 then the data is not linear correlated. In this case either the data points are distributed randomly in space or they form a nonlinear shape.

The Pearson's correlation coefficient is no ideal measure of the correlation as a view on figure 2.7 clarifies: The correlation coefficients of the data shown top right and bottom left are similar. But for the plot bottom left a nonlinear correlation is obvious whilst in the first one no correlation is apparent. This coefficient is simple to compute and compare and therefore it is sensible to use it as one but not the only one measure.

Table 2.2 shows which domain parameters are varied and discussed in chapter 3. Further the expected observations are listed.

parameter (where discussed)	meaning of parameters	expectation
$L_{fraction}$ (Chp 3.1)	size of $L_1 + L_2$ in relation to S	If $L_{fraction}$ decreases the linear correlation increases and therefore the absolute value of $\langle u \rangle_c$ increases. If $\langle u \rangle_1$ and $\langle u \rangle_2$ are plotted for each $L_{fraction}$ a correlation (but not linear) is apparent.
L_{Ratio} (Chp 3.1)	Relation between L_1 and L_2 ; $\left(= \frac{L_1}{L_2} \right)$	If L_{Ratio} is near 1, no influence is expected. If L_{Ratio} increases or decreases with respect to 1, the linear correlation should decrease.
$L_{Position}$ (Chp 3.2)	Location of the center of both domains in space	No influence of $L_{Position}$ should be observed as far as temporal interval for comparing the average densities is sufficient large. If the correlation is influenced: - prove whether it is caused by then initial conditions OR - prove whether it depends on the choice of the temporal interval in which the average densities are compared
L_{Zero} (-)	Distance between A_1 and A_2	Not discussed here. L_{Zero} is set to 0.
size and location of temporal interval for comparing the average densities and computing correlation coefficients. (Chap 3.2)		If the interval is sufficient large, then the location should have no influence. Open question: How large is sufficient large?

Table 2.2: Domain parameters which are varied and the expected observations.

3 Correlation of average Densities

If not mentioned otherwise, the simulations discussed below are performed with the parameter set A of pde parameters, the initial conditions a and $D_u/D_v = 1$ and the domain parameters are set to $L_{Ratio} = L_1/L_2 = 1$ and $L_{position} = 0$ (center).

3.1 Size of the Domains

One can expect, that the linear correlation between $\langle u \rangle_1$ and $\langle u \rangle_2$ increases when L decreases. This will be discussed at first. In figure 3.1 three plots with $\langle u \rangle_1$ on the x- and $\langle u \rangle_2$ on the y-axes for different sizes of L are shown.

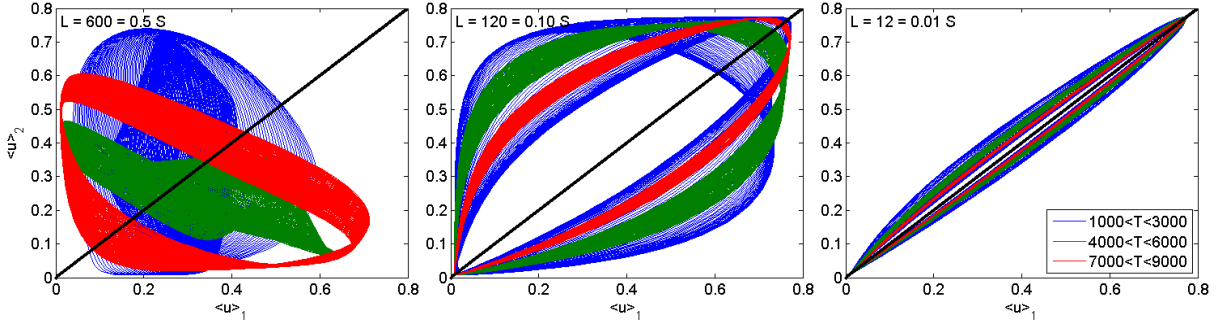


Figure 3.1: Plots of the $\langle u \rangle_1$ - $\langle u \rangle_2$ -phase plane for different values of L . Size of L decreasing from $L = 0.5S$ (left) and $L = 0.1S$ (center) to $L = 0.01S$ (right). In each plot a correlation between $\langle u \rangle_1$ and $\langle u \rangle_2$ is observable but with decreasing L the linear correlation increases.

L	$\langle u \rangle_c (L_{Position})$							$\overline{\langle u \rangle_c}$	$Var(\langle u \rangle_c)$
	-0.3	-0.2	-0.1	0	0.1	0.2	0.3		
1200				-0.2335				-0.2335	
900			0.0193	-0.2037	-0.3727			-0.1857	0.0387
600		-0.2826	-0.4302	-0.4302	-0.2769	-0.0442		-0.2928	0.0250
300	0.3076	0.1818	0.1013	0.0865	0.1692	0.3654	0.6020	0.2591	0.0333
120	0.8078	0.7763	0.7554	0.7467	0.7567	0.7997	0.8891	0.7902	0.0024
60	0.9445	0.9353	0.9289	0.9255	0.9267	0.9366	0.9675	0.9379	2,15E-04
12	0.9976	0.9972	0.9970	0.9968	0.9968	0.9970	0.9986	0.9973	4,26E-07
1.2	1.0000	1.0000	1.0000	1.0000	1.0000	1.0000	1.0000	1.0000	4.12E-11

Table 3.1: For eight sizes of L the value of $\langle u \rangle_c$ is computed at different positions of the domains (numbers $\{-0.3, -0.2, \dots, 0.3\}$ in the second line of the heading). For a better comparison of the correlation coefficients the mean value $\overline{\langle u \rangle_c}$ and variance $Var(\langle u \rangle_c)$ of the $\langle u \rangle_c$'s is given in two columns on the right. The gray coloured correlation coefficients are those of the plots in figure 3.1. The influence of the position on the correlation coefficients is discussed in section 3.2

Figure 3.1 shows a clear dependency between $\langle u \rangle_1$ and $\langle u \rangle_2$ similar to a limit cycle. Dependency does not mean linear correlation but any shape which does not look random like the plot top right in figure 2.7. For decreasing L the cycles converges to the black line which is a line through the origin and with a gradient of 1. Thus, the linear correlation increases. The correlation coefficients in table 3.1 show the same. The gray coloured ones in the table are those belonging to the plots in figure 3.1.

Table 3.1 shows correlation coefficients for $\langle u \rangle_1$ and $\langle u \rangle_2$. The values in the table are attained by the same pde solution as above. In this case the time series $\langle u \rangle_1$ and $\langle u \rangle_2$ are computed for different positions of A_1 and A_2 . Further the coefficients are computed for the temporal interval $[1000, 10000]$. It is sensible not to start with $t = 0$ because of the influence of the initial conditions. The influence of the initial conditions is briefly discussed in the summary to this chapter in section 3.6. For a better overview, the average value and variance of the different correlation coefficients for each domain size are computed.

The average correlation coefficients in table 3.1 increase for decreasing L with $L \leq 300$. The variances of the correlation coefficients show, that for $L = 600$ and $L = 300$ the correlation coefficients at the different positions vary more, than for smaller L . If you look at the red lines of the left plot of figure 3.1 the reason becomes clear: A slightly linear correlation (negative) is present. For high L there is no linear correlation but by coincidence a alignment of $\langle u \rangle_1$ and $\langle u \rangle_2$ can form which looks as if a linear correlation was existent. This is the case for the red line. Therefore we can expect different correlation coefficients at different positions for high L . If L is small, the variance is also small and thus the correlation coefficients are quite similar. With a look at the plot on right-hand side of figure 3.1 this can be expected. Hence we can assume reasonably that small L lead to a high linear correlation between $\langle u \rangle_1$ and $\langle u \rangle_2$ and high L to nearly random correlation coefficients.

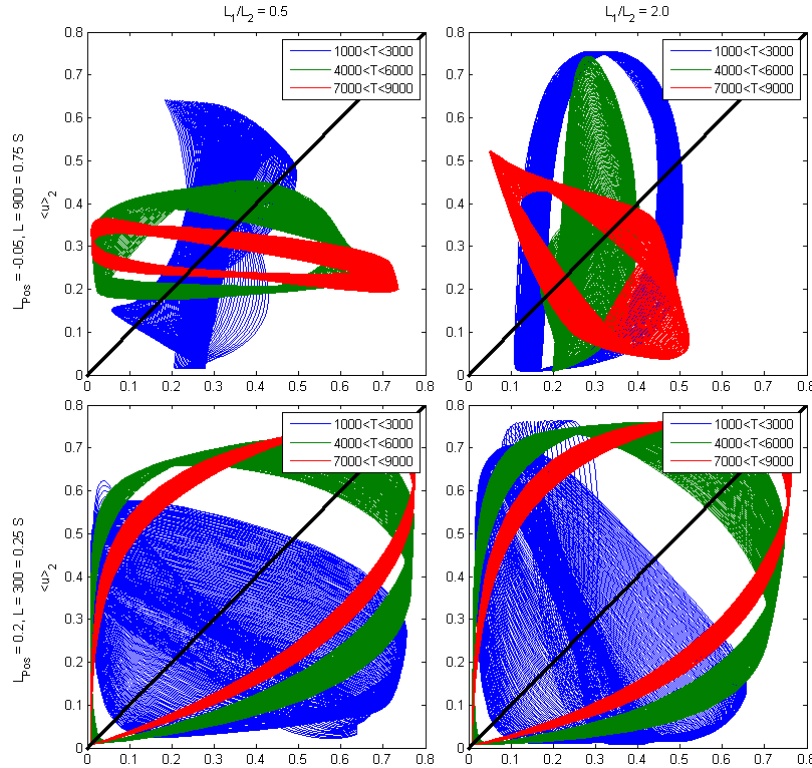


Figure 3.2: Plots of the $\langle u \rangle_1$ - $\langle u \rangle_2$ -phase plane for each two different values of L and $L_{Ratio} = L_1/L_2$. $L_{Position}$ is -0.05 in the top row and 0.2 in the bottom row. The corresponding correlation coefficients $\langle u \rangle_c$ are given in table 3.3

L_{ratio}	L	$\overline{\langle u \rangle_c}$	L_{ratio}	L	$\overline{\langle u \rangle_c}$	L_{ratio}	L	$\overline{\langle u \rangle_c}$
0.5	1,2	1.0000	0.5	120	0.7996	0.5	900	-0.0462
2		1.0000	2		0.7978	2		-0.1304
0.5	12	0.9974	0.5	300	0.3024	0.5	1200	-0.2402
2		0.9974	2		0.2835	2		-0.1119
0.5	60	0.9405	0.5	600	-0.1652			
2		0.9403	2		-0.2383			

Table 3.2: As in table 3.1 the mean value $\overline{\langle u \rangle_c}$ of the correlation coefficients of the time series at different $L_{Position}$'s for given L_{Ratio} and L are shown. The single values at the different positions are not shown.

As next different choices of L_{Ratio} are considered. In section 2.4 it was assumed that $L_{Ratio} = r$ with $r \in [1, \infty[$ and $L_{Ratio} = r^{-1}$ lead to nearly equal time series of $\langle u \rangle_i$ and correlations between them. Table 3.2 and figure 3.2 show some data to discuss this assumption. If $L \leq 300$, the $\overline{\langle u \rangle_c}$'s for $L_{Ratio} = 0.5$ and $L_{Ratio} = 2$ in table 3.2 differ only in maximal ± 0.02 . If L is larger, the deviation is much larger. Hence we conclude, that the effect of $L_{Ratio} = r$ and $L_{Ratio} = r^{-1}$ on the correlation of the average populations densities is identical for $L \leq 300$. Figure 3.2 can be interpreted in the same way. The top row shows plots for $L = 900$ and bottom for $L = 300$. The columns contain plots for $L_{Ratio} = 0.5$ (left) and $L_{Ratio} = 2$ (right). If plots within each row are compared, the similarity in the bottom row is high except for the blue trajectory. In the first row, no similarity is present. This confirms the observations made in table 3.2. Therefore it can be assumed, that L_1 and L_2 are interchangeable without problems for small and medium L ($L \leq 300$).

L	L_{Ratio}	0.5	2	1	9	99
900		-0.0501	-0.1519	-0.1519	-0.0382	0.4372
300		0.4246	0.3346	0.0865	0.1103	0.1772
60				0.9255	0.9260	0.9270

Table 3.3: Correlation coefficients $\langle u \rangle_c$ corresponding to the plots in figures 3.2 and 3.3

Now we consider the effect of different L_{Ratio} 's on the correlation of $\langle u \rangle_1$ and $\langle u \rangle_2$. Figure 3.3 shows some plots for varying L and L_{Ratio} . $L_{Position}$ is 0 for all plots. If L is small (bottom row of fig 3.3), L_{Ratio} has no noticeable influence. For medium L as shown in the center row an effect of L_{Ratio} is existent but not large. With increasing time the effect declines. Finally for large L the influence of L_{Ratio} is clear as visible in the top row of plots: The three cycles align in a similar shape and direction. This leads to a larger correlation coefficient for larger L_{Ratio} 's. The values in the first row of Table 3.3 confirm it. Consideration of time series for other values of L and $L_{Position}$ lead to the same observations. Hence it can be concluded, that L_{Ratio} has no significant influence on the correlation between $\langle u \rangle_1$ and $\langle u \rangle_2$ for small and partly medium L .

3.2 Different Locations of the Domains

If we hold all parameters and the sizes of L_1 and L_2 constant and only vary the position of L then the correlation between $\langle u \rangle_1$ and $\langle u \rangle_2$ should stay constant in an interval of natural variation. Depending on the size of L this variation deviates. A first processing of the data gained by the solved PDE showed a strange result: When moving A_1 and A_2 from left to right in space the correlation coefficients grew. Therefore we go further into detail than the first sentence lets the reader expect.

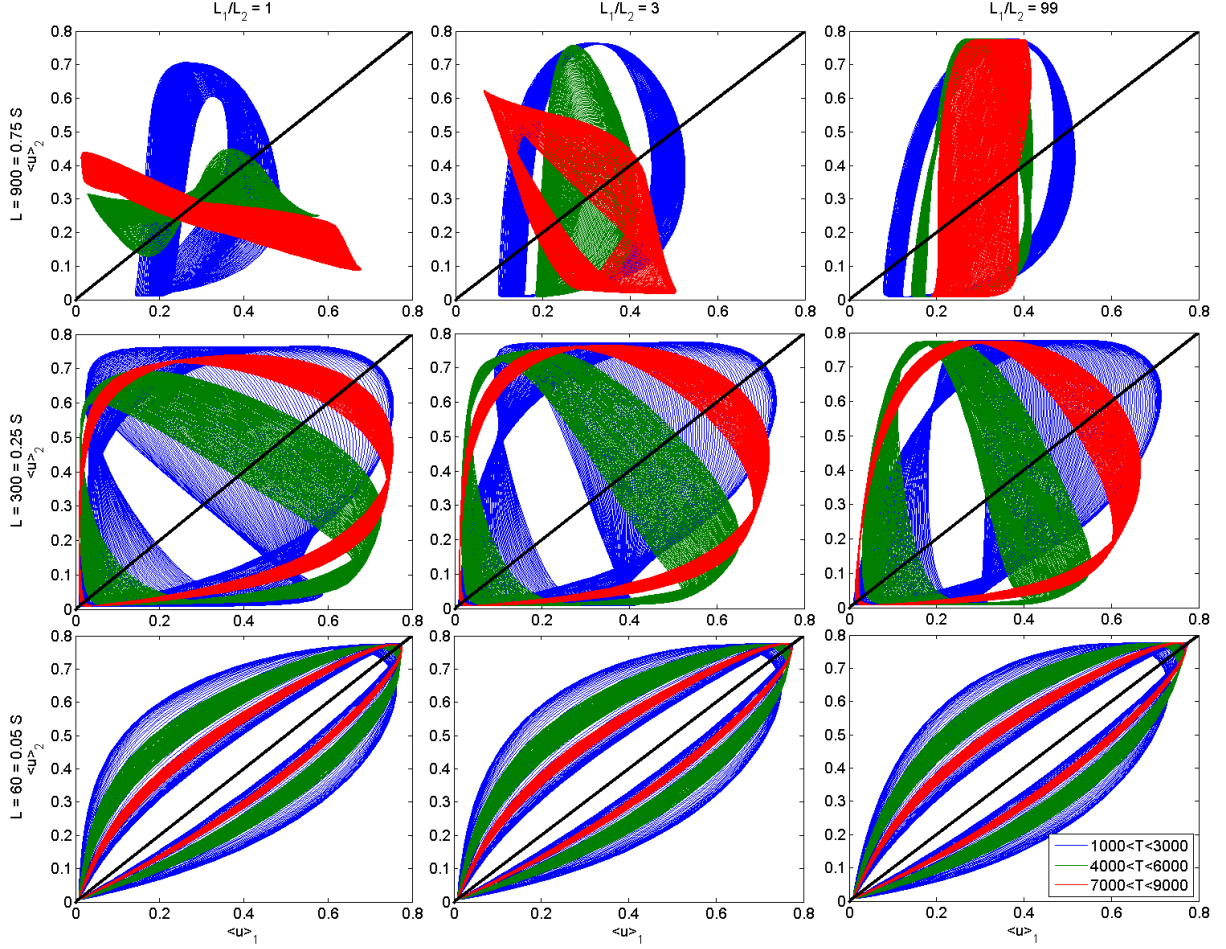


Figure 3.3: Plots of the $\langle u \rangle_1$ - $\langle u \rangle_2$ -phase plane for different values of L and $L_{Ratio} = L_1/L_2$. In each column L_{Ratio} and in each row L is constant. $L_{Position} = 0$ for all plots. The corresponding correlation coefficients $\langle u \rangle_c$ are given in table 3.3

Table 3.4 (which contains actually four tables, but the colouring is simpler done in Excel) shows correlation coefficients for two different values L , seven positions of L and two different sets of initial conditions. Normal initial conditions means set a. The term *inverted initial conditions* is explained further below when the bottom row is actually discussed. At first only the tables in the top row are discussed. In figure 3.4 the correlation coefficients $\langle u \rangle_1$ and $\langle u \rangle_2$ are plotted for the same L as in the tables but less positions.

Column “1000 < t < 3000” in both tables of the top row of table 3.4 is important to note. Depending on the position of L (e.g. -0.3 and 0.2) the correlation coefficients differ strongly. It means, that for a considerable large time interval of 2000 time units the correlation between $\langle u \rangle_1$ and $\langle u \rangle_2$ is still depending on the position of the domains or respectively on the point of view of an observer. Column “5000 < t < 9000” in the top row tables of table 3.4 and the plots of figure 3.4 show the same. The blue lines show the different correlations most clearest: Strong linear correlation in the plots on the left hand side (partly covered by the green lines) and a shape similar to a rectangle with a low linear correlation one the right. This observation is valid for different L . Again smaller L leads to a larger linear correlation.

In the bottom row of table 3.4 data of simulations with the same parameters as in the top row is shown but the initial conditions are inverted. Inverted initial conditions in this case means, that the initial densities from the right side of the space are now on the left and the other way around. Or mathematically spoken: $v_0^{inv}(0) = v_0(X)$ and general $v_0^{inv}(x) = v_0(X - x)$,

"normal" initial conditions			Correl. Coefficient of $\langle u \rangle_1$ and $\langle u \rangle_2$			
L_1/L_2	L	Position	$1,000 < t < 10,000$	$1,000 < t < 5,000$	$1,000 < t < 3,000$	$5,000 < t < 9,000$
1	120	-0,3	0,827	0,979	0,981	0,685
1	120	-0,2	0,791	0,932	0,975	0,638
1	120	-0,1	0,764	0,792	0,965	0,715
1	120	0	0,749	0,671	0,859	0,789
1	120	0,1	0,748	0,588	0,566	0,854
1	120	0,2	0,773	0,576	0,383	0,910
1	120	0,3	0,846	0,699	0,517	0,953

"normal" initial conditions			Correl. Coefficient of $\langle u \rangle_1$ and $\langle u \rangle_2$			
L_1/L_2	L	Position	$1,000 < t < 10,000$	$1,000 < t < 5,000$	$1,000 < t < 3,000$	$5,000 < t < 9,000$
1	60	-0,3	0,950	0,995	0,995	0,909
1	60	-0,2	0,940	0,981	0,994	0,896
1	60	-0,1	0,932	0,936	0,991	0,921
1	60	0	0,927	0,899	0,958	0,943
1	60	0,1	0,925	0,874	0,861	0,961
1	60	0,2	0,930	0,868	0,803	0,977
1	60	0,3	0,954	0,910	0,854	0,988

inverted initial conditions			Correl. Coefficient of $\langle u \rangle_1$ and $\langle u \rangle_2$			
L_1/L_2	L	Position	$1,000 < t < 10,000$	$1,000 < t < 5,000$	$1,000 < t < 3,000$	$5,000 < t < 9,000$
1	120	-0,3	0,889	0,780	0,640	0,969
1	120	-0,2	0,800	0,611	0,388	0,933
1	120	-0,1	0,756	0,570	0,450	0,883
1	120	0	0,746	0,622	0,707	0,823
1	120	0,1	0,755	0,728	0,949	0,753
1	120	0,2	0,776	0,860	0,970	0,676
1	120	0,3	0,808	0,973	0,978	0,638

inverted initial conditions			Correl. Coefficient of $\langle u \rangle_1$ and $\langle u \rangle_2$			
L_1/L_2	L	Position	$1,000 < t < 10,000$	$1,000 < t < 5,000$	$1,000 < t < 3,000$	$5,000 < t < 9,000$
1	60	-0,3	0,967	0,935	0,892	0,992
1	60	-0,2	0,937	0,875	0,798	0,983
1	60	-0,1	0,927	0,868	0,825	0,969
1	60	0	0,925	0,885	0,907	0,953
1	60	0,1	0,929	0,916	0,988	0,932
1	60	0,2	0,935	0,957	0,993	0,909
1	60	0,3	0,944	0,994	0,995	0,896

Table 3.4: Four tables each with correlation coefficients (coloured columns in the tables) computed at different positions in space and over different temporal intervals. The temporal intervals are $[1000, 10000]$, $[1000, 5000]$, $[1000, 3000]$ and $[5000, 9000]$. For each table different initial conditions for solving the pde and different domain sizes L are chosen: tables left hand side: $L = 120 = 0.1S$; right: $L = 60 = 0.05S$; tables at the top: normal initial conditions; bottom: inverted initial conditions. $L_{Ratio} = 1$ for all tables.

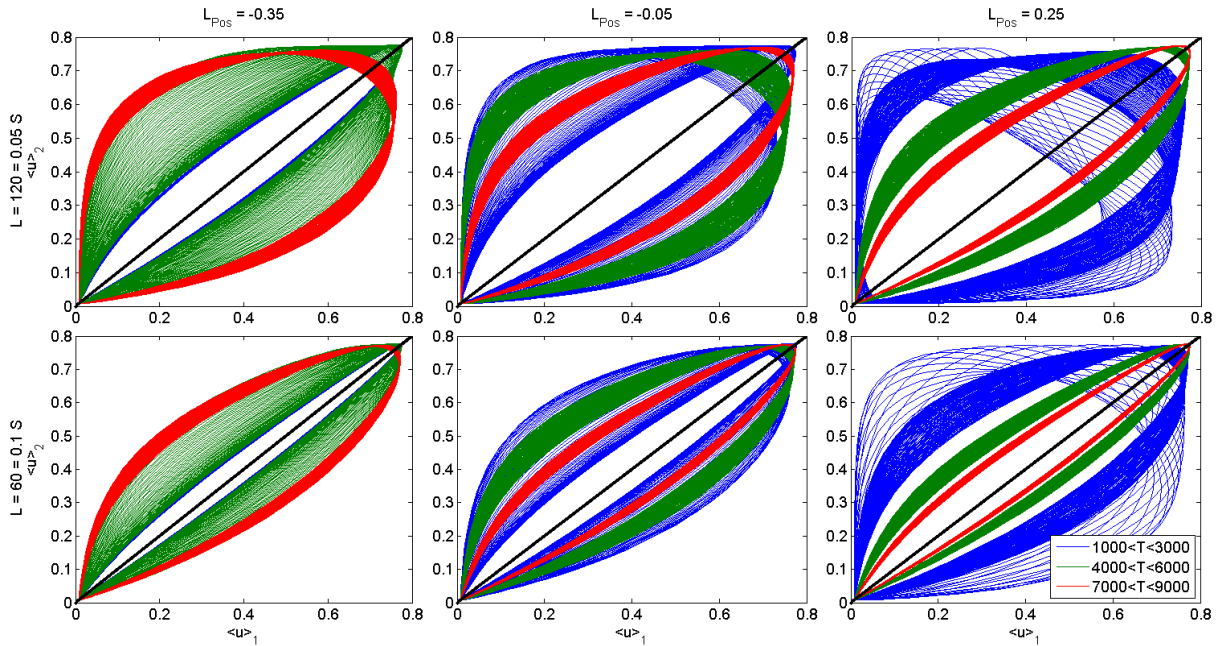


Figure 3.4: Plots of the $\langle u \rangle_1$ - $\langle u \rangle_2$ -phase plane for different values of $L_{Position}$ and L . In each row L and in each column $L_{Position}$ is constant. $L_{Ratio} = 1$ for all plots. The corresponding correlation coefficients $\langle u \rangle_c$ are given in table 3.5

L	$L_{Position}$	-0,35	-0,05	0,25
120		0,8273	0,7493	0,8464
60		0,9502	0,9268	0,9542

Table 3.5: Correlation coefficients $\langle u \rangle_c$ corresponding to the plots in figure 3.4.

whereas $v_0(x)$ are the initial conditions of v at location x under normal initial conditions and $v_0^{inv}(x)$ under inverted initial one. As can be seen clearly, the correlation coefficients are mirror inverted with respect to the positions of the domains. Therefore the spatial variation of the correlation coefficients depends on the initial conditions.

All in all it has been shown, that the correlation coefficients of $\langle u \rangle_1$ and $\langle u \rangle_2$ should be computed for a reasonable large temporal interval of at least 5000 time units. Furthermore the position dependency of the correlation coefficient is caused by the initial conditions and is not a system inherent property. Moreover it is shown, that the initial conditions effect the correlation of the average densities still after several thousand time units.

3.3 Comparison of average Predator- and Prey Densities

Till now only the population density u was considered and v was ignored. If analysis of $(\langle u \rangle_1, \langle u \rangle_2)$ and $(\langle v \rangle_1, \langle v \rangle_2)$ lead to the same results then the analysis of one is enough. Table 3.6 shows some correlation coefficients in comparison.

L_{ratio}	$L_{Position}$	$\langle u \rangle_c$	$\langle v \rangle_c$	L
1	0.00	-0.2335	-0.2280	1200
1	-0.05	-0.0831	-0.0968	900
1	0.10	-0.2769	-0.2852	600
3	-0.15	-0.1226	-0.1238	600
1	0.10	0.1692	0.1315	300
1	-0.25	0.7907	0.7492	120
1	0.00	0.7467	0.6990	120
3	-0.30	0.9452	0.9282	60
1	0.10	0.9968	0.9956	12

Table 3.6: Comparison of $\langle u \rangle_c$ and $\langle v \rangle_c$ for parameter set A and initials conditions a . In each row $|\langle u \rangle_c - \langle v \rangle_c| \leq 0.05$.

As it is clear to see in table 3.6, $\langle u \rangle_c$ and $\langle v \rangle_c$ differ in less than ± 0.05 from each other. The plots in figure 3.5 show the $\langle u \rangle_1$ - $\langle u \rangle_2$ - and $\langle v \rangle_1$ - $\langle v \rangle_2$ -phase planes for three different values of L . The trajectories of $\langle u \rangle$ and $\langle v \rangle$ are the same except of a scaling factor. Hence the correlation for u is equal to the one of v . Therefore it is reasonable to consider only u or v .

3.4 Parameter Set C

The results for parameter set C are only shortly discussed, because qualitatively they do not differ from those for parameter set A. Have a look on table 3.7. If L increases (tables from left to right) the correlation coefficient $\langle u \rangle_c$ for set C decreases. For large L (right table) the variability of the $\langle u \rangle_c$ at different positions is larger than for small L (left table). A change of L_{Ratio} (not shown) has the same effect as obtained for parameter set A. Therefore the use of parameter set

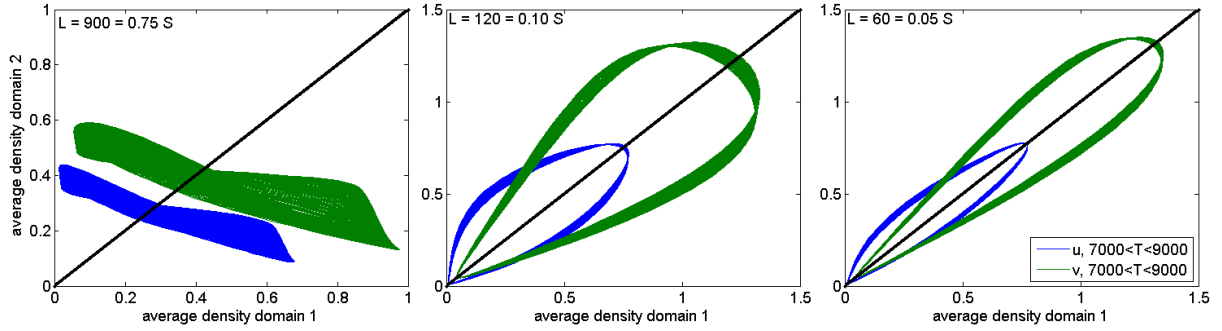


Figure 3.5: Plots of the $\langle u \rangle_1 - \langle u \rangle_2$ - respectively $\langle v \rangle_1 - \langle v \rangle_2$ -phase plane for different values of L . $L_{Ratio} = 1$ and $L_{Position} = 0$ for all plots. The shape of the blue and green trajectories in each plot is the same. It differs only in size.

C leads qualitatively to the same results as the use of set A. $\langle u \rangle_c$ for set C is larger than for set A. This means that the linear correlation of the mean densities in both domains is larger for set C. Hence the results obtained using the parameter sets A and C are quantitatively not comparable.

L	L_{Pos}	$\langle u \rangle_c$		L	L_{Pos}	$\langle u \rangle_c$		L	L_{Pos}	$\langle u \rangle_c$	
		A	C			A	C			A	C
60	-0.3	0.9445	0.9978	120	-0.3	0.8078	0.9911	600	-0.2	-0.2826	0.7306
60	-0.2	0.9353	0.9973	120	-0.2	0.7763	0.9891	600	-0.1	-0.4302	0.6515
60	-0.1	0.9289	0.9965	120	-0.1	0.7554	0.9859	600	0	-0.4302	0.5183
60	0	0.9255	0.9951	120	0	0.7467	0.9804	600	0.1	-0.2769	0.2715
60	0.1	0.9267	0.9926	120	0.1	0.7567	0.9703	600	0.2	-0.0442	-0.1950
60	0.2	0.9366	0.9869	120	0.2	0.7997	0.9478				
60	0.3	0.9675	0.9695	120	0.3	0.8891	0.8774				

Table 3.7: Correlation coefficients of simulations with the parameter sets A (column 3) and C (column 4) for different values of L (column 1) and $L_{Positions}$ (column 2)

3.5 Different Diffusion Coefficients

D_u	D_v	$\overline{\langle u \rangle_c}$		
		$\bar{L} = 12$	$\bar{L} = 60$	$\bar{L} = 120$
1	4	0.9144	0.4654	0.3770
1	1	0.9974	0.9403	0.7976
4	1	0.8999	0.3167	0.1870

Table 3.8: As in table 3.1 the mean value $\overline{\langle u \rangle_c}$ of the correlation coefficients of the time series at different $L_{Position}$'s for given D_u/D_v and L are shown. The single values at the different positions are not shown.

If both diffusion coefficients D_u and D_v are scaled with the same factor q the effect is equal to scaling the space with \sqrt{q}^{-1} . In other words: If we scale the diffusion coefficients with q and the space with \sqrt{q} nothing changes. The same should count for L : If the diffusion coefficients are increased and the absolute value of L not, L increases with respect to the velocity of spatial transport. Hence the linear correlation decreases. But what happens for changing ratio between the diffusion coefficients D_u/D_v ? One could expect, the system is scaled a bit and thus the

correlation coefficient for a special L decreases. The expectation can be confirmed by the data in table 3.8.

Table 3.8 shows: If one of the diffusion coefficients raises, the linear correlation decreases for unchanged L . Regarding the first sentences of section 3.5 the correlation coefficient of $D_u/D_v = 1/4$ or $D_u/D_v = 4$ and $L = 60$ should be equal or smaller than the one of $D_u/D_v = 1$ and $L = 120$. If the $\langle u \rangle_c$'s in table 3.8 are regarded it becomes obvious that the effect of scaling D_u with 4 is larger than scaling L with $\sqrt{4} = 2$. We will not go deeper into this but remember it for later work. Another interesting observation to note is, that $\langle u \rangle_c$ is smaller for $D_u/D_v = 4$ than for $D_u/D_v = 0.25$. Also here, we will not go further into detail.

3.6 Summary first Analysis and Outlook

Before we enlarge our model and make it more complicated, we will sum up the most important points of chapter 3. Figure 3.6 shows two 3D plots with L_{Ratio} and $L_{Position}$ on the x-axis respectively and with each the correlation coefficient $\langle u \rangle_c$ on the z- and the size of both domains L on the y-axis. The most observations in the left plot are already mentioned in section 3.1. For small L the linear correlation of the mean densities is high and $\langle u \rangle_c$ is near 1. When L increases, $\langle u \rangle_c$ decreases to 0 and further below and it reaches a minimum at about $L = 600$. The correlation coefficient is negative in the minimum. Therefore a linear correlation with negative gradient is present. But it is quite small because $\langle u \rangle_c > -0.5$ and it's value depends on $L_{Position}$ as the right plot shows. For increasing L above $L = 600$ the correlation coefficient increases again to values around 0. L_{Ratio} has nearly no influence if L is small. But for increasing L its influence growth. If L is large and L_{Ratio} is increased (starting with $L_{Ratio} = 1$), $\langle u \rangle_c$ increases at first strong and then the gradient declines. From $L_{Ratio} = 20$ to 100 only a small increase in $\langle u \rangle_c$ takes place and its value is around 0.5. This observation is new and is not mentioned above in section 3.1 or anywhere else. Why $\langle u \rangle_c$ converges to about 0.5 is not completely intuitively clear. One possible explanation is the following: If we have two large domains both influence each other in a small region around their contact point. Outside of this region the oscillations in both domains are independent of each other. Therefore the average densities are quite uncorrelated. If we have one large and one small domain, the large domain influences the other one strongly. Thus the oscillations in the small domain adapt slightly to those in the large one and the oscillations in both domains show a medium or large correlation.

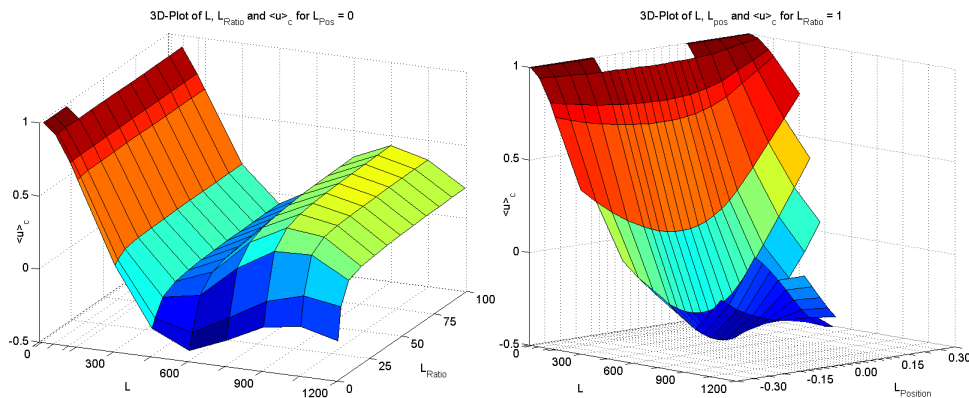


Figure 3.6: Two 3D-plots with correlation coefficient $\langle u \rangle_c$ on the z-axis, the size of both domains L on the y-axis and L_{Ratio} (left plot) and $L_{Position}$ (right plot) on the x-axis respectively.

Have a look on the right plot of figure 3.6. If L is small, $L_{Position}$ has no influence on the correlation coefficients. Contrary, if L is medium or large - not too large, because then we have

too less possible positions - $\langle u \rangle_c$ depends strongly on $L_{Position}$. This was already mentioned and discussed in section 3.2.

Furthermore, in section 3.3 we consider whether the predator and the prey density have to be regarded or whether one of the densities is sufficient. We obtained the result, that working with one density is sufficient. In section 3.4 the results obtained by two different parameter sets are compared. Changing the pde parameters leads qualitatively to the same results. Quantitatively the correlations coefficients $\langle u \rangle_c$ differ. Finally in section 3.5 the influence of the ration D_u/D_v is discussed briefly. The correlation coefficients do not change as expected. Therefore in further works the influence of the diffusion coefficients D_u and D_v should be regarded more in detail.

The correlation coefficients which are discussed in this chapter (chapter 3) are computed over the temporal intervals [1000,5000] or [1000,10000]. In section 3.1 we argue, that we start the computation at $t = 1000$ to avoid the influence of the initial conditions. However, as we see in table 3.4 of section 3.2 inverted initial conditions lead to differences in the results beyond $t = 5000$. As mentioned in section 2.3 varying the initial conditions can lead to chaotic oscillations. Later in subsection 4.2.2 a third kind of oscillations induced by another choice of the initial conditions is observed. Therefore another big topic for further works is the influence of the initial conditions on the average populations densities of two or more spatial domains, on the correlation coefficients between them and on the system behaviour in general.

The next planned step is to add noise to the model to get a more realistic system behaviour. In chapter 5 one kind of noise is introduced and discussed. This noise should have been added to our model. Unfortunately it does not lead to a more realistic system behaviour. Defining a new kind of noise, adding it to our model and analysing the results is out of the temporal scope of this work. Therefore we discuss some other interesting findings of our simulations in the chapters 4 and 6. In further works a new kind of noise should be defined and applied to our model. section 5.5 lines out another way of defining noise.

4 Variation of Parameters

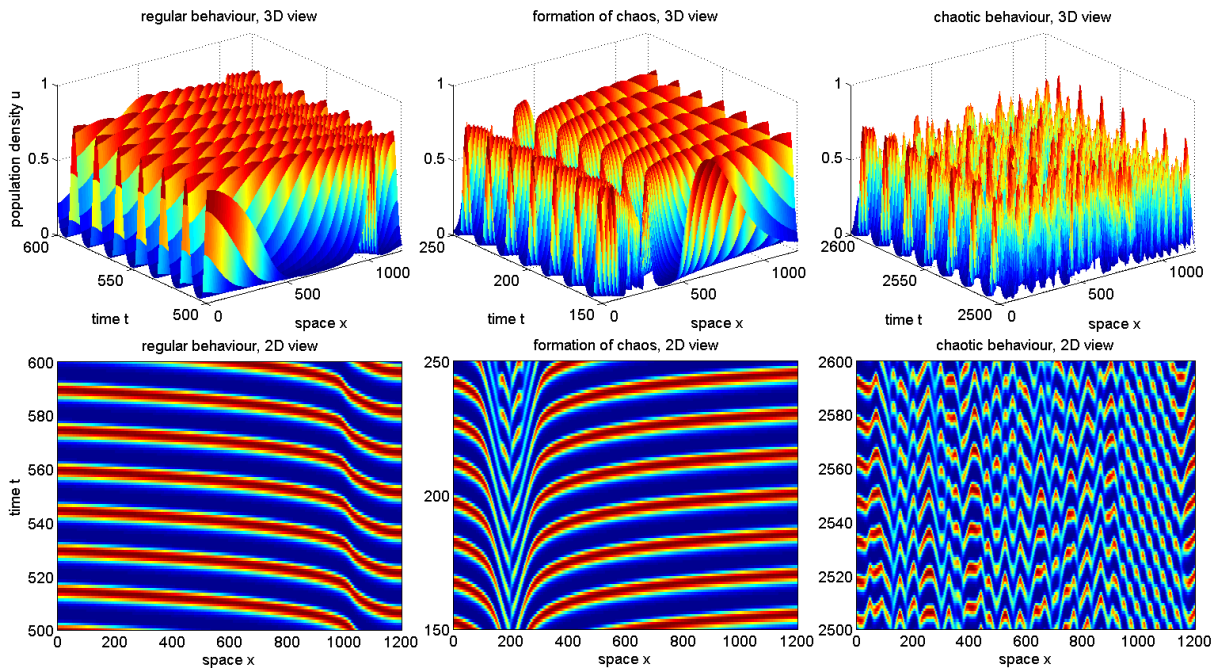


Figure 4.1: Different kinds of plots with different visualised data. **Different columns:** One the left hand side data of simulations with parameter set A and initial conditions a is plotted for the temporal interval $[500, 600]$. The system behaviour is regular. In the center and on the right hand side data of simulations with parameter set C and initial conditions b is plotted for two different temporal intervals. For the plots in the center the temporal interval is $[150, 250]$. At $x = 200$ chaotic oscillations emerge. On the right hand side the temporal interval $[2500, 2600]$ is used. In the plotted period of time, chaos prevails. **Different rows:** The top row shows 3d plots of the given data. On the x-axis the *space* x , on the y-axis the *time* t and on the z-axis the *prey's populations density* u is plotted. The color of the graph corresponds to the value on the z-axis. The bottom row shows 2d color plots of the same data as in the top row. X- and y-axes are the same as in the plots of the top row. The color at each point in the plot depends on the value of the populations density at the point. Dark blue stands for a small density and dark red for a large one. In our work the absolute value of the populations density is not regarded. Therefore we forgo to plot an extra color legend to each 2d color plot.

In this section and the following two, results of simulations with different variations of parameter sets and initial conditions are presented, discussed and compared with each other. For the visualisation of the results two different kinds of plots are used. Those are to see in figure 4.1. In the top row of this figure 3d plots are arranged and in the bottom row 2d color plots. In both kinds of plots the x-axis shows the space x and the y-axis the time t . The population density of the prey or predator (In figure 4.1 it is the prey.) is plotted at the z-axis of the 3d plot and is indicated by the color of the graph. At the 2d color plots only the color of a point in the spatio-temporal plane of the plot indicates relatively the populations density. The color dark

red stands for the largest values of the density within the plotted spatio-temporal interval and dark blue for the smallest. The absolute values of the densities do not interest us. Therefore the relative illustration of the data is sufficient and we forgo to plot a legend with the absolute values corresponding to the color.

Till now we worked with regular behaving systems only. The two plots in the left column of figure 4.1 show a section of such a system for a small spatio-temporal interval. Parameter set A and initial conditions a are used. In this and the following chapter the development of chaos and chaotic oscillations are considered. Therefore we shortly present how the *normal* onset of chaos and the chaotic oscillations look like. With *normal* we mean the chaos induced by the initial conditions b or more general those with $v(t=0, x) = v^*$ for at least one $x \in]0, X[$. As we discuss later, further mechanisms exist which lead to chaos. The plots in the center and right hand side columns of figure 4.1 show simulation results for parameter set A and initial conditions b for two different periods of time. The onset of chaos is plotted in the center column for $t \in [150, 250]$. The chaotic oscillations start at $x = 200$ and expand in both directions. The plots on the right hand side show chaotic oscillations over the whole spatial domain for $t \in [2500, 2600]$.

4.1 Chaos through parameter variation

In order to get to know the range if the system behaviour - constituted by the equations 1.3 and 1.4 - some pde parameters are varied. The set 'a' of initial conditions is kept unchanged. Results of two runs are plotted in figure 4.2. The plots in the center and the bottom row show results of the same run. The parameters $H = 0.3$, $m = \mathbf{0.6}$ and $k = 1.9$ are used. The runs to the plots in the top row were performed with the parameters $H = 0.3$, $m = \mathbf{0.8}$ and $k = 1.9$. As clearly to see in figure 4.2 some parameter sets lead to the evolution of chaos. It is not sure, whether the onset of chaos for some parameter sets is system inherent or a problem of numerical accuracy. One comment to a possible problem of numerical accuracy. Comparing the limit cycles in the u-v-phase plane (not shown here) of simulations with different parameter sets leads to the following observation: If the limit cycle (before the onset of chaos) is considerably close to the u- and v-axes the onset of chaos can be expected. Therefore it could be, that small values of u and v are rounded to 0 which possibly leads to the onset of chaos. We choose a parameter set which leads to chaos even for initial conditions a (regular oscillations expected) and perform four simulations with changed initial conditions and this set. In one of the four cases no chaos appeared till $t = 4000$. The other three initial conditions did not inhibit the onset of chaos. With this we stop speculating about explanations, let the problem unsolved and only present further observations.

The plots in figure 4.3 show the *normal* onset of chaos using parameter set A and initial conditions b on the left hand side and the onset of chaos induced by changed parameters on the right hand side. The mechanism in both cases look similar but the way till the mechanism starts working is different. As described in section 2.1 and repeated at the beginning of chapter 4 the *normal* onset of chaos is caused by the initial conditions. At the point x_0 with $v(t=0, x_0) = v^*$ the populations are spatially separated and the population density is near 0 as can be seen in the left plot of figure 4.3. The period time of the oscillations spatially close to x_0 is smaller than the period time at a larger distance. Regard the area of maximum density (dark red) as a function t_i of x . We need the index i because there is more than one maximum in temporal direction. $i = 1$ indicates the first maximum density in temporal direction for increasing t with $t \leq 0$, $i = 2$ the second one and so on. The gradient $\partial t_i / \partial x$ near x_0 increases with increasing i . Reaching some critical value it can not increase further and chaos breaks out. A similar argumentation is used in section 4.3. Another view on this is, that the movement or diffusion of the population near x_0 decreases with increasing t . At some time point the velocity is too

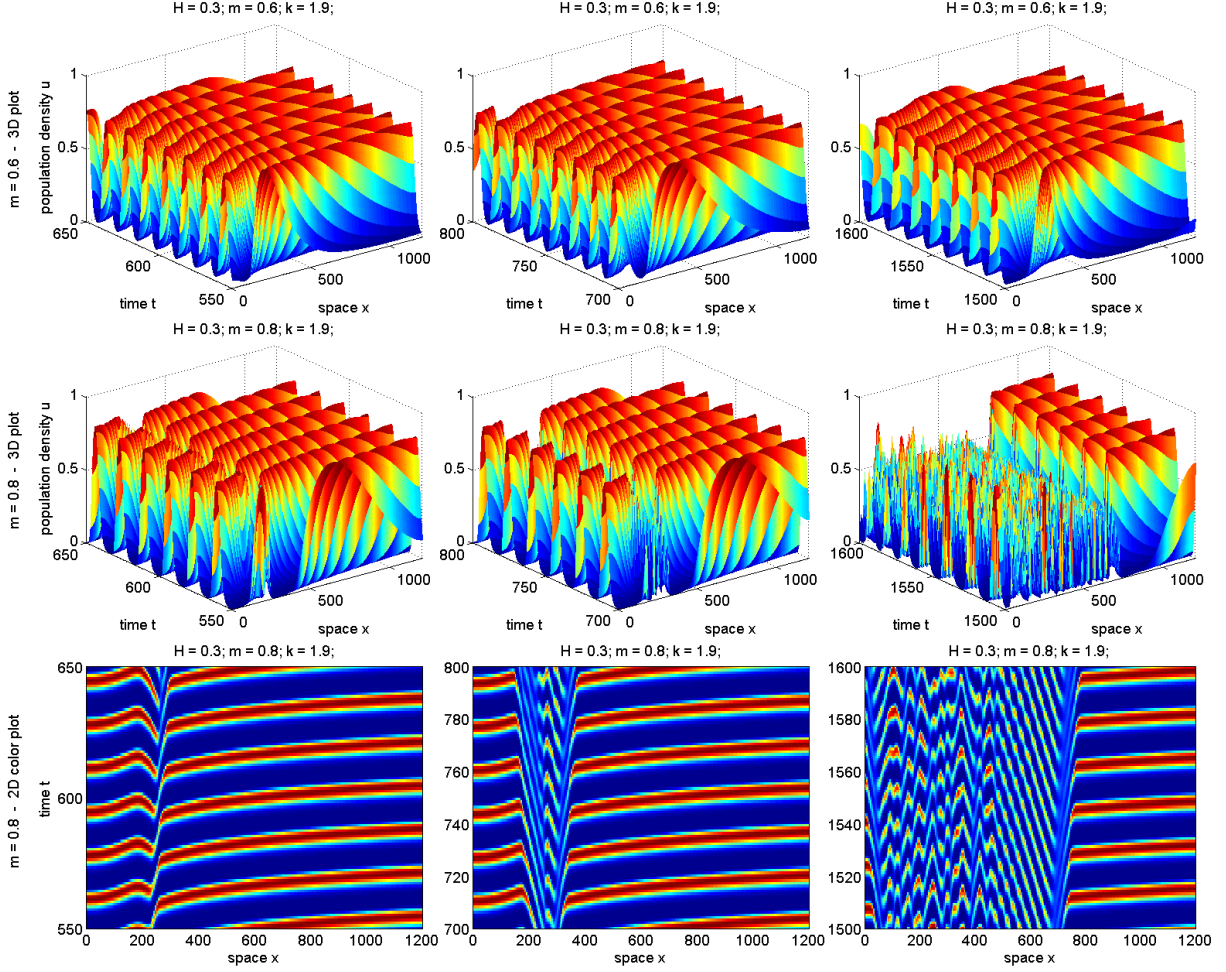


Figure 4.2: Plots to simulations with two different parameter sets. The parameters H and k in both sets are equal with $H = 0.3$ and $k = 1.9$. For the plots in the top row the parameter m is given by $m = 0.8$ and in the center and bottom rows by $m = 0.6$. The initial conditions a are used for all simulations. The center and bottom row differ in the way of visualisation (center: 3d plot, bottom: 2d color plot). The data in both rows is equal. The plots in the three columns show the system behaviour at different periods of time (left: 550 to 650, center: 700 to 800, right: 1500 to 1600). If the parameters $H = 0.3$, $m = 0.8$ and $k = 1.9$ with initial conditions a are used (first row), the system behaves regular. If the parameter m is changed to 0.6 and the rest is unchanged (second and third row), chaos evolves in the system. The evolution of the chaos in this case differs from the *normal* evolution of chaos in figure 4.1. In figure 4.3 the onset of chaos for both cases is compared directly.

slow which leads to chaos. In the plot on the right hand side of figure 4.3 no gap splits the population spatially. At one point x_1 in space the populations starts moving slower. Or in other words: The population is split in two domains with only a small connection left between them. At this x_1 the same situation prevails as at x_0 while the *normal* onset of chaos. The mechanism as described above by a critical gradient $\partial t_i / \partial x$ or a too slow velocity of the population acts here. It is striking, that x_1 has about the same value as x_0 . Two simulations with slightly varied initial conditions are performed (not plotted here). The parameters ϵ and x_0 are the same as for the initial conditions 'a': $\epsilon = 0.0004$, $x_0 = 0$. For the one simulation δ is set to 0.008 and for the other one to 0.015. x_1 is further left for $\delta = 0.008 < 0.01$ and further right for $\delta = 0.015 > 0.01$. Moreover the chaos evolves slower for larger δ . The two simulations show, that $x_1 \approx x_0$ in figure

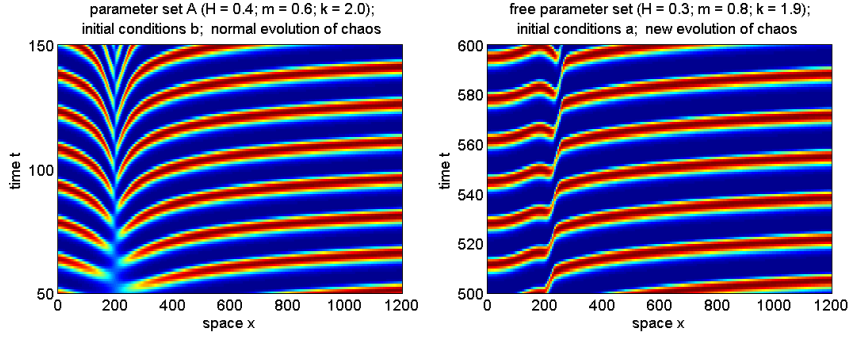


Figure 4.3: The onset of chaos for two different sets of parameters and initial conditions is plotted. For the simulation visualised in the plot on the left hand side the parameter set A and initial conditions b are used. This plot shows the same data as those in the center and right columns of figure 4.1 for other periods of time. On the right hand side of this figure, simulation results for the parameters $H = 0.3$, $m = 0.6$ and $k = 1.9$ and initial conditions a are plotted. These results are equal to those plotted in the center and bottom rows of figure 4.2. Chaotic oscillations itself are not visible in both plots. The evolution of a disturbance which leads to chaos is clear to see and different in both plots. In the plot on the left hand side there exists a gap at $x_0 = 200$. This means, that the populations oscillations left and right of x_0 are separated from each other. The closer a position x in space is to x_0 the smaller the period times of the population oscillations at this position become. Contrary, in the plot on the right hand side the population oscillations are connected over the whole space (Not at the same time.). The connection fades away by ongoing time. At some time point chaos arises. In this case it happens also at about $x_1 = 200$. For different initial conditions the spatial point of the onset of chaos varies.

4.3 is a coincidence.

Finally we want to give an overview about possible system behaviour and the associated parameter space of the pde parameters. As discussed in the second and third paragraph of section 2.1 (between equations 2.1 and 2.2) the nontrivial stationary point (u^*, v^*) is unstable with a stable limit cycle if $H < (1 - p) / (1 + p)$ and stable or a saddle point otherwise. Hence for $H > (1 - p) / (1 + p)$ the system behaviour is not interesting. But it should be mentioned here. For $H < (1 - p) / (1 + p)$ two possibilities exist. In some cases the populations densities oscillate regular and in other ones chaos arises as we see in figure 4.2. Table 4.1 illustrates for a cutout of the parameter space for which parameter sets which system behaviour can be expected. The green areas indicate sets where $H > (1 - p) / (1 + p)$ is given. The yellow areas indicate regular oscillations on a limit cycle and the red ones chaotic oscillations. The yellow and red marked parameter combinations are all tested in simulations. The light red marked combinations are not tested, however we expect chaos. The question mark '?' indicates combinations for which no simulations are performed. Additionally we are not sure which system behaviour results.

4.2 Varying the growth rate

We multiply a new factor α as growth rate with the logistic growth of the prey in equation 1.3 and get a new system given by the equations 4.1 and 4.2. Instead of adding and varying α we could vary m , k , $v(t = 0, x)$, X and T to get the same results (see subsection 4.2.2 for more details). Because working only with α is simpler, we do this. Simulation results for $\alpha = 1.1$ are plotted in figure 4.4. The figure is discussed in subsection 4.2.1.

H = 0.3		H = 0.4							
		k →							
		1.6	1.7	1.8	1.9	2.0	2.1	2.2	
m ↓									
0.5		?	?	?					
0.6									
0.7									
0.8									
0.9									
0.10									
0.11									



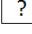

	limit cycle with onset of chaos		stable focus (not of interest)
	? unknown behaviour		limit cycle with regular oscillations

Table 4.1: Systembehaviour depending on the parameter set. Green areas: stable stationary point $((1 - p) / (1 + p) < H < (1 - p) / p$, with $p = m/k$); yellow and red areas: theoretically stable limit cycle around unstable stationary point ($H < (1 - p) / (1 + p)$) but only in some cases regular oscillations (yellow) and in others chaos (red) (results of simulations); light red: no simulations but chaos for sure; '?' (Question mark): no simulations performed

$$u_t = u_{xx} + \alpha \cdot u(1 - u) - \frac{u}{u + H}v \quad (4.1)$$

$$v_t = v_{xx} + k \frac{u}{u + h}v - m(t) \cdot v \quad (4.2)$$

4.2.1 Simulation results for changed growth rate

In the simulations before this chapter α is equal 1. Here we increase α . Decreasing it does not lead to qualitative new results. Increasing it does. Figure 4.4 shows plotted data of simulations with $\alpha = 1.1$. The time is increasing from the left to the right column (left $t \in [300, 400]$, center $t \in [2000, 2100]$ and right $t \in [9000, 9100]$). In the bottom row the same data as in the top row is displayed. The oscillations in the plots on the left hand side look similar to those which later evolve to chaos (e.g. compare to fig 4.1 center). As the plots in the center and on the right hand side of figure 4.4 document, no chaotic oscillations arise. Instead, new oscillations in spatial direction appear. They develop at about $x = 100$ and propagate in both directions. Finally, these oscillations occupy the whole spatial domain (not to see in fig 4.4). If α is increased, the point x at which the new oscillations develop moves to the right. The plots in figure 4.5 indicate this.

In some areas the development of the population density looks like a wave which travels through space. The topic of travelling waves is a huge one in the area of the modelling of population and chemical reaction dynamics. Sherratt and Smith [2008] gives a good up-to-date overview over methods, models and real world observations concerning this topic. Here we mention and describe our observations briefly and do not go into detail. Figure 4.6 shows some of the observed travelling waves. They are marked by a black bar. The plots in the top row present data for the time intervals [4000, 4100], [5000, 5100], and [6000, 6100]. The wave marked by the black bar moves slowly with about 100 spatial units per 1000 time units

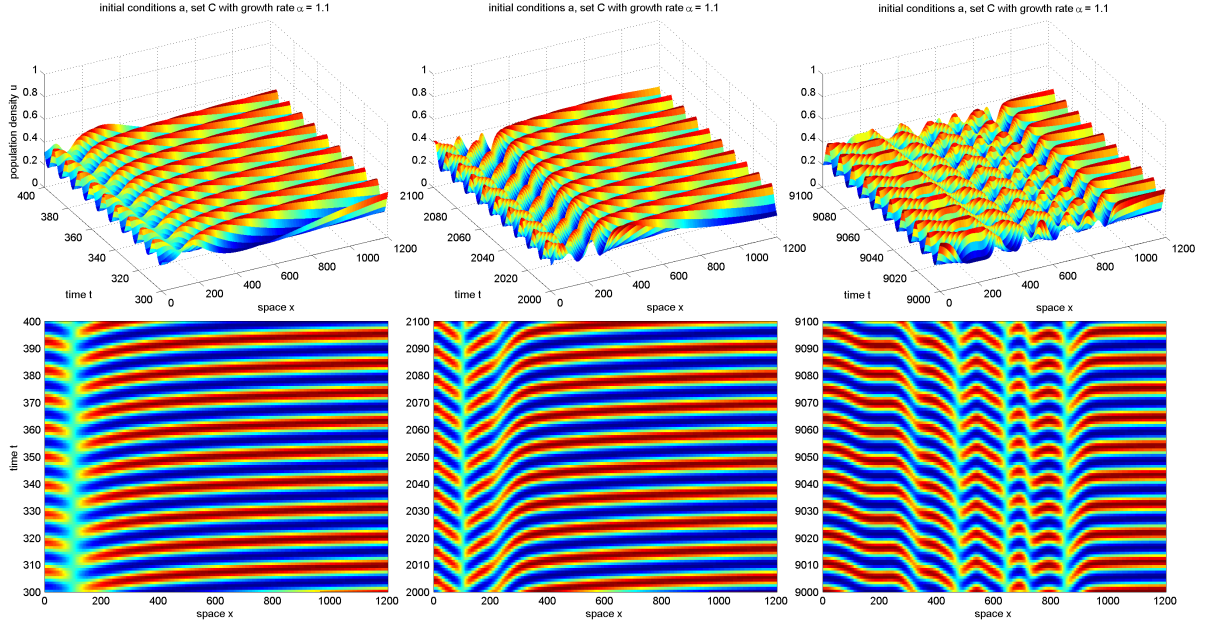


Figure 4.4: Plotted results of simulations with parameter set C, growth rate $\alpha = 1.1$ and initial conditions a for three different temporal intervals (from left to right: $t \in [300, 400]$, $t \in [2000, 2100]$ and $t \in [9000, 9100]$). In the top row the results are plotted in 3d with the space x on the x-, the time t on the y- and the population density u on the z-axis. The bottom row contains 2d color plots which show the same data as the plots in the top row. At $x = 100$ the population density does not oscillate in time for $t \in [300, 400]$ and $t \in [2000, 2100]$. The population is nearly split in two parts. The plots on the right hand side show, that for large t ($t \in [9000, 9100]$) the anomaly at $x = 100$ vanished or moved.

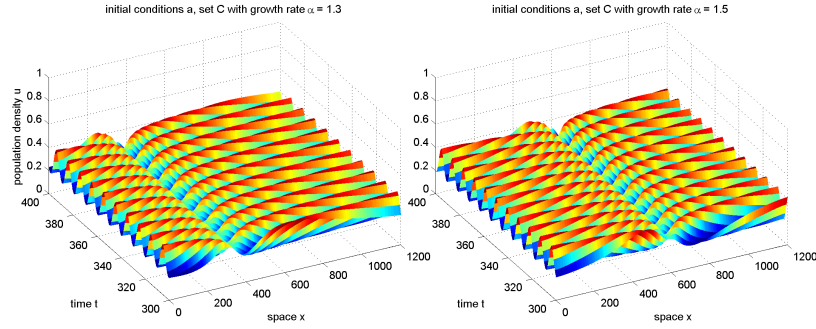


Figure 4.5: Plotted results of simulations with parameter set C, initial conditions a and two different growth rates α (left: $\alpha = 1.3$, right: $\alpha = 1.5$). The gap where no temporal oscillations occur is not located at $x = 100$ as in simulations with $\alpha = 1.1$. For $\alpha = 1.3$ it is located at approximately $x = 350$ and for $\alpha = 1.5$ at 650 .

(≈ 0.1 [spatial units] / [time unit]) from left to right. The shape of the wave nearly does not change. In figure 4.7 the population density u is plotted against the time for three values of t out of the above mentioned intervals. The travelling wave is marked by a black box. In the area left of the wave no further not by time deformed waves are existent. The bottom row contains three plots for the temporal intervals $[8000, 8100]$, $[10000, 10100]$ and $[12000, 12100]$. In each plot two travelling waves are marked by a black bar. The right one is the same as in the plots of the top row. The left one is new and evolved after $t = 6100$. Both waves move with a velocity of approximately 0.1 [spatial units] / [time unit] and their shapes deform only slightly. Further

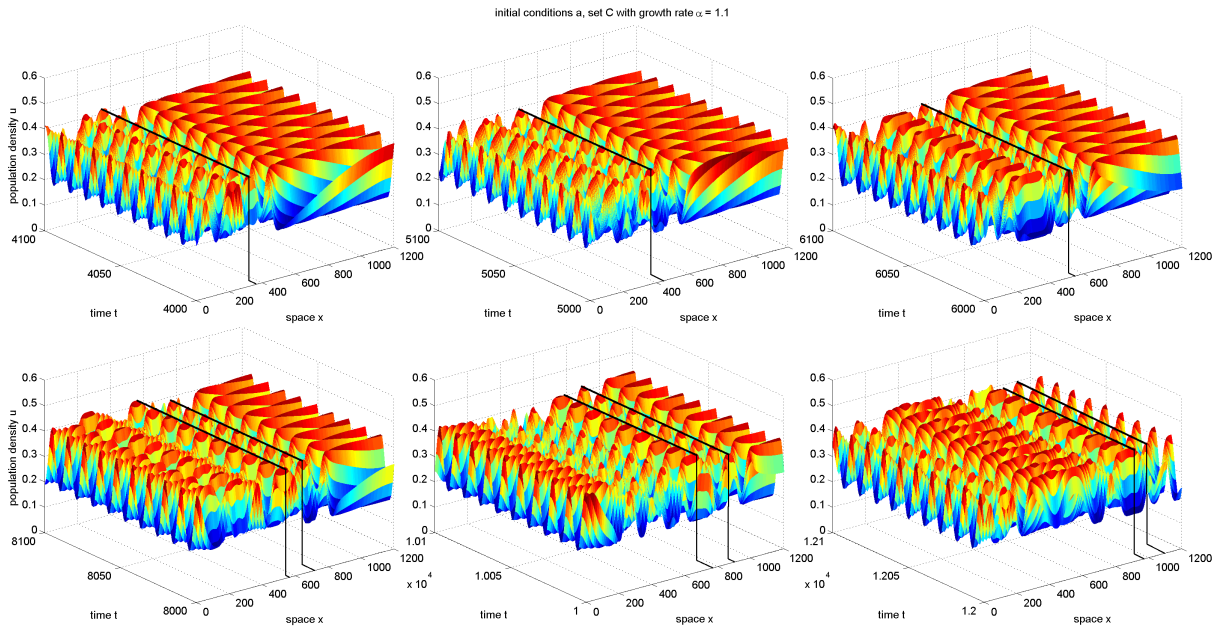


Figure 4.6: Simulation results (initial conditions a, parameter set C, growth rate $\alpha = 1.1$) are plotted for six different temporal intervals. In the plots in the top row the advection of a population peak (or wave) is marked by a black bar. The shape of the wave does not change while the wave travels from left to right. In the plots in the bottom row two travelling waves are marked. The right one in each plot matches to the one marked in the top plots. The left one arose after $t = 6100$. Unfortunately the latter wave is slightly deformed as a comparison of the plots on the left and on the right hand side reveal: The wave is stretched. The velocity of the first wave constitutes approximately 0.1 [spatial units] / [time unit]

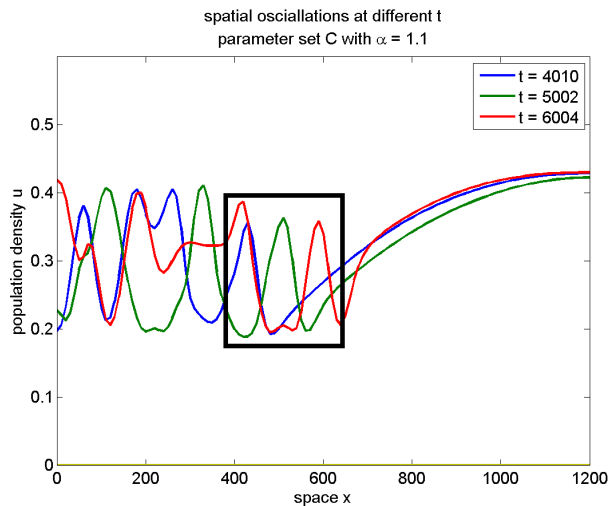


Figure 4.7: The prey's population density u is plotted against the space x for three different time points. This figure and figure 4.6 (initial conditions a, parameter set C, growth rate $\alpha = 1.1$) are based on the same data. The travelling wave which is marked by a black bar in figure 4.6 is marked by a black box in this figure. For $t = 4010$ (blue) the wave is near the left boundary of the box, for $t = 5002$ (green) it is in the center and for $t = 6004$ (red) it is near the right boundary.

examination of the travelling waves is out of the temporal scope of this work.

4.2.2 Attempts to explain the simulation results

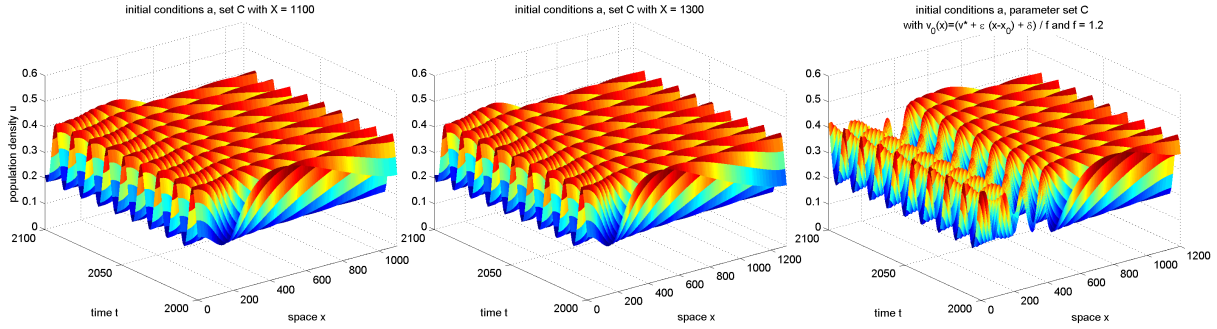


Figure 4.8: Plotted results of simulations with parameter set C and initial conditions a. On the left hand side and in the center the spatial extent X of the system is varied from $X = 1200$ (normal size, not shown) to 1100 (left) and to 1300 (center). The results plotted on the right hand side are obtained by dividing the *normal* initial values of the predator density v by a factor f . Instead of $v * +\epsilon(x - x_0) + \delta$ the formula $(v * +\epsilon(x - x_0) + \delta) / f$ is used for computing $v_0(x)$. In this case $f = 1.2$. Between $x = 300$ and $x = 400$ a gap exists as in the plots of figures 4.4 and 4.5.

Another direction worth to consider and go into detail is to seek for a reason why the new oscillations appear. Instead of changing α , other model parameters could be changed. If we consider equation 1.1, we see that changing α means multiplying the parameter a with a factor f with $f = \alpha$. Consider we replace a by $a \cdot f$, change f and keep $\alpha = 1$. Then all parameters und variables which contain a are changed:

$$m = \mu / (a \cdot f) \quad (4.3)$$

$$k = \kappa \cdot \gamma / (a \cdot f) \quad (4.4)$$

$$v = V \cdot \gamma / (u_1 \cdot a \cdot f) \quad (4.5)$$

$$t_{dimensionless} = t_{with\ dimensions} \cdot a \cdot f \quad (4.6)$$

$$T_{dimensionless} = T_{with\ dimensions} \cdot a \cdot f \quad (4.7)$$

$$x_{dimensionless} = x_{with\ dimensions} \cdot \sqrt{a \cdot f / D} \quad (4.8)$$

$$X_{dimensionless} = X_{with\ dimensions} \cdot \sqrt{a \cdot f / D} \quad (4.9)$$

The change of m and k (equations 4.3 and 4.4) does not lead to results as observed in subsection 4.2.1. The scaling of x and t (equations 4.8 and 4.6) is not important till comparing results to real world data. It could be sensible to scale the spatial and temporal step sizes Δx and Δt by \sqrt{f} . We did not do it. T (equation 4.7) has no effect on the simulations results. We set X (equation 4.9) to 1100 and 1300 instead of 1200 and perform a simulation for each value with parameter set C and no other changes. The results are plotted in figure 4.8 on the left hand side and in the center. The variation of only X has not the effect as observed in subsection 4.2.1. If a is multiplied by f then v has to be divided by f (equation 4.5). Therefore also $v_0(x)$ has to be divided by f (see equation 4.10). On the right hand side of figure 4.8 results of simulations with changed initial conditions are plotted (equation 4.10, $f = 1.2$). Contrary to the changes of the other parameters and variables, the change of v_0 does lead to similar results as obtained in subsection 4.2.1: A gap between $x = 300$ and $x = 400$ splits the population in two parts.

$$v_0(x) = v(t=0, x) = (v^* + (\epsilon(x - x_0) + \delta)) / f \quad (4.10)$$

Finally through figure 4.8 we conclude, that new behaviour obtained in subsection 4.2.1 by varying α is qualitatively reproducible by varying the initial values of the predator population. As far as we know it is a new observation, that varying the initial conditions not only leads to simple regular oscillations or chaos but also to more complex regular oscillations. In proceeding works with the model a focus should be set on further variations of the initial conditions.

4.3 Spatially Varying parameters

For all simulation results presented in the chapters before, the pde parameters m , k , H and α are kept constant in space and time during each simulation. In this section we vary some parameters in space and describe and discuss the obtained simulation results. The spatial variation of parameters can be implemented arbitrarily complex. We decide to increase the growth rate α (introduced in section 4.2) and the mortality rate m linearly in space. The equations 4.11 and 4.12 show the spatial dependence. $\langle \alpha \rangle$ and $\langle m \rangle$ are equal to the values of α and m defined in the used parameter set if not mentioned otherwise (e.g. for set A we get $\langle \alpha \rangle = 1$ and $\langle m \rangle = 0.6$). In the simulations we present, either α or m depend on space and not both at once. Therefore, either σ_1 or σ_2 is equal zero.

$$\alpha(x) = \langle \alpha \rangle \left(1 + \sigma_1 \frac{x}{X} \right) \quad (4.11)$$

$$m(x) = \langle m \rangle \left(1 + \sigma_2 \frac{x}{X} \right) \quad (4.12)$$

In figure 4.9 results of simulations with parameter set C, initial conditions a and variations of σ_1 and σ_2 are plotted. The plots in each row show data of the same simulations but at two different times. The plots in the first row of figure 4.9 show the *normal* system behaviour and are included for comparison only. The used values of σ_i for each row are written down in table 4.2.

row	σ_1	σ_2	comment
top	0 %	0 %	<i>normal</i> run without spatial gradient
center	5 %	0 %	α increasing from left to right
bottom	0 %	5 %	m increasing from left to right

Table 4.2: Values of σ_1 and σ_2 for the simulations which results are plotted in figure 4.9 and some comments.

Consider the center row in figure 4.9: The period length of the spatial oscillations in the left hand side plot is larger than in the right hand side one. As well, the movement velocity of population peaks on the left hand side is larger than on the right hand side. Thus, the period length and the velocity decrease with increasing time. Compared to the center row, the period length in the plots in the top row is larger. Moreover the direction of the movement of population peaks is inverted (top row: left to right; center row: right to left) and the velocity is also larger.

Consider the bottom row: The population density u is temporal constant in both plots for large x (left plot: $x \geq 900$; right plot: $x \leq 700$). We call this area a *beach* because it looks like one: Waves arrive from the left side at a slowly increasing area (More correctly they depart from the beach.). Through increasing the mortality m from the left to the right, the stability

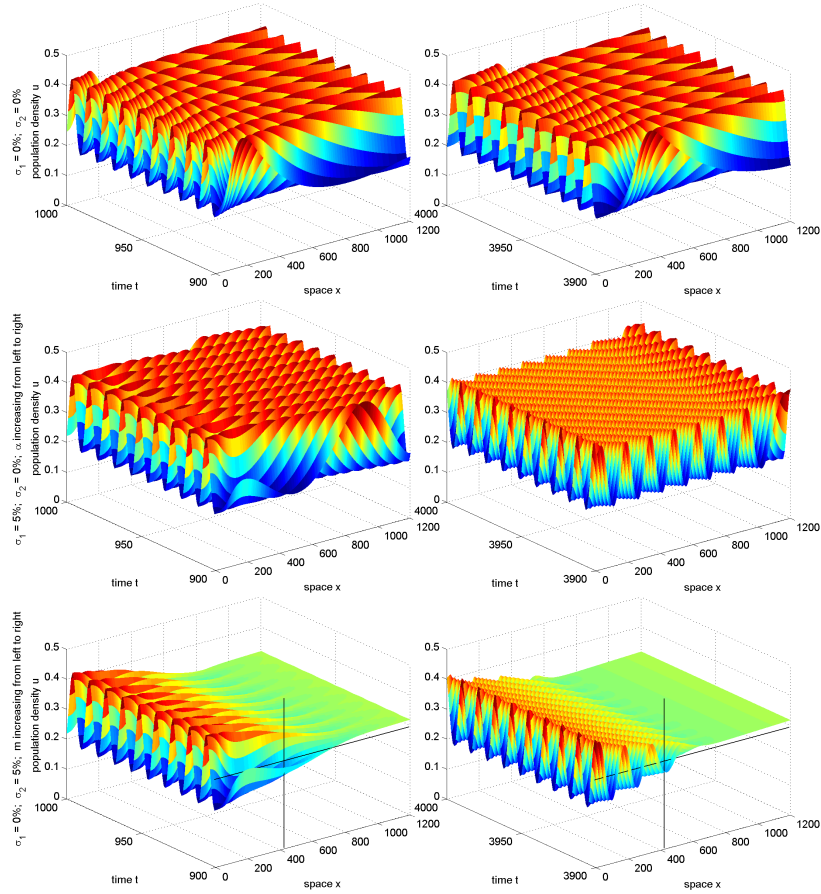


Figure 4.9: Spatial Gradient in parameters leads to travelling waves; top row: predator’s mortality rate m and prey’s growth rate α constant in space ($m = 0.8$, $\alpha = 1.0$); center row: predator’s mortality rate m is constant in space and prey’s growth rate α increases linearly from the left ($x = 0$) to the right ($x = 1200$) by 5% ($m = 0.8$, $\alpha_{x=0} = 1.00$, $\alpha_{x=1200} = 1.05$); bottom row: predator’s mortality rate m increases linearly from the left to the right by 5% and prey’s growth rate α is constant in space ($m_{x=0} = 0.80$, $m_{x=1200} = 0.84$, $\alpha = 1.0$); For $m = 0.8$ the non-trivial steady state is unstable and for $m = 0.84$ it is stable. At $m = 0.8143$ the stability changes in terms of a Hopf bifurcation (see the corresponding text or section 2.1 for more details). The black lines in the plot of the bottom row indicate the position (vertical line) and stationary population density u^* (horizontal line) of the Hopf bifurcation.

of the nontrivial stationary state changes from unstable to stable. At $H = (1 - p) / (1 + p) = (k - m_{Hopf}) / (k + m_{Hopf})$ the Hopf bifurcation occurs (see section 2.1). If we rewrite this with respect to m_{Hopf} we get equation 4.13. Replacing $m(x)$ in equation 4.12 by the right hand side of equation 4.13 and rewriting it with respect to x leads to equation 4.14. For $X = 1200$, $\langle m \rangle = 0.8$, $k = 1.9$ and $H = 0.4$ the value of x_{Hopf} is 428.5714. This value is marked by the black vertical line in the plots. The black line parallel to the x-axis indicates the nontrivial stationary state u^* at the bifurcation. It is computed by $u^* = \frac{m_{Hopf} \cdot H}{k - m_{Hopf}} = \frac{1 - H}{2}$ and its value is 0.3. Right of the intersection of both lines, (u^*, v^*) is stable. As to see in both plots in the bottom of figure 4.9 the waves cover a larger area than the stability of (u^*, v^*) lets expect and the beach begins further right. The direction of movement of the waves is equal to that in the plots in the center row and unequal to that in the plots in the top row of figure 4.9.

$$m_{Hopf} = k \cdot \frac{1 - H}{1 + H} \quad (4.13)$$

$$x_{Hopf} = \frac{X}{\sigma_2} \cdot \left(\frac{k}{\langle m \rangle} \cdot \frac{1 - H}{1 + H} - 1 \right) \quad (4.14)$$

The observations can be generalised for other values of σ_1 and σ_2 . If σ_1 or σ_2 are increased, the velocity of the waves decreases. In subsection 4.3.2 the dependence of the velocity on σ_1 and σ_2 is discussed. If σ_2 is larger than 0 and m_{Hopf} is larger than m_{Hopf} a beach appears on the right hand side of the space. The area covered by the beach increases with increasing σ_2 . If parameter set C is used as for figure 4.9, for $\sigma_2 = 5\%$ already half of the spatial domain is covered by the beach. To have more space with waves and less with beach we use another parameter set and call it E. Set E which is equal to set C except for the value of $\langle m \rangle$: $\langle m_{setC} \rangle = 0.8$ and $\langle m_{setE} \rangle = 0.75$.

First of all, we are interested in impact of the initial conditions. If we spatially invert the initial conditions in a system with spatially homogeneous pde parameters the oscillations are also inverted spatially. How do the oscillations for inverted initial conditions look like if α or m changes in space? This is topic in the following section.

4.3.1 Effects of variation in the initial conditions

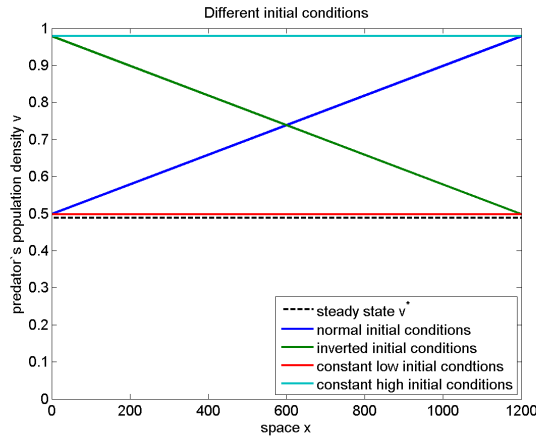


Figure 4.10: Different initial conditions of the predator's populations density plotted against the space. $v^* = 0.4885$ is the steady state of the predator's populations density. Parameter set E is used. The initial conditions are defined as follows:

- *normal* initial conditions a (blue line): $v_0(x) = v^* + 4 \cdot 10^{-4} \cdot x + 0.01$;
- *inverted* initial conditions a (green line): $v_0(x) = v^* - 4 \cdot 10^{-4} \cdot (x - 1200) + 0.01$;
- *constant low* initial conditions (red line): $v_0(x) = v^* + 0.01$;
- *constant high* initial conditions (cyan line): $v_0(x) = v^* + 0.49$;

In this subsection we vary the initial conditions and discuss the resulting effects. If not mentioned otherwise, the simulations are performed with parameter set E. Four different initial conditions are used here. They are plotted in figure 4.10. Figure 4.11 shows plots with results of simulation with parameter set E and the four given initial conditions. The time increases from the left hand side plot to the right hand side one. σ_2 is set to 2% in each simulation. The initial conditions used in the different rows are noted at the left hand side of each row and in table 4.3.

Comparing the associated plots in the first and the second row reveals, that the travelling wave velocity is smaller for the inverted initial conditions. Moreover there is an anomaly in the waves

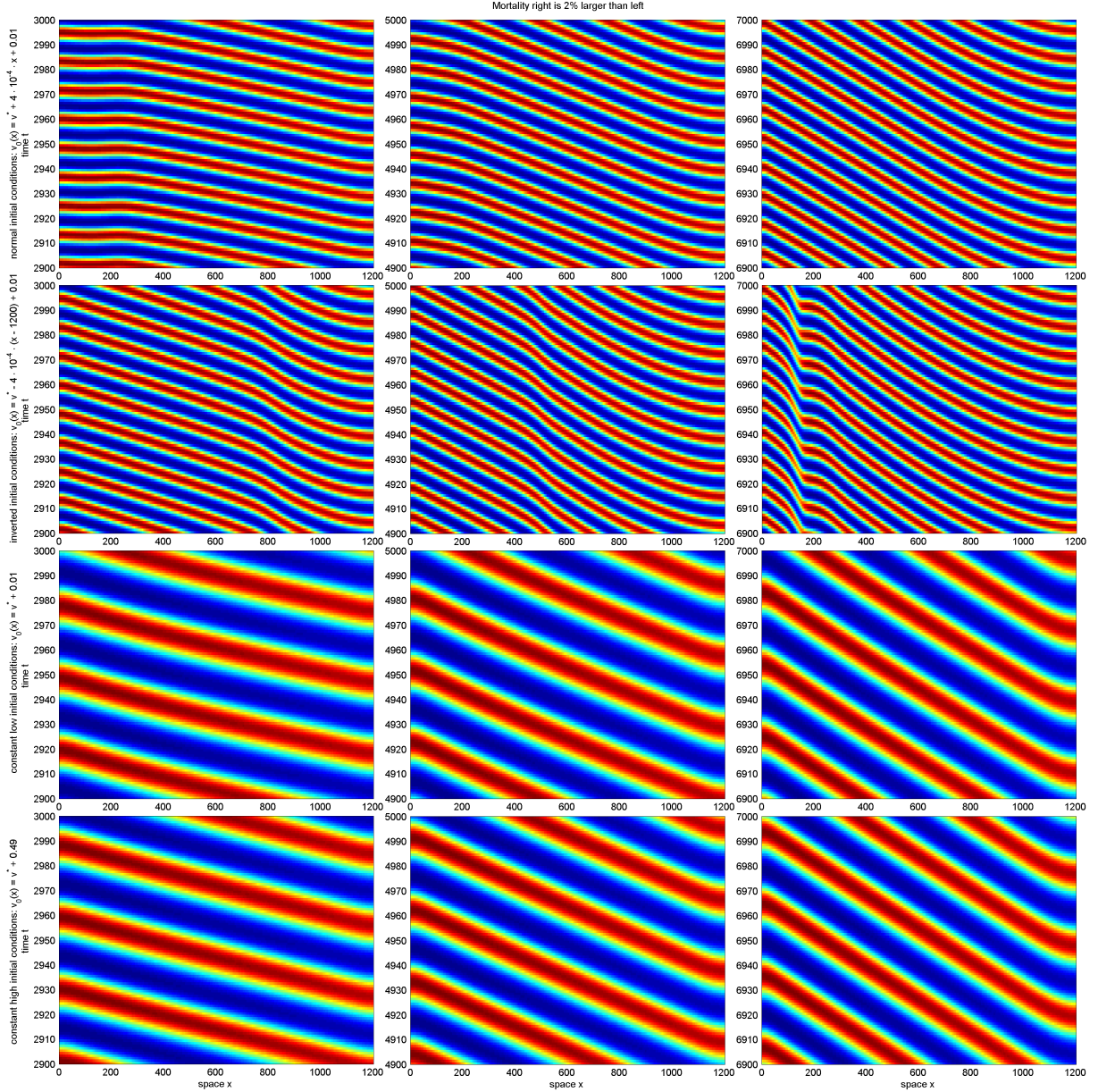


Figure 4.11: Plots for spatially increasing mortality (m_{right} is 2% larger than m_{left}), different initial conditions and at different times. Top row: Initial conditions a (normal ones); second row: inverted initial conditions a ($x_0 = 1200$, $\delta = 0.01$ and $\epsilon = -0.0004$); third row: constant low initial conditions ($x_0 = 0$, $\delta = 0.01$ and $\epsilon = 0$); bottom row: constant high initial conditions ($x_0 = 0$, $\delta = 0.49 = 4 \cdot 10^{-4} \cdot 1200 + 0.01$ and $\epsilon = 0$); columns from left to right: $t \in [2900, 3000]$, $t \in [4900, 5000]$ and $t \in [6900, 7000]$. The plots in the second row show a perturbation in the oscillations compared to the plots in the top line. The perturbation moves from right to left in space while the wave length of the perturbed oscillation decreases. The plots in the third and in the bottom row show oscillations with equal temporal and spatial period length. For all initial conditions the velocity of the travelling waves decreases with increasing time. Parameter set E is used.

which moves from the right to the left and grows. This anomaly also appears in simulations with normal initial conditions for larger t (see subsection 4.3.2). If spatially constant initial conditions are used, the period time and period length of the oscillations are independent of the

row number in fig 4.11	line color in fig 4.10	initial conditions
1	blue	initial conditions a (from now on called <i>normal</i> initial conditions)
2	green	spatially inverted initial conditions a (called: <i>inverted</i> initial conditions)
3	red	spatially constant initial conditions with $v_0(x) = 0.01$ (called: <i>constant low</i> initial conditions)
4	cyan	spatially constant initial conditions with $v_0(x) = 0.49$ (called: <i>constant high</i> initial conditions)

Table 4.3: Description of the initial conditions in figures 4.10 and 4.11

value of v_0 as the plots in the third and fourth row show. In general the period length of the travelling waves is smaller if the initial conditions vary in space. Although it does not matter if $v_0(x)$ increases or decreases with increasing x . Moreover the velocity of the travelling waves is approximately equal for normal and constant initial conditions. It is notably, that travelling waves arise and decelerate for each of the four tested initial conditions. Therefore we can assume, that not a particular combination initial conditions and spatially varying parameters induce the travelling waves, but that only through introducing spatially varying parameters these waves arise.

4.3.2 Velocity of travelling waves

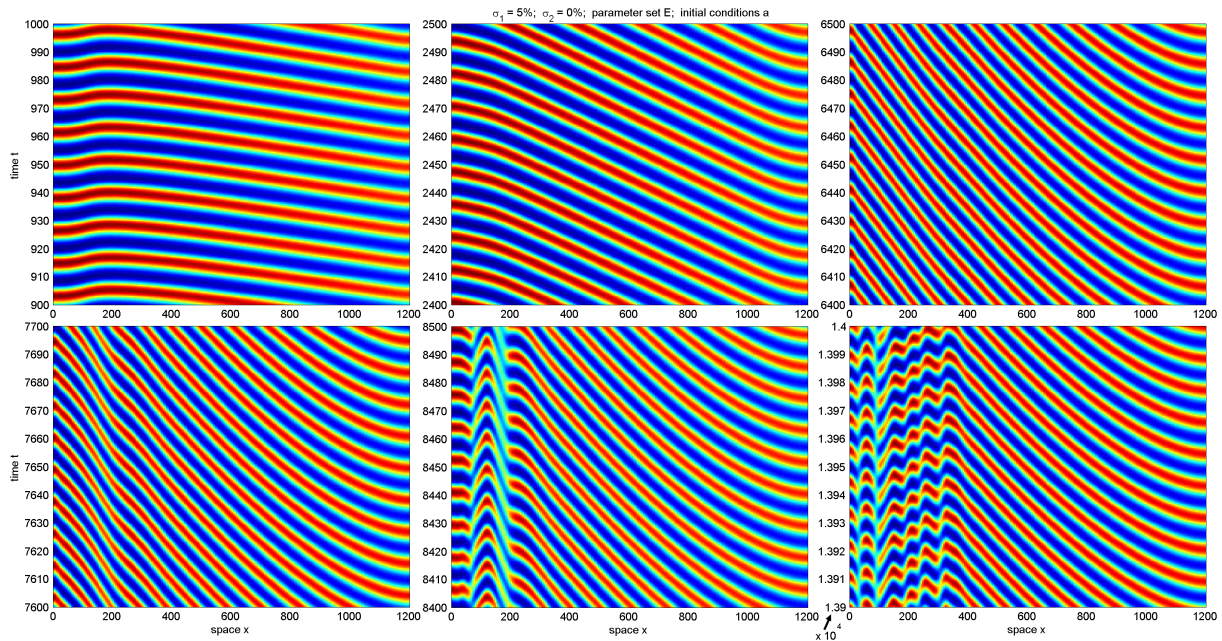


Figure 4.12: Plots with results of one simulation with parameter set E, $\sigma_1 = 5\%$ and $\sigma_2 = 0\%$. From top left to bottom right the time increases. In table 4.4 and the text below (or above) the transformation of the spatio-temporal oscillations is described briefly.

In figure 4.12 we see results of a simulation with parameter set E and growth rate α spatially increasing by $\sigma_1 = 5\%$ plotted for six different time intervals. The plots show, that the spatio-temporal oscillations change with advancing time. The following description is summarised in table 4.4. At first (top left plot) on the right and on the left boundary of the space population

plot	movement of the waves
top left	waves arise at the left and right boundary, move towards $x \approx 200$ and vanish there
top center	waves arise at the right boundary and move to the left; at first they are fast, then decelerate till $x \approx 1000$, move with constant velocity till $x \approx 200$ and finally accelerate again;
top right	waves arise at the right boundary and move to the left: at first they are fast, then decelerate till $x \approx 200$ and then move with constant velocity till they arrive at the right boundary; The constant velocity here is slower than in the top center plot.
bottom left	like top right but an anomaly appears at $x \approx 200$ where the waves' velocities fluctuate
bottom center	like bottom left but the anomaly expands in space and chaos-like oscillations arise
bottom right	the anomaly continues expanding compared to the plot bottom center

Table 4.4: A brief description of the transformation of the spatio-temporal oscillations in the plots of figure 4.12.

maxima arise and move to the center. They *collide* at $x \approx 200$ and vanish while at the boundaries new waves arise. In the second plot (top center) waves are generated only on the right hand side, move to the left (negative velocity) and vanish at the left hand side. Their velocity is high at the left boundary, decreases till $x \approx 1000$, remains constant till $x \approx 300$ and finally increases again. The wave movement in the third plot (top right) is similar to the that in the second one. It differs near the left boundary: The wave's velocity continues decreasing till the wave vanishes and does not increase again. The fourth plot (bottom left) shows the emergence of an anomaly at $x \approx 200$. Near it the velocity of the waves fluctuates. In the fifth (bottom center) and sixth (bottom right) plot this anomaly expands in space and some oscillations which could be chaotic oscillations arise. We did not test whether they are chaotic one or not. The evolution of the system behaviour for other values of σ_1 is qualitative equal to the just described one in figure 4.12. If σ_1 is larger, the process is faster and, if σ_1 is smaller, the process is slower.

In figure 4.12 the waves decelerate from the first to the second, from the second to the third and from the third to the fourth plot. In the fourth plot the deceleration stops and the anomaly appears. It seams, that the waves' velocities converge towards a minimal velocity at which possibly chaotic oscillations arise. This observation is comparable to that of simulations with other values of σ_1 . We compute the velocity of the travelling waves in the area where the velocity is constant and plot it against the time in figure 4.13. The different line colors indicate different values of σ_1 . The black dots mark the onset of chaotic oscillations. In the following we discuss the absolute values of the velocities. Therefore, decreasing means *value moves towards zero*. It is obvious, that the velocities converge towards one constant value at which chaos sets on. If σ_1 is large, the velocity decreases faster compared to a smaller σ_1 . Moreover, the chaotic oscillations arise earlier if σ_1 is larger. The critical minimal absolute velocity at which the chaos emerges is between 6 and 9 [*spatial units*] / [*time unit*] for each σ_1 as table 4.5 illustrates but it increases slightly with decreasing σ_1 . We are not sure if the final velocity really increases or if the observed correlation between σ_1 and the final velocity is a result of our velocity computations which are described in the next paragraph.

The automation of the velocity computation in the region where the velocity is nearly constant is complicated. Each time step the positions of the density maxima have to be computed. The positions of the maxima of two consecutive have to be compared to compute the velocity. In advance, it is not clear in which direction a maximum moves. If the maxima move too fast, the

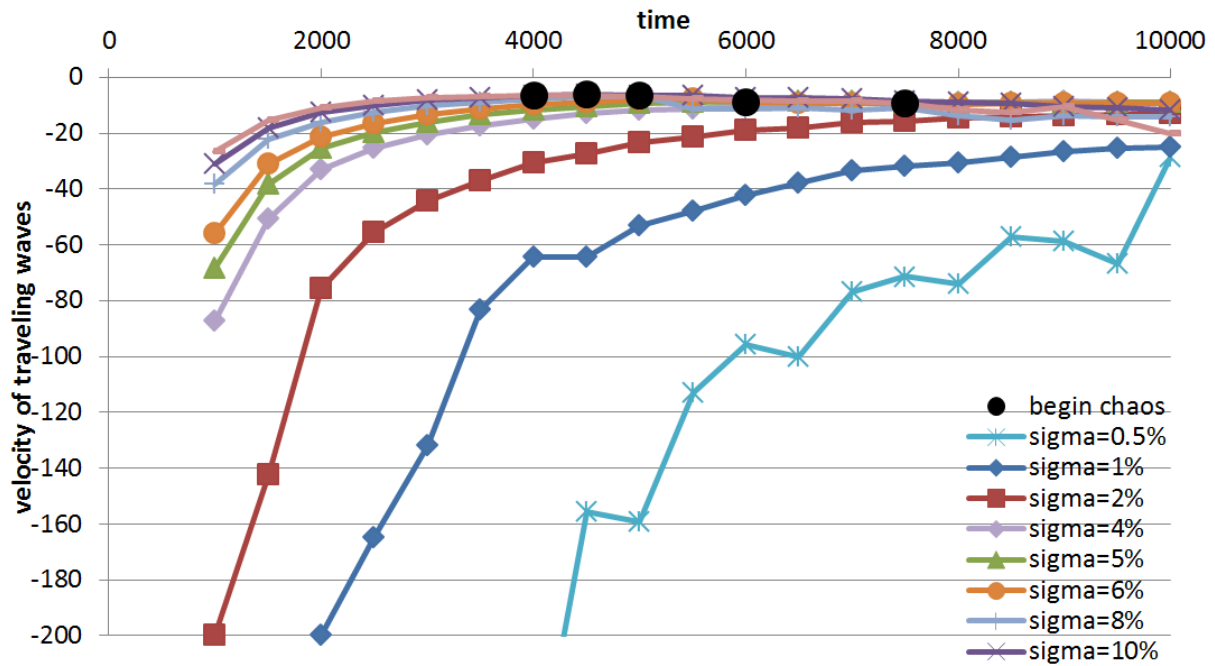


Figure 4.13: Minimal (referred to the absolute value) velocities (computed within the area where the velocity is constant) plotted against the time t for different values of $\sigma_1 = \sigma$. The velocities decrease (referred to the absolute value). They decrease faster if σ_1 is larger. At some minimal velocity chaotic oscillations arise. The black dots mark the onset of them. After the chaotic oscillations started, the velocities do not decrease anymore. These observations are presented more clearly in figure 4.14. The velocities at which chaos arises are written down in table 4.5 for different values of σ_1 .

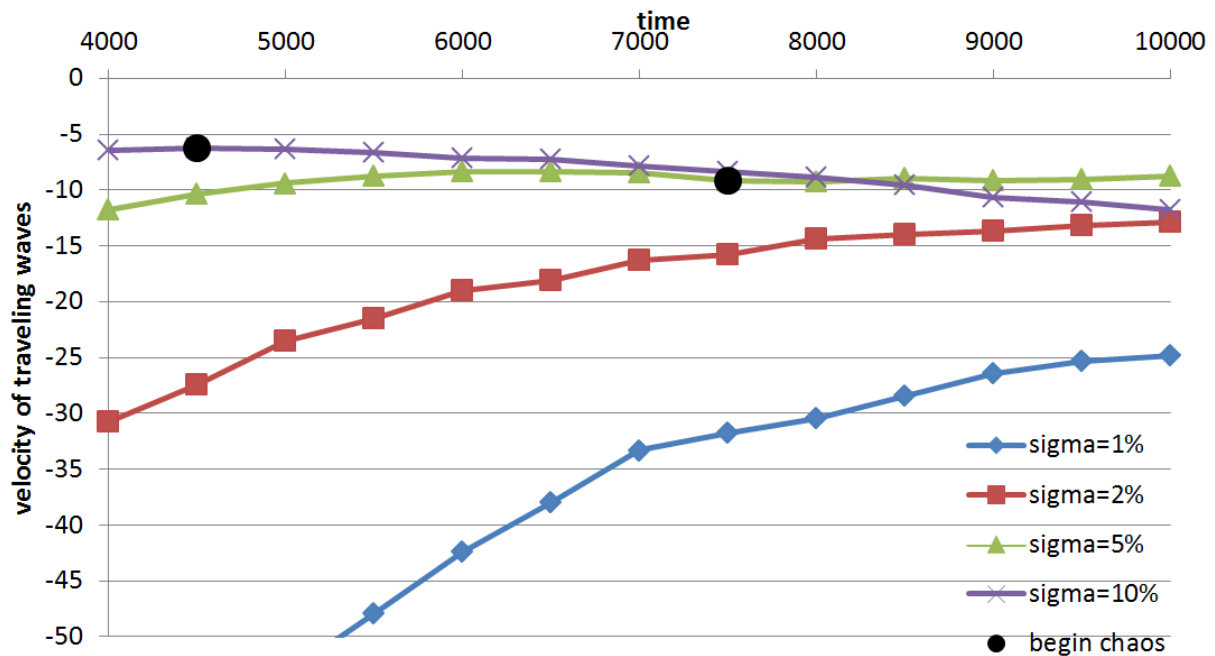


Figure 4.14: Like figure 4.13 but less data and the scaled axes.

wrong maxima could be compared for computing the velocity. At the left and right boundary

σ_1	time t	velocity
12 %	4000	6.79
10 %	4500	6.49
8 %	5000	7.01
6 %	6000	7.65
5 %	7500	8.46
4 %	14000	8.77
3 %	> 50000	
2 %	> 50000	
1 %	> 50000	

Table 4.5: Velocity and time at which chaos arises for different values of σ_1 . The velocity is negative because the waves move from the left to the right. We discuss absolute velocities. Each 500th time unit the system behaviour is checked and the velocity is computed.

maxima appear and disappear from time to time. This can be an error source. Finally, it is difficult to implement the automated determination of the region with constant velocity. Nevertheless, we implemented a automated velocity computation but it did not work well. Because we did not want to include an existing package from a third person and familiarise us with it, we computed the velocity by hand - supported by some tricks - for each 500th time unit. The observation, that the final absolute velocity before chaos arises increase with decreasing σ_1 , could be a results of these discrete computations. This should be checked in another project.

4.4 Summary Parameter Variation

In this chapter we varied the parameters of the pde system (equations 1.3 and 1.4) in different ways and produced some interesting results. We started with a variation of the predator's mortality rate in section 4.1 and produced chaotic oscillations without a change of the initial conditions. The onset of chaos in this case does not look like the normal onset of chaos induced by the initial conditions as figure 4.3 clarifies. It is no clear whether the chaotic oscillations either would arise in the analytic solution (if it was existent) as well or are a result of numerical inaccuracy. Moreover we found further sets of pde parameters which led to chaotic oscillations without a change of the initial conditions, too. In table 4.1 we presented a discrete cutout of the parameter space of H , m and k and added the resulting system behaviour.

In section 4.2 we extended the model by a prey's growth rate α . The modified model is given by the equations 4.1 and 4.2. Increasing the growth rate led to anomalous regular oscillations which start a one point x_1 in space and spread over the whole space (figure 4.4). The point x_1 depends on the value of α as long as $\alpha > 1$ as we showed in figure 4.5. Additionally, in figures 4.6 and 4.7 we found some population peaks which look like travelling waves. Instead of introducing and varying α the initial predator density $v_0(x)$ can be declined to induce qualitatively the same oscillations as the plot on the right hand side of figure 4.8 illustrates. Because the initial conditions cause the new oscillations and because its onset looks similar to the one of chaos, we expect that these new regular oscillations are near the boundary to chaotic oscillations.

Finally in section 4.3 the growth rate α and the mortality m were varied linearly in space. The decency is defined by the equations 4.11 and 4.12. The variation of one the two parameters in space leads to travelling waves as the plots in the center and bottom row of figure 4.9 show. The velocity of the waves and the wave length decrease with increasing time. If the non-trivial steady state (u^*, v^*) is stable in one part of the space and instable in the other, the population

density becomes temporally constant in the first part and oscillates regular in the second one. The oscillations reach a bit into the spatial part where the steady state is stable. The point where the stability changes is called Hopf bifurcation (bottom row of figure 4.9). The travelling waves arise independent of the initial conditions as figure 4.11 shows but they differ in length and velocity depending on the initial conditions. The waves start moving fast, then decelerate and at some minimal critical velocity chaotic oscillations arise (see figure 4.12). The larger the spatial gradient of the growth rate α the faster is the deceleration and earlier the onset of chaos. Figures 4.13 and 4.14 illustrate this well. These figures and the data in table 4.5 suggest that the critical velocity depends on the spatial gradient of α . We are not sure whether this relation is correct or it is a coincidence caused by our way to compute the velocities only each 500th time unit. If the arising oscillations are chaotic ones, is not clear as well.

5 Introduction of Noise

5.1 Motivation II: Why noise?

There are two main reasons why to add noise to a population model. One is the Moran Effect: Through spatially correlated noise a spatial synchronising of population densities takes place. An example for spatially correlated noise is the influence of atmospheric weather systems (rain, drought/heat) on animal populations. For more information concerning the Moran Effect I refer to (Ranta et al. [1997a], Royama [1982]).

The other reason for noise in a model is to make the simulation more realistic: Real world data is expected to be noisy. The simulations we performed for the preceding chapters are deterministic ones. Diffusion reaction partial differential equations in general define a mean expected density at each point in time and space. Therefore the solution is the most probable density distribution. Especially extreme events are not included in the results. To make real observations and simulation results better comparable it is sensible to add noise. Different spatial scales of noise correlation are imaginable. Large scale correlations through atmospheric influences are one possibility (see further Ranta et al. [1995], Ranta et al. [2000]). Medium and small scale correlations through forest fires, floods or large groups of riflemen are another one. Also noise without any spatial correlation would be sensible: A lynx is killed by a falling tree or a car or a hare has a very secure hiding and gets more offspring than normally. In this work we use noise correlated on a large spatially scale.

Our further technical procedure is similar to that in Petrovskii et al. [2010]. The difference is that Petrovskii et al. [2010] analysed the suppression of chaotic oscillations through noise in a system with initial conditions which should lead to chaos. In opposite we work with a system using initial conditions which should lead to regular oscillations. As we will see below in 5.4, regular oscillations can be converted to chaotic ones in the presence of noise.

5.2 Application and Implementation of the Noise I

We use the equations 4.1 and 4.2 in which the prey's growth rate α , the Michaelis-Menten constant H , the food utilisation rate k and the predator's mortality m are parameters. Following we add noise to α and m separately. In Petrovskii et al. [2010] noise was only added to one of the rates but not to both at the same time. In the general case the prey and predator are affected differently by the weather. If we have for example frogs (predator) and insects (prey), heavy rain has another influence on the frog population than on the insect population. Therefore Petrovskii et al. [2010] adds noise either to the one rate or the other. For more information I refer to Milne et al. [1965] and Blackshaw and Petrovskii [2007]. Our analysis is motivated by the Canadian snowshoe hare and the Canadian lynx. The effect of the weather on both species can be considered to be similar. Nevertheless we add noise to the growth or the mortality rate separately. The food utilisation rate k and the Michaelis-Menten constant H are kept unchanged.

The noise is added accordingly to Petrovskii et al. [2010] and similar to the equations 4.11 and

4.12:

$$\alpha(t) = \langle \alpha \rangle (1 + \sigma_1 \eta(t)) \quad (5.1)$$

$$m(t) = \langle m \rangle (1 + \sigma_2 \eta(t)) \quad (5.2)$$

$\langle a \rangle$ and $\langle m \rangle$ are the mean growth and the mean mortality rates as in section 4.2. The η are uniformly distributed uncorrelated random numbers within the interval $[-1; 1]$. To generate the η 's we used the Mersenne Twister (Matsumoto and Nishimura [1998], Matsumoto [1998]) as implemented in Matlab 2010a and 2010b as generator algorithm *mt19937ar*. For further information see the documentation of Matlab R2010a [MathWorks, 2010a] or R2010b [MathWorks, 2010b] in the chapter *Creating and Controlling a Random Number Stream* or the publications of Matsumoto. The chosen initial values for the generator are documented and can be forwarded on request. The generator is only used to generate the η 's and no other random numbers. σ_1 and σ_2 scale the influence of the random numbers with $\sigma_i \in [0; 1]$. Thereby $\sigma_i = 0$ relates to 0 % noise and $\sigma_i = 1$ to 100 %. η is not drawn new each time step but keeps constant for a time period of the length T_0 after which it is redrawn from the interval $[-1; 1]$. This kind of noise is also called kangaroo type of noise (van Kampen [1992]). Figure 5.1 illustrates this. η is independent of x and at each position x in space the same noise is applied to *alpha* and *m*.

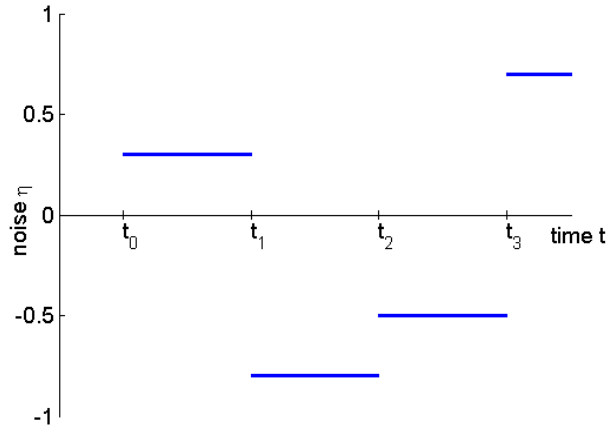


Figure 5.1: The random number η is used for a temporal period of the length T_0 and redrawn after that. $\eta \sim \text{Uniform}[-1; 1]$ and $t_{i+1} = t_i + T_0$.

Why did we choose the noise in the above described way? The argumentation is equal to that of Petrovskii et al. [2010]. We assume the noise is the effect of a atmospheric weather systems of a large spatial scale or climate variations. Those weather systems have a size of the order of 10^3 km (Monin [1986]). Therefore the noise can be expected to be homogeneous in space. Furthermore the systems provide a similar weather for some period of time. The replacement of an old weather systems by a new one occurs on a small time scale compared to the time scale of constant weather. See Monin [1986] for more details. T_0 relates to the temporal period of constant weather. Both systems need not to be correlated to each other and therefore it is sensible to choose η as non-correlated random numbers. In general the resulting kind of noise is called white noise. Steele [1985] and Vasseur and Yodzis [2004] discuss why white noise seems to be more appropriate than colored noise (= correlated random numbers). We call our noise kangaroo type noise because we hold a random number for a certain time before we generate a new one which is reminiscent of jumps of a kangaroo.

A further reason for the kangaroo type of noise is of technical nature. The application of schemas for non-stochastic pdes on stochastic pdes can lead to problems and wrong solutions. The noise in our case stays constant for several time steps. Therefore the given system of partial differential equations does not need to be considered as system of stochastic pdes. Thus the

numerical schemas mentioned in section 2.2 are still valid. This saves time and computation capacity.

5.3 First Observations I: Strong dependence on size of time steps

Till now we used $\Delta x = 0.1$ (spatial step) and $\Delta t = 0.1$ (time step) in our numeric solution (see section 2.2). We worked primary with parameter set A and initial conditions a (regular behaviour) applied on the system of partial differential equations given by equations 1.5 and 1.6. For this purpose $\Delta t = 0.1$ is sufficient. As soon as we add noise, some problems emerge and the time step has to be chosen smaller. Δx will not be discussed because its value of 0.1 is small enough in all cases.

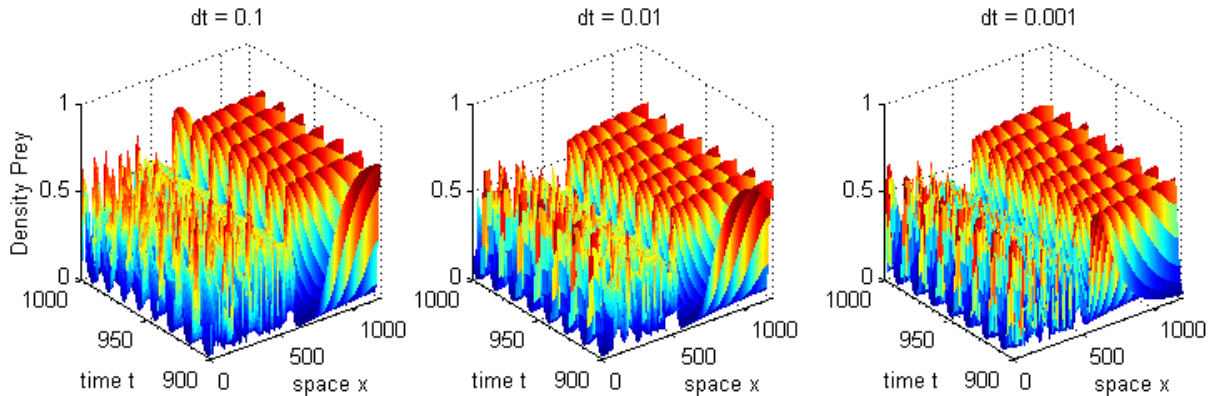


Figure 5.2: The prey density for the given system with parameter set A, initial conditions b (chaos) and no noise. Three different sizes of time steps Δt are used for solving the pde system numerically. They are given above each plot. Decreasing Δt decreases the period time of the regular oscillations. The chaotic oscillations also differ for different sizes of the time steps but the general system behaviour does not change.

We choose parameter set A and initial conditions b for chaotic behaviour. Figure 5.2 shows plots for three different choices of Δt . On the right-hand side of each plot regular oscillations prevail and on the left hand side chaotic oscillations. If Δt is decreased the period time of the regular oscillation is decreased slightly. It seems as the oscillations are phase shifted for different Δt . This is the effect of the different period times. The chaotic oscillations in each plot differ a little bit but the overall system behaviour is unchanged.

We will go into detail on the oscillations in temporal direction and consider the reaction terms of the pde system 1.3 and 1.4 only. Thus we get a system of ordinary differential equations as follows (5.3, 5.4).

$$u_t = u(1 - u) - \frac{u}{u + H}v \quad (5.3)$$

$$v_t = k \frac{u}{u + h}v - m \cdot v \quad (5.4)$$

Figure 5.3 shows plots of numeric solutions of this system for different Δt (colors), different times (left to right) and using different numeric schemata (top and bottom row). For the results in the top row the euler schema is applied and for those in the bottom row the Runge-Kutta schema 4th order (RK4) [cf. Hairer et al., 2010]. Which line color and line style corresponds to which Δt is given in the legend bottom right. Parameter set C is used. Set A leads to

similar results. The density of the prey population is plotted. The predator population shows qualitatively the same system behaviour. If Δt is decreased, the period time and the amplitude of the oscillation decrease. The latter conclusion is obvious. The first conclusion concerning the period time follows through comparison of the plots on the left hand site and in the center. The left ones show a small phase shift between the different coloured lines and the centred ones a larger shift. The unique explanation for this observation is a difference in the period time of the different oscillations. Compare both schemata: The deviation of the amplitude for different Δt is nearly equal for Euler and RK4. Whereas the deviation of the period time is smaller when using the Runge-Kutta 4 schema (compare plots in the center). The plots on the right-hand site show that even for $\Delta t = 0.01$ the RK4 schema leads to a deviating period time. The difference in the amplitude between $\Delta t = 0.010$ and $\Delta t = 0.005$ is small for both schemata. Therefore the Runge-Kutta schema is not reasonable better than the Euler. Hence in a view of runtime performance it is sensible to use the Euler schema. The amplitude of the oscillation converges to a constant value for $\Delta t \rightarrow 0$, whereas for $\Delta t \leq 0.01$ the amplitude has an acceptable value. Thus $\Delta t = 0.01$ seems to be a good value for simulations, ignoring the deviation of the period time. Nevertheless, it has to be emphasised, that the system behaviour is the same for all four sizes of Δt . The diffusion term without the reaction is not considered here.

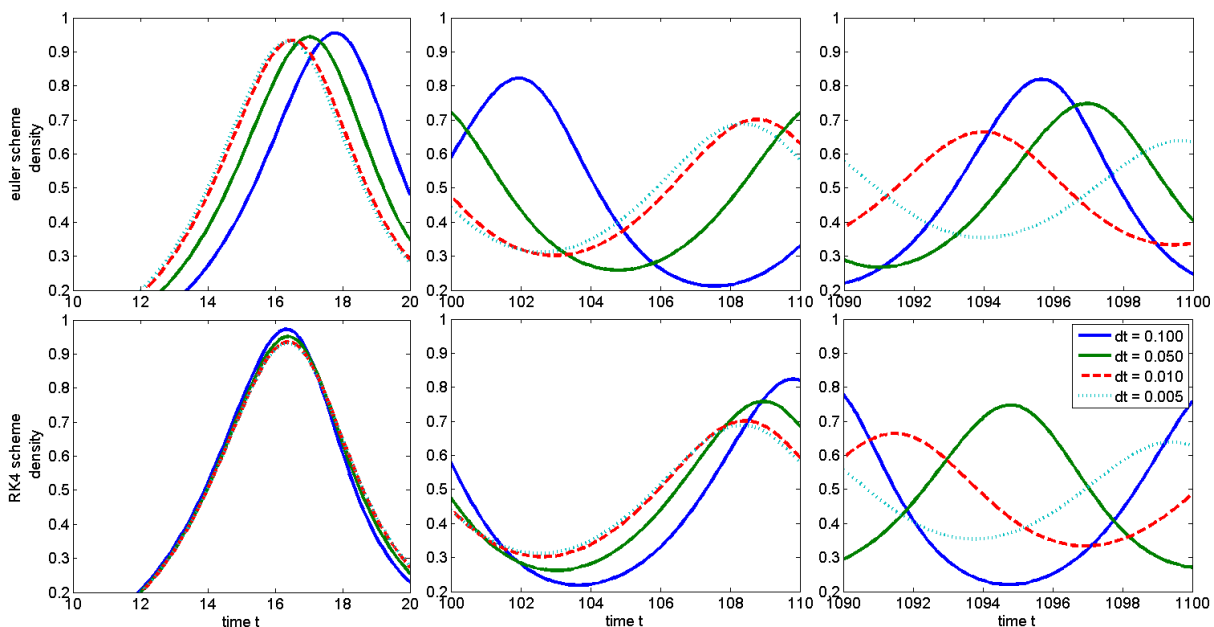


Figure 5.3: Numerical solutions for the reaction part of the pde system 1.5 and 1.6 for parameter set C. The top row shows numerical solutions obtained by using the Euler Schema and the bottom row by the Runge-Kutta Schema fourth order (RK4). The different colors represent different sizes of time steps Δt . The mapping is given in the legend bottom right. The different plots in each row show the prey population at different times (see x-axes). For both schemata $\Delta t > 0.01$ leads very early to obvious differences in period time and amplitude of the oscillations compared to smaller time steps. Using the Runge-Kutta Schema (bottom row) the results for different Δt differ less. For large times (plots on the left hand site) even a difference between the solutions for $\Delta t = 0.01$ and $\Delta t = 0.005$ using the RK4 is quite clear to see in the phase shift of the oscillation. At the same time the amplitudes for these two time steps are nearly equal. Therefore $\Delta t = 0.01$ looks as a good choice between accuracy and performance.

In chapter 3 we are interested in the correlation between mean densities. The larger amplitudes and period times in simulations with $\Delta t = 0.1$ compared to $\Delta t \geq 0.01$ can be considered as

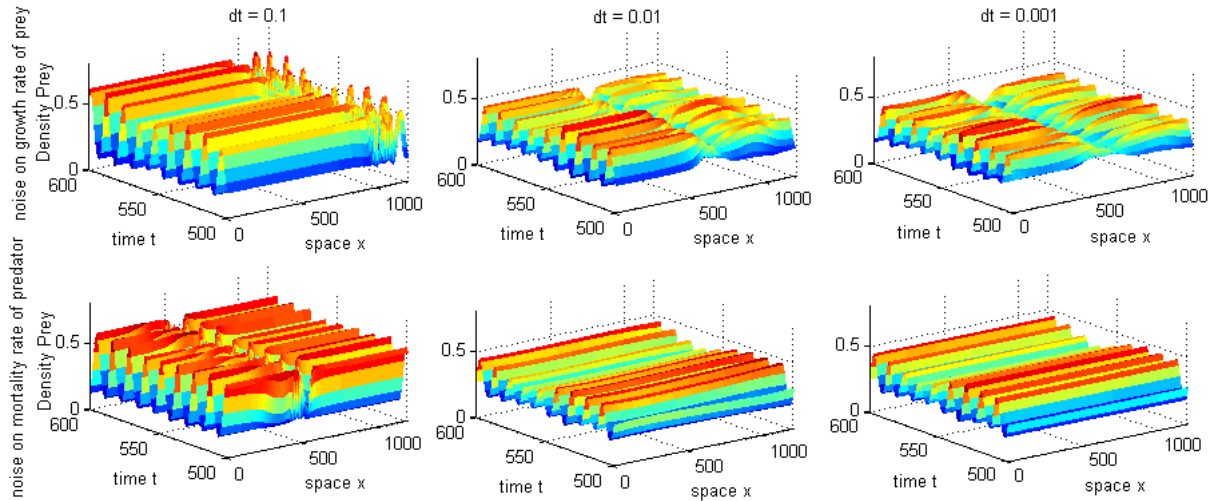


Figure 5.4: The prey density of simulations with parameter set C, initial conditions a (regular oscillations) and noise (noise intensity $\sigma = 0.1$) is plotted here. Three different sizes of time steps Δt are used for solving the pde system numerically. They are given above each plot. The plots in the top row show simulations with noise on the growth rate of the prey and those in the bottom row show simulations with noise on the mortality rate of the predator. Between $\Delta t = 0.1$ in the left column and $\Delta t = 0.01$ and 0.001 in the center and right column the system behaviour differs strongly. Whereas for $\Delta t = 0.1$ in the bottom row we get chaotic oscillations at about $x = 500$ which later spread over the whole space (not shown), we get nice spatially homogeneous oscillations with varying amplitudes for $\Delta t = 0.01$ and 0.001 in the bottom row. In the top row something similar happens.

simulations with $\Delta t = 0.01$ and additionally amplitude and period time scaled by constant factors. If the values of a time series are scaled and the time frame of it is stretched the correlation coefficient for two of these time series should not be affected by the scaling and stretching. Therefore the correlation coefficients in chapter 3 stay the same. The other pure qualitative observations are also not affected. Bearing in mind that smaller Δt increases the computing time, $\Delta t = 0.1$ was a good choice for the parameter set A and C and initial conditions a in chapter 3.

When noise is introduced a problem with the choice of Δt appears. Figure 5.4 points it out. Noise of the intensity $\sigma_i = 0.1$ is added to the growth rate of the prey (top row) and to the mortality rate of the predator (bottom row). Δt is varied as in figure 5.2. In both rows chaotic oscillations arise for $\Delta t = 0.1$. Time passing, the chaotic domains expand and finally the whole area is occupied by chaotic oscillations (not shown). For $\Delta t \leq 0.01$ instead the results differ: If noise is applied to the predators mortality (bottom row), the oscillations stay regular and the densities become spatially homogeneous. If noise is applied to the preys growth rate (top row), the oscillations look more interesting than those without noise but finally (not shown) the densities become spatially homogeneous. Since the system behaviour changes for different Δt , the choice of Δt is crucial after introducing noise into the model. Our observations lead to the assumption, that $\Delta t = 0.01$ is a sufficient small value. For smaller values the systems behaviour does not change significantly anymore.

5.4 First Observations II: Different system behaviour for different sets of parameters

In their work Petrovskii et al. [2010] used initial conditions which lead to chaotic system behaviour. They applied noise of different intensities and analysed the chaos suppressing influence of this noise. The effect of noise on a system with regular behaviour was not within the scope their analysis. One can expect that noise applied to a system with regular behaviour leads to more realistic and more interesting oscillations whilst the behaviour stays non-chaotic. As we see below this expectation is not fulfilled. Depending on the system parameters we get chaotic oscillations or spatially homogeneous densities.

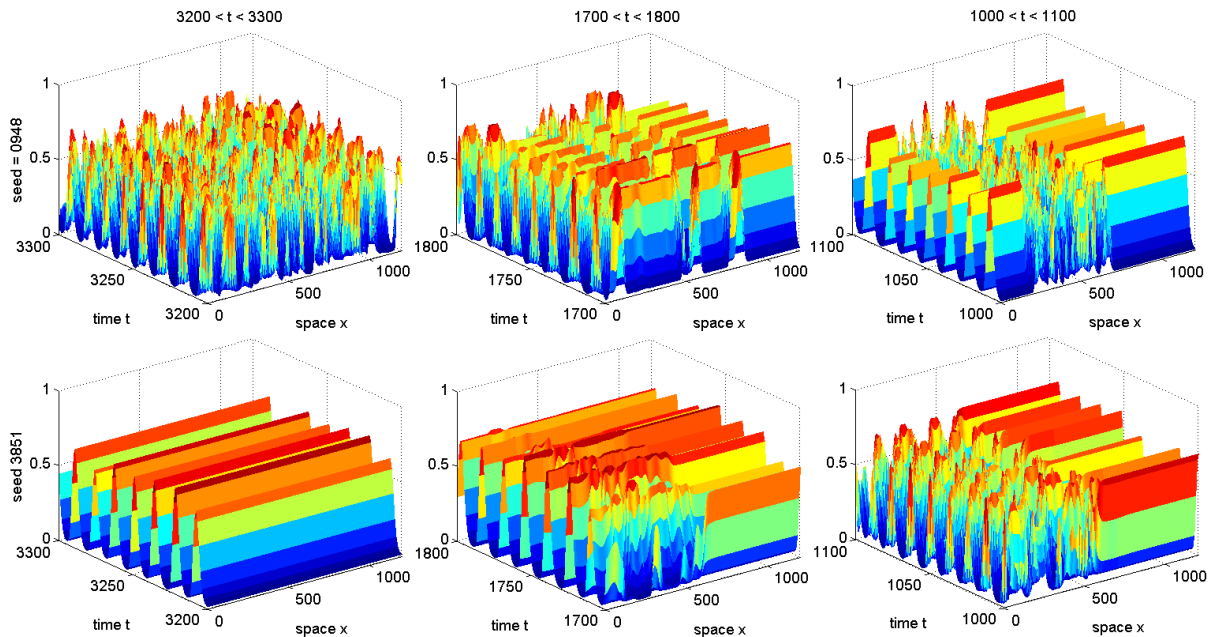


Figure 5.5: Noise of the intensity $\sigma = 20\%$ on the predator's mortality rate of parameter set A, $\Delta t = 0.01$ ($\Delta t = 0.001$ leads to the same qualitative behaviour). The initial values (seeds) of the used sets of random numbers are given in front of each row if someone should try to reproduce my results with my code. As initial conditions the set a is used and as pde parameter set the set A.

As discussed in section 5.3 the system shows non-chaotic behaviour for parameter set C with noise of the intensity 10% and $\Delta t \leq 0.01$. Consider figure 5.4 again. The plots in the center and on the right hand side of the bottom row show spatially homogeneous densities. The corresponding plots in the top row show some interesting behaviour in space but simulating further in time (not plotted), the densities here become also homogeneous in space. This observation is valid for all generated set of random numbers we tested. Thus, we do not get more interesting regular oscillations as expected but more *boring* ones. Just as well we could only solve the reaction terms without diffusion. One reason for this could be the Moran effect which was mentioned at the beginning of section 5.1. We will not discuss this deeper but realise, that parameter set C with noise added as defined above is not usable for our analysis.

If parameter set C leads to spatially homogeneous densities one can expect that set A with noise leads to the same results. That is not always the case as can be seen in figure 5.5. In the two rows simulation results for two different sets of random numbers are shown. Noise of the intensity 20% is applied on the mortality rate of the predator. The data is plotted for the time intervals [1000, 1100] (right), [1700, 1800] (center) and [3200, 3300] (left). In both simulations a

noise applied on	system behaviour	noise intensity σ					
		5%		10%		20%	
		numb.		numb.		numb.	
		abs.	rel.	abs.	rel.	abs.	rel.
mortality	chaos	18	100.0%	17	94.4%	10	55.6%
	homogeneous	0	0.0%	1	5.6%	6	33.3%
	unclear	0	0.0%	0	0.0%	2	11.1%
growth rate	chaos	12	66.7%	17	94.4%	9	50.0%
	homogeneous	5	27.8%	1	5.6%	5	27.8%
	unclear	1	5.6%	0	0.0%	4	22.2%

Table 5.1: On the growth rate and the mortality (each separate, see left column) of parameter set A eighteen different sets of random numbers are applied. The noise intensities 5%, 10% and 20% are used (see first row). Three different system behaviours are observed: chaotic (as in figure 5.5 top row), spatially homogeneous (as in figure 5.5 bottom row) or no clear prevailing of the two before mentioned over the whole runtime. The absolute (columns *abs.* in the table) and relative numbers (columns *rel.* in the table) of cases where each behaviour occurred for the different noise intensities σ is given in this table.

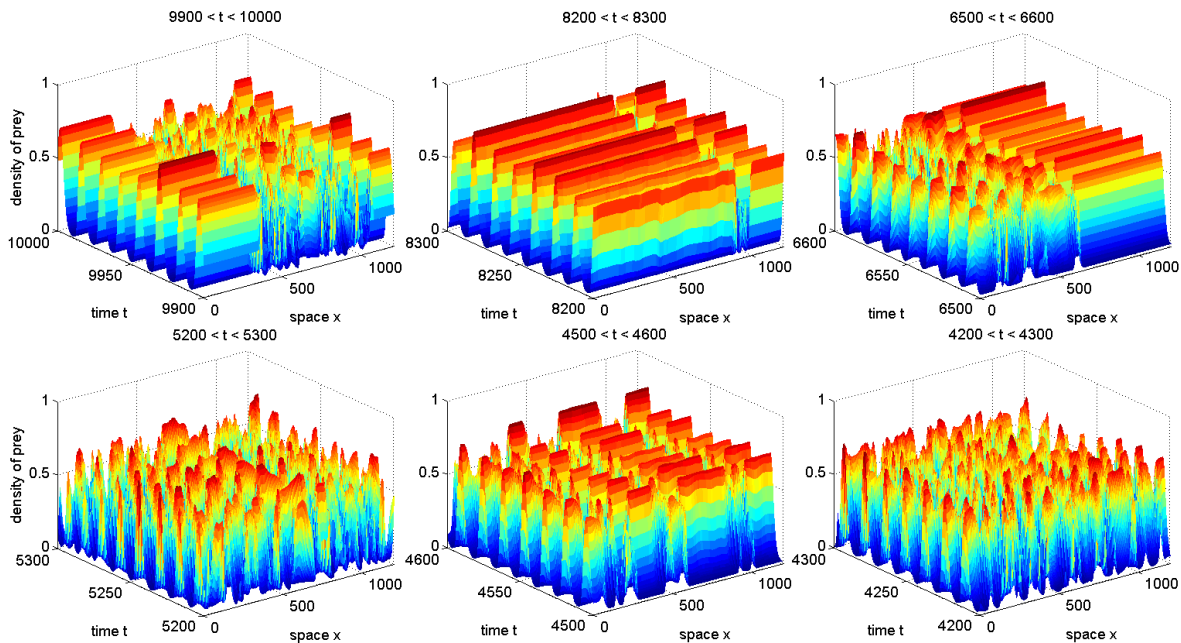


Figure 5.6: Simulations with parameter set A, initial conditions a, 20% noise on the growth rate α ; At $t = 4200$ (plot bottom right) chaos prevails. Some regions of regular oscillations arise between $t = 4300$ and $t = 4500$ as to see in the plot bottom center. These regions fade till $t = 5200$ (plot bottom left) but arise again until $t = 6500$ (plot top right). At $t = 8200$ (plot top center) the chaotic regions are shrunken to one short region. Till $t = 9900$ (plot top left) this one region grew again.

region of chaotic oscillations exists at $t = 1000$ (right). For seed 0948 (= initial value for random number generator) the region of chaotic oscillations splits up and the new regions *move* in space (plot top center). Later in time chaos prevails in the whole space (plot top left). For seed 3851 the chaotic oscillations decay until $t = 1800$. After that the densities are spatially homogeneous. In ten of eighteen cases (= eighteen different sets of random numbers) chaos prevailed finally. Table 5.1 gives an overview over results of simulations with other noise intensities.

In some cases this system exhibits not only chaos dominated or regular oscillations dominated behaviour but also a mixed behaviour, denoted as *unclear* in the table. Figure 5.6 shows plots of one of these cases. At $t = 4200$ (plot bottom right) chaos prevails. Some regions of regular oscillations arise between $t = 4300$ and $t = 4500$ as to see in the plot bottom center. These regions fade till $t = 5200$ (plot bottom left) but arise again until $t = 6500$ (plot top right). At $t = 8200$ (plot top center) the chaotic regions are shrunken to one short region. Till $t = 9900$ (plot top left) this one region grows again. We did not perform simulations for $T \geq 10000$ and thus do not know the final system behaviour.

For now we have an interesting new system behaviour which alternates between regular and irregular oscillations. Perhaps some connection exists to the findings in section 4.2 where new spatial oscillations are cause by the variation of the growth rate α . Here the parameter set A and in section 4.2 the set C is used, but in both cases α is varied. In further studies one could go deeper into detail at this spot.

5.5 Summary, Outlook and Noise II

In this chapter we defined noise and added it to the pde system (equations 1.3 and 1.4). The aim was to obtain more realistic oscillations. In general noise can lead to a more realistic system or to a spatial synchronisation of the oscillations. The latter effect can happen, if the noise is correlated on a large spatial scale. This effect is called Moran Effect. We decided to use spatially homogeneous noise of a kangaroo type in time (see figure 5.1) and added it to the prey's growth rate α or the predator's mortality rate m (equations 5.1 and 5.2). Spatially homogeneous noise represents influences of the weather or the seasons. Technically it is practical to use kangaroo type noise and add it to some pde parameters as reasoned in section 5.2.

Section 5.3 describes a problem we met concerning the choice of the time step Δt after we added noise. The size of Δt is sufficient for solving the deterministic pde system represented by the equations 1.3 and 1.4. The period time and amplitude of oscillations depend slightly on Δt as figure 5.3 illustrates but the system behaviour itself is not affected (figure 5.2). Therefore the results in chapter 3 need not to be reproduced by simulations with smaller choices of the time step. In chapter 4 we already used a smaller Δt . If noise is added to one of the parameters the system behaviour depends on the size of the time step. Figure 5.4 shows clearly that for $\Delta t = 0.1$ the behaviour is distinguishable from that for $\Delta t = 0.01$ and $\Delta t = 0.001$. $\Delta t = 0.01$ seems to be sufficient small.

In section 5.4 the effect of noise on the system behaviour using the parameter sets A and C is discussed. The temporal oscillations synchronise spatially in simulations with parameter set C for each set of random numbers we tested. It could be the results of the Moran Effect. Using parameter set A leads to different system behaviours. In some cases the population densities homogenise in space as for set C (figure 5.5 bottom row) and in some others chaotic oscillations arise and spread over the whole space (5.5 top row). Additionally, a coexistence of both system behaviours is possible as figure 5.6 shows. We did not clarify whether the state of coexistence lasts for ever or one behaviour prevails after a long period of time.

Finally we have a problem: Parameter set C with noise applied leads to less realistic system behaviour and parameter set A with noise leads to unpredictable system behaviour. Before the

latter case is not analysed more in detail, it is not sensible to use the simulations results for other studies - e.g. those of chapter 3. There are three different ways to proceed further: a) We wait till the system with parameter set A and noise is analysed more in detail. b) We find another parameter set which leads to the system behaviour we want when applying the noise as defined in section 5.2. c) We apply another kind of noise on the system and look what happens.

How could other kind of noise look like? We could combine the approach of spatially varying parameters (section 4.3, equations 4.11 and 4.12) with random numbers as defined in section 5.2 (text in section and equations 5.1 and 5.2). The parameters α and m would be defined as follows in equations 5.5 and 5.6:

$$\alpha(x) = \langle \alpha \rangle \left(1 + \sigma_1 \eta(t) \frac{x}{X} \right) \quad (5.5)$$

$$m(x) = \langle m \rangle \left(1 + \sigma_2 \eta(t) \frac{x}{X} \right) \quad (5.6)$$

Nice concerning this solutions: Everything is implemented already and therefore we have not much work with coding. Also other spatial relations are imaginable. With this suggestion for a second kind of noise we close this chapter and proceed with the work on the chaotic system in chapter 6.

6 Chaotic System

6.1 Islands of Order

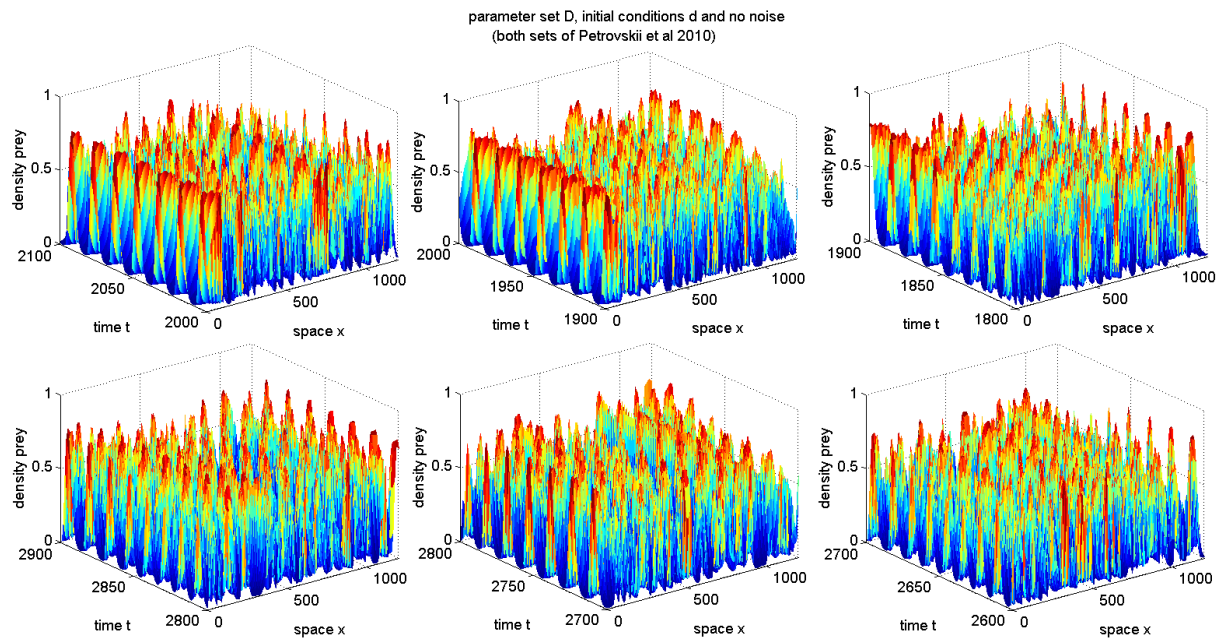


Figure 6.1: Islands of Order in the Chaos; Results of simulations with parameter set D, initial conditions d and no noise are plotted for different time intervals. In the top row from right to left data of the following time intervals is plotted: [1800, 1900], [1900, 2000] and [2000, 2100]. In the bottom row the intervals are [2600, 2700], [2700, 2800] and [2800, 2900]. At $t \approx 1850$ and $0 \leq x \leq 200$ (plot top right) regular oscillations emerge and persist till at least $t = 2100$ (plot top left). In doing so the size of the region declines which starts at about $t = 2050$. In the plot in the bottom row the islands of regular oscillations are not as obvious. At the position $500 \leq x \leq 700$ and the time $t = 2680$ emerges an island which disappears already at $t = 2720$. This island is not counted because the period of time of its existence is too short. The regular oscillations which arise at $850 \leq x \leq 1050$ and $t = 2670$ are counted because they last till some time between 2800 and 2850.

During oscillations of spatio-temporal chaos some regions arise in which the oscillations seem to be regular. In figure 6.1 results of simulations with parameter set D and initial conditions d are plotted for the time intervals [1800, 2100] (top row) and [2600, 2900] (bottom row). A region of regular oscillations is good to see in the plots of the top row at $0 \leq x \leq 200$. Existing regions in the plots of the bottom row are listed in the caption of figure 6.1. We call the regions of regular oscillations also *islands of order* (in an ocean of spatio-temporal chaotic oscillations)

We counted these islands and computed the ratio between whole area and area with regular oscillations. With *region/area* we name here the plane which is spanned by the space and time. The whole area has a size of $X \times T$. If we count and measure each region of regular oscillations

with a size of at least 150×200 ($x \times t$), we find about 20 regions which cover about 5% of the whole area. If we count and measure each region of regular oscillations with a size of at least 130×150 ($x \times t$), we find about 65 regions which cover about 10% of the whole area.

6.2 Chaos Suppression through noise

In Petrovskii et al. [2010] the suppression of spatio-temporal chaos through adding noise on some system parameters was observed. They computed the probability of chaos suppression depending on the intensity of the noise (cf. figure 4 and 5 in Petrovskii et al. [2010]). The noise is defined in the same way as in section 5.2 of this report. Interesting is, that the dependency of the chaos suppression probability on the noise intensity can not be described by a entire monotone increasing or entire monotone decreasing function as could be expected. In Petrovskii et al. [2010] was remarked, that the shape of the function depends on the chosen parameters of the system of partial differential equations (the same system as 1.3 and 1.4). Also the choice of the random number generator could have an influence (personal communication). Here we want to reproduce the results of Petrovskii et al. [2010]. Therefore we used the same set of pde parameters and initial conditions but another implementation of the numeric schemata and another random number generator.

The parameter set of Petrovskii et al. [2010] we called set D in section 2.3 on page 15. Their set of initial conditions is our set d (also section 2.3). These initial conditions lead to the formation chaos in the middle of the space $[0, 1200]$ at $x = 600$.

Petrovskii et al. [2010] used a linear congruential generator of the form $X_{n+1} = (aX_n + b) \bmod j$ with *appropriately chosen parameters* a , b and j . For more information about choosing a , b and j I refer to L'Ecuyer [1999]. We used the Mersenne Twister as described in section 5.2.

We ran simulations with fourteen different noise intensities and each fifty different sets of random numbers. Table 6.1 shows the absolute number of cases (= sets of random numbers) with chaos suppression and the relative number. The latter one is equal to the probability of chaos suppression.

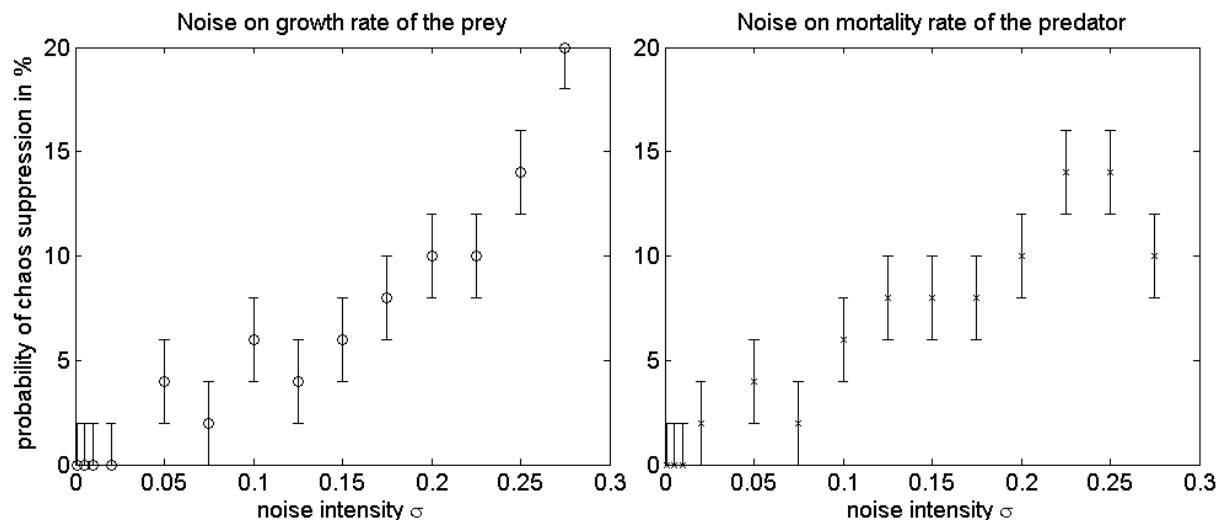


Figure 6.2: Data of table 6.1 visualised. Comparable to figures 4 and 5 on page 8 of Petrovskii et al. [2010]. The errorbars indicate the change of the probability if one case of chaos suppression is changed to non-suppression or the other way around ($\pm 2\%$).

Noise on the growth rate of the prey and *noise on the mortality rate of the predator* is long to

σ	noise on growth rate		noise on mortality rate	
	number of sets with chaos suppression		number of sets with chaos suppression	
	absolute of 50	relative	absolute of 50	relative
0,1 %	0	0 %	0	0 %
0,5 %	0	0 %	0	0 %
1,0 %	0	0 %	0	0 %
2,0 %	0	0 %	1	2 %
5,0 %	2	4 %	2	4 %
7,5 %	1	2 %	1	2 %
10,0 %	3	6 %	3	6 %
12,5 %	2	4 %	4	8 %
15,0 %	3	6 %	4	8 %
17,5 %	4	8 %	4	8 %
20,0 %	5	10 %	5	10 %
22,5 %	5	10 %	7	14 %
25,0 %	7	14 %	7	14 %
27,5 %	10	20 %	5	10 %

Table 6.1: Chaos Suppression through noise: Noise of the intensity σ is added to the growth rate of the prey α (second and third column) and the mortality of the predator m (fourth and fifth column). For each σ (different rows) fifty different realisations of random numbers are used. Columns two and four give the absolute numbers of random number sets for which chaos is suppressed. Columns three and five contain the relative numbers and hence the probability of chaos suppression. The data is visualised in figure 6.2

write and much to read. Therefore we write *10 noise* for noise on the growth rate α and *01 noise* for the other, respectively. In doing so, *10 noise* does not mean *ten noise* but *one zero noise*. *one zero* means noise on growth rate and no noise on mortality rate. Accordingly *zero one* stands for no noise on growth rate and noise on mortality, *one one* for noise on both and *zero zero* for no noise on anything. Furthermore we write the chaos suppression probabilities as percentage numbers between 0 % and 100 % and the noise intensities as decimal numbers between 0 and 1 for a better readability.

Now we compare our plots in figure 6.2 which represents the data of table 6.1 with the figures 4 and 5 on page 8 of Petrovskii et al. [2010].

For small noise intensities σ ($\sigma < 0.02$) the probability of chaos suppression is equal zero. This is consistent with the results of [Petrovskii et al., 2010]. If we increase the noise intensity in our simulation, the chaos suppression probability increases, too. For 10 noise and 01 noise each two anomalies appear at which the suppression probability decreases unexpected: One is at $\sigma = 0.075$ in both cases, one at $\sigma = 0.125$ for 10 noise and the other one at $\sigma = 0.275$ for 01 noise. The latter decrease of chaos suppression probability at $\sigma = 0.275$ in our simulations is similar to the decrease in figure 5 of Petrovskii et al. [2010]. With this observation the consistency between the two works ends. In our simulations the chaos suppression probability exceeds only in one case a probability of 15 %. Whereas the results of [Petrovskii et al., 2010] show a strong increase of this probability till about 75 % for 10 noise and 45 % for 01 noise each at a noise intensity of 0.05. Moreover the results in figures 4 and 5 of Petrovskii et al. [2010] exhibit a decrease of the chaos suppression probability, if σ increases beyond 0.05. For larger noise intensities the probability increases again which leads to another local maximum at $\sigma = 0.3$ for 10 noise and

at $\sigma = 0.2$ for 01 noise. 10 noise leads to a third smaller local maximum at about 0.175. These results are contrary to our results with monotonically increasing suppression probabilities.

To sum everything up, comparing the quantitative results of [Petrovskii et al., 2010] and our ones shows some parallels: a) no chaos suppression for low noise intensities and b) a decrease of the chaos suppression probability for noise intensities σ larger than 0.20 on the mortality of the predator. Clearly the differences prevail: Our chaos suppression probabilities increase nearly monotonically and stay below 20 % whereas in [Petrovskii et al., 2010] there probabilities fluctuate between 0 % and 75 %. One possible explanation is the small sample size of sets of random numbers. We used 50 different sets for each σ and [Petrovskii et al., 2010] between 10 and 15. We did not check how many different sets are needed for a good statistical comparison. Another possible explanation is that in both works different random number generators are used. The one qualitative result is equal in Petrovskii et al. [2010] and here: Chaotic oscillations are suppressed by noise as defined in section 5.2.

7 Summary and Outlook

Motivated by the snowshoe hare and the Canadian lynx, we introduced a spatio-temporal predator-prey-population model which consists of two coupled partial differential equations. It has one non-trivial and two trivial stationary states. Regarding stability, the non-trivial one can be saddle point, a stable knot, a stable focus, an unstable focus with a limit cycle or an unstable knot. The stability of an unstable focus with a limit cycle is the most appropriate for our work because the system variables oscillate. Hence we chose the pde parameter to get this stability. Remarkable at this system is, that for a fix set of parameters only depending on the initial conditions chaotic or non-chaotic (regular) oscillations evolve. Therefore we introduced two sets of initial conditions which lead to chaos (set b) and regular oscillations (set a). In this work we solved the pde system in one spatial dimension only. In principle, it can be solved in arbitrary many dimensions.

After introducing the model theoretically we came back to reality. Real world observations of the snowshoe hare, the Canadian lynx and other species consist of average population countings in large spatial areas. The model produces spatial continuous populations densities. This situation led us to the questions: How do the simulation results look like if the continuous population densities are averaged over large spatial domains like real world observations are by nature? Which influence do size and position of the domains have on the correlation between the average densities in both domains?

To answer these questions we defined two spatial domains in the space and computed the average populations densities within these domains for each time step. The results are four time series: $\langle u \rangle_1$, $\langle u \rangle_2$, $\langle v \rangle_1$ and $\langle v \rangle_2$. $\langle u \rangle_1$ and $\langle u \rangle_2$ are the time series of the prey population and the domains 1 and 2. $\langle v \rangle_1$ and $\langle v \rangle_2$ are those of the predator population, respectively. We compared $\langle u \rangle_1$ and $\langle u \rangle_2$ in two ways. We plotted a $\langle u \rangle_1$ - $\langle u \rangle_2$ -phase plane and discussed it and computed the Pearson's correlation coefficients $\langle u \rangle_c$ and $\langle v \rangle_c$ of the two time series. The following results were obtained and presented in chapter 3: The linear correlation between $\langle u \rangle_1$ and $\langle u \rangle_2$ declines if the size of the domains is increased. For large sizes a correlation is still present but it is nonlinear. The relation between the sizes of both domains has only a small influence on $\langle u \rangle_c$. Unlike expected, $\langle u \rangle_c$ depends strongly on the position of the domains in space. The larger the temporal interval for computing the correlation coefficient, the smaller the dependency on the position. Thus this problem of the spatial dependency can be solved by simulating over a sufficient large time interval. Especially here the influence of different initial conditions is interesting. The results of regarding u and v are quite similar. Hence $\langle v \rangle_1$ and $\langle v \rangle_2$ need not to be discussed separately. The above described qualitative results stay equal if other sets of pde parameters are used. Therefore we limit our work to one parameter set. Finally we varied the ratio between the diffusion coefficients of both coupled pdes and got results we did not expect. Here we do not go into detail but recommend to regard this ratio in further works.

The above mentioned topic is important to work on but for the directly subsequent work we recommend another focus. The five following steps should be performed next in any order:

- Vary distance between the two domains.
- Work with two spatial dimensions.
- Test further initial conditions.

- Find another measure for comparing $\langle u \rangle_1$ and $\langle u \rangle_2$ instead of the correlation coefficient.
- Add noise to the system.

The first, second and third steps are self-explanatory and consist mainly of writing correct programme code. Step four is open and deserves the study of literature. These steps were not treated in this work and are to-dos for further works. Noise should make the regular oscillations of the system more interesting and, above all, more realistic. We do not want chaotic oscillations which we could already get without much effort, if we wanted to. The implementation of noise and its application were performed in chapter 5 which we discuss now.

The first implementation of noise should be as simple as possible. We added noise to the growth rate of the prey and the mortality rate of the predator separately. It seemed sensible to follow Petrovskii et al. [2010] in the definition and implementation of the noise. To avoid instability of the numerical solution the random numbers were kept constant in the whole space and for a previously defined period of time T_0 . Hence, we talk of *spatially homogeneous noise of kangaroo type in time*. The first result we got from the simulations with noise was, that the length of the time step Δt we had chosen in chapter 3 is too long. We tested different Δt in simulations of the model without noise and got slightly varying amplitudes and period time of the oscillations. The system behaviour and the qualitative results in chapter 3 were not affected. After adding the noise we had to decrease the size of the time step by one order of magnitude to get correct results. *Correct* means that the results did not change anymore after decreasing Δt further. Noise was added in simulations with two different sets of pde parameters. Using the one parameter set the population densities became spatially homogeneous after a short period of time. The temporal oscillation were similar to those of the model without diffusion. This behaviour is not useful for our work and not useful in general because the spatial dimension is redundant. Adding noise to simulations with the other parameter set leads to spatio-temporal chaos or to spatially homogeneous oscillations. In most cases one of both system behaviours prevails after some time but in some cases a coexistence of both behaviours exists. This system behaviour is also not the one we wanted to achieve by adding the noise. Nevertheless, the observations we made are interesting for other applications. In nature chaotic and more or less regular oscillations of populations are present. Depending on place, time and species the one or the other kind of oscillations prevails. With this information in the mind, a relative simple system which behaviour changes between chaotic and regular behaviour is sensible to analyse more in detail. Noise added to simulations with the two parameter sets we test and probably other parameter sets, too, leads to no system behaviour we wanted for our further work on the topic of chapter 3. Therefore we suggested another definition of noise in the end of chapter 5 but did not implement and test it.

In chapter 4 we varied some of the pde parameters and described and discussed the results. By changing the mortality rate of the predator we induced chaotic oscillations without changing the initial conditions or adding noise. The onset of chaos does not look like the *normal onset* of chaos induced by appropriate initial conditions. We are not sure, whether the chaos either is caused by numerical inaccuracy or would also be present in the analytical solution. The time step in our simulations was as small as the one we used in chapter 5 for our simulations with noise. Possibly Δt has to be chosen smaller. The values of the population densities u and v are partly near 0. If they are too small, they could be rounded to 0 or a negative number. This could induce chaotic oscillations as well. We made a map for which parameter sets we got chaos (tab. 4.1). In further works it should be worked with these sets in order to check whether numerical errors are present. Additionally we added a growth rate to the prey's logistic growth term and increased it. This lead to less regular regular oscillations. These oscillations arise at one point and spread over the whole space. The onset looks similar to that of spatio-temporal chaos but chaos does not start. It seems, that some single travelling waves arise and move through the space. Dividing the initial values of the predator density $v_0(x)$ by some factor larger than

1 leads to qualitatively the same results. Because the variation of the initial conditions can induce chaos, the less regular regular oscillations could be regular oscillations near the boundary to spatio-temporal chaos. These oscillation and the used initial conditions and parameter set should be analysed more in detail. They could be used as more realistically looking regular oscillations for the further work on the topic of chapter 3. In the end of chapter 4 we increased the growth rate of the prey and the mortality rate of the predator linearly in space and produced travelling waves in doing this. During ongoing time the velocity of the waves decreases till some critical value. A larger spatial gradient of the parameter increase leads to a faster decrease of the wave velocity. Variations of the initial conditions affect the wave length in space and time but do not influence the velocity of the waves. If the critical velocity is reached, oscillations, which look like chaotic oscillations, arise at one point and spread over the whole space. The value of the critical velocity seems to depend slightly on the spatial gradient of the parameter increase. We are not sure, whether this dependency is either real or caused by the way and time in and at which we compute the velocities. If the arising oscillations are chaotic ones or just look like them, is not sure as well. Also this third part of chapter 4 is worth to be regarded more in detail.

Finally in chapter 6 we worked with chaotic oscillations only. When spatio-temporal chaos prevails, small areas of regular oscillations emerge, exist for some time and then fade away. We call these areas *regular islands* or *islands of regular oscillations*. Are the islands seeds of regular oscillations which are suppressed by spatio-temporal chaos again? We do not know. But we counted and measured the islands. Depending on the size and time of existence from which we regard an island as such, we got 5% to 10% coverage of the spatio-temporal plane by these islands. This percentage is quite large and more than we expected. The countings were performed for only one set of pde parameters and for the temporal interval $[0, 10000]$. In further works the interval should be enlarged and other sets should be used. Secondly, we wanted to reproduce the results of Petrovskii et al. [2010]. In Petrovskii et al. [2010] the suppression of spatio-temporal chaos through noise is regarded. Here we did the same as in chapter 5 with the difference, that we used initial conditions which cause chaotic oscillations. Adding noise leads to the three cases: chaotic oscillations, spatial homogeneous regular oscillations and coexistence of both. This time, we counted the cases in which finally spatial homogeneous oscillations prevail for different intensities of noise. The qualitative result of Petrovskii et al. [2010], that chaos is suppressed by noise in some cases, we confirmed in our work. Quantitative dependencies between the noise intensity and the probability of chaos suppression were not reproducible. Potential reasons for the latter result are: We used another random number generator than Petrovskii et al. [2010]. The sample size of sets of random numbers was to small. We tested fifty different sets for fourteen different noise intensities each. Possibly much more are needed?

The given pde system provides much potential for further work as became clear in chapters 3, 4, 5, 6 and this summary. Variations of initial and boundary conditions are nearly completely ignored in this work. The manifold alternatives working with a system of two coupled pdes is amazing and the logic following question is: What to do with more complex systems?

Bibliography

- Rod P. Blackshaw and Sergei V. Petrovskii. Limitation and regulation of ecological populations: a meta-analysis of tipula paludosa field data. *Math. Model. Nat. Phenom.*, 2(4):46–62, 2007.
- Klaus Brauer. Loesungsmethoden bei partiellen differentialgleichungen (methods for solving partial differentialequations). (lecture notes, summer semester 2005), 2005.
- Helen Chitty. The snowshoe rabbit enquiry, 1943-46. *Journal of Animal Ecology*, 17(1):pp. 39–44, 1948.
- Helen Chitty. The snowshoe rabbit enquiry, 1946-48. *Journal of Animal Ecology*, 19(1):pp. 15–20, 1950.
- LaMont C. Cole. Population cycles and random oscillations. *The Journal of Wildlife Management*, 15(3):pp. 233–252, 1951.
- LaMont C. Cole. Some features of random population cycles. *The Journal of Wildlife Management*, 18(1):pp. 2–24, 1954.
- Samuel Daniel Conte and Carl W. De Boor, editors. *Elementary Numerical Analysis: An Algorithmic Approach*. McGraw-Hill Higher Educatio, 3rd edition, 1980.
- Andre M. DeRoos, Edward Mccauley, and William G. Wilson. Mobility versus density-limited predator–prey dynamics on different spatial scales. *Proceedings: Biological Sciences*, 246 (1316):pp. 117–122, 1991.
- Rick Durrett and Simon A. Levin. Lessons on pattern formation from planet wator. *Journal of Theoretical Biology*, 205(2):201 – 214, 2000.
- Charles S. Elton. Periodic fluctuations in the numbers of animals their causes and effects. *J Exp Biol*, 2(1):119–163, 1924.
- Charles S. Elton and Mary Nicholson. The ten-year cycle in numbers of the lynx in canada. *Journal of Animal Ecology*, 11(2):pp. 215–244, 1942.
- J. Patrick Finerty. Cycles in canadian lynx. *The American Naturalist*, 114(3):pp. 453–455, 1979.
- Ernst Hairer, Syvert P. Norsett, and Gerhard Wanner, editors. *Solving Ordinary Differential Equations I*, volume 8 of *Springer Series in Computational Mathematics*. Springer, Berlin Heidelberg, 2nd edition, 2010.
- Eberhard Hopf. Abzweigung einer periodischen losung von einer stationaren losung eines differentialsystems. *Ber. Math-Phys. Sachsische Adademie der Wissenschaften Leipzig*, 94:1–22, 1942.
- Charles J. Krebs, B. S. Gilbert, Stan Boutin, Anthony R.E. Sinclair, and James N. M. Smith. Population biology of snowshoe hares. i. demography of food-supplemented populations in the southern yukon, 1976-84. *Journal of Animal Ecology*, 55(3):pp. 963–982, 1986.
- Charles J. Krebs, Rudy Boonstra, Stan Boutin, and Anthony R.E. Sinclair. What drives the 10-year cycle of snowshoe hares? *BioScience*, 51(1):pp. 25–35, 2001.

- Pierre L'Ecuyer. Tables of linear congruential generators of different sizes and good lattice structure. *Math. Computation*, 68(225):249–260, January 1999.
- Edward N. Lorenz. Deterministic nonperiodic flow. *Journal of Atmospheric Sciences*, 20:130–148, mar 1963.
- Alfred J. Lotka. *Elements of Physical Biology*. Baltimore, Williams and Wilkins, 1925.
- Alfred J. Lotka. *Thorie analytique des associations biologiques. Premire partie. Principes*. Paris, Herman + Cie, 1934.
- Duncan A. MacLulich. Fluctuations in the numbers of the varying hare (*lepus americanus*). Technical report, University of Toronto Press, 1937.
- Duncan A. MacLulich. The place of change in population processes. *The Journal of Wildlife Management*, 21(3):pp. 293–299, 1957.
- Horst Malchow, Sergei V. Petrovskii, and Alexander B. Medvinsky. Numerical study of plankton-fish dynamics in a spatially structured and noisy environment. *Ecological Modelling*, 149(3): 247 – 255, 2002.
- Jerrold E. Marsden and Marjorie McCracken. *The Hopf Bifurcation and Its Applications*, volume 19 of *Applied mathematical sciences*. Springer, New York, 1st edition, 1976.
- MathWorks. Matlab r2010a documentation: Creating and controlling a random number stream, 2010a. URL <http://www.mathworks.com/help/releases/R2010a/techdoc/math/brn4ixh.html>.
- MathWorks. Matlab r2010b documentation: Creating and controlling a random number stream, 2010b. URL <http://www.mathworks.com/help/techdoc/math/brn4ixh.html>.
- Makoto Matsumoto. Mersenne twister home page. Internet: Homepage of M. Matsumoto at the Dept. Math. Hiroshima-Univ., 1998. URL <http://www.math.sci.hiroshima-u.ac.jp/~m-mat/MT/emt.html>.
- Makoto Matsumoto and Takuji Nishimura. Mersenne twister: A 623-dimensionally equidistributed uniform pseudorandom number generator. *ACM Transactions on Modeling and Computer Simulation*, 8(1):3–30, 1998.
- Alexander B. Medvinsky, Sergei V. Petrovskii, Irene A. Tikhonova, Horst Malchow, and Bailian Li. Spatiotemporal complexity of plankton and fish dynamics. *SIAM Review*, 44(3): 311–370, 2002.
- Leonor Michaelis and Maud Menten. Die kinetik der inverinwirkung. *Biochem. Z.*, 49:333–369, 1913.
- A. Milne, R. Laughlin, and R. E. Coggins. The 1955 and 1959 population crashes in the leatherjacket, *tipula paludosa meigen*, in northumberland. *Journal of Animal Ecology*, 34(3): pp. 529–544, 1965.
- Andrei S. Monin. *An Introduction to the Theory of Climate*. Reidel Publishing Company, Netherlands, 1st edition, 1986.
- Cathleen S. Morawitz, James B. Serrin, and Yakov G. Sinai, editors. *Selected works of Eberhard Hopf with commentries*. Number 17 in Collected Works. American Mathematical Society, 2002. ISBN 978-0821820773.
- James D. Murray. *Mathematical biology*. Springer-Verlag GmbH, 1st edition, 1989.

- James D. Murray. *Mathematical Biology II: Spatial Models and Biomedical Applications*, volume 2. Springer, Berlin, 3rd edition, 2003.
- James D. Murray. *Mathematical Biology I: An Introduction*, volume 1. Springer, Berlin, 3rd edition, 2008.
- Mercedes Pascual and Simon A. Levin. From individuals to population densities: Searching for the intermediate scale of nontrivial determinism. *Ecology*, 80(7):2225–2236, 1999.
- Sergei V. Petrovskii and Horst Malchow. A minimal model of pattern formation in a prey-predator system. *Mathematical and Computer Modelling*, 29(8):49 – 63, 1999.
- Sergei V. Petrovskii and Horst Malchow. Wave of chaos: New mechanism of pattern formation in spatio-temporal population dynamics. *Theoretical Population Biology*, 59(2):157 – 174, 2001.
- Sergei V. Petrovskii, Bai-Lian Li, and Horst Malchow. Quantification of the spatial aspect of chaotic dynamics in biological and chemical systems. *Bulletin of Mathematical Biology*, 65(3): 425 – 446, 2003.
- Sergei V. Petrovskii, Bai-Lian Li, and Horst Malchow. Transition to spatiotemporal chaos can resolve the paradox of enrichment. *Ecological Complexity*, 1(1):37 – 47, 2004.
- Sergei V. Petrovskii, A. Morozov, Horst Malchow, and Michael Sieber. Noise can prevent onset of chaos in spatiotemporal population dynamics. *The European Physical Journal B - Condensed Matter and Complex Systems*, 78:253–264, 2010.
- Esa Ranta, Veijo Kaitala, Jan Lindstrom, and Harto Linden. Synchrony in population dynamics. *Proceedings of the Royal Society of London. Series B: Biological Sciences*, 262(1364):113–118, 1995.
- Esa Ranta, Veijo Kaitala, Jan Lindstrm, and Eero Helle. The moran effect and synchrony in population dynamics. *Oikos*, 78(1):pp. 136–142, 1997a.
- Esa Ranta, Jan Lindstrom, Veijo Kaitala, Hanna Kokko, Harto Linden, and Eero Helle. Solar activity and hare dynamics: A cross-continental comparison. *The American Naturalist*, 149 (4):pp. 765–775, 1997b.
- Esa Ranta, Per Lundberg, Veijo Kaitala, and Jouni Laakso. Visibility of the environmental noise modulating population dynamics. *Proceedings: Biological Sciences*, 267(1455):pp. 1851–1856, 2000.
- Robert Davis Richtmyer and Keith William Morton. *Difference Methods for Initial-Value Problems*. Krieger Pub Co, 2nd edition, 1994.
- Otto E. Rössler. An equation for continuous chaos. *Physics Letters A*, 57:397–398, jul 1976.
- T. Royama. *Analytical Population Dynamics*. Chapman & Hall, London, 1982.
- H.R. Schwarz and R. Koeckler, editors. *Numerische Mathematik*. Vieweg+Teubner, 7th edition, 2009.
- Jonathan A Sherratt and Matthew J Smith. Periodic travelling waves in cyclic populations: field studies and reactiondiffusion models. *Journal of The Royal Society Interface*, 5(22):483–505, 2008.
- N. Shigesada and K. Kawasaki. *Biological Invasions: Theory and Practice*. Oxford Series in Ecology and Evolution. Oxford University Press, USA, 1rd edition, 1997.

- Anthony R.E. Sinclair, Charles J. Krebs, James N. M. Smith, and Stan Boutin. Population biology of snowshoe hares. iii. nutrition, plant secondary compounds and food limitation. *Journal of Animal Ecology*, 57(3):pp. 787–806, 1988.
- Anthony R.E. Sinclair, John M. Gosline, Gerald Holdsworth, Charles J. Krebs, Stan Boutin, James N. M. Smith, Rudy Boonstra, and Mark R. T. Dale. Can the solar cycle and climate synchronize the snowshoe hare cycle in canada? evidence from tree rings and ice cores. *The American Naturalist*, 141(2):pp. 173–198, 1993.
- C.H. Smith. Spatial trends in canadian snowshoe hare, *lepus americanus*, population cycles. *Canadian Field-Naturalist*, 97(2):pp. 151–160, 1983. URL <http://people.wku.edu/charles.smith/essays/SMITH83.htm>.
- James N. M. Smith, Charles J. Krebs, Anthony R.E. Sinclair, and Rudy Boonstra. Population biology of snowshoe hares. ii. interactions with winter food plants. *Journal of Animal Ecology*, 57(1):pp. 269–286, 1988.
- J H Steele. A comparison of terrestrial and marine ecological systems. *Nature*, 313(6001): 355–358, 1985.
- Michael Tabor. *Chaos and Integrability in Nonlinear Dynamics: An Introduction*. Wiley-Interscience, 1. edition, 1989. ISBN 978-0471827283.
- N.G. van Kampen. *Stochastic Processes in Physics and Chemistry*. Elsevier, Amsterdam, 1992.
- David A. Vasseur and Peter Yodzis. The color of environmental noise. *Ecology*, 85(4):1146–1152, 2004.
- Vito Volterra. Fluctuations in the abundance of a species considered mathematically. *Nature*, 118:558–560, oct 1926.
- Vito Volterra. *Leons sur la Thorie Mathmatique de la Lutte pour la Vie*. Gauthier-Villars, 1931.
- WikiCommons, E Pluribus Anthony, Andrew pmk (Wikimedia Commons User), and Kaveh (Wikimedia Commons User). Political map of canada. Internet: Wikimedia Commons; No Copywrite, June 2007. URL http://commons.wikimedia.org/wiki/File:Political_map_of_Canada.png.
-